



**AALBORG UNIVERSITY**  
DENMARK

**Aalborg Universitet**

## **Kinetics of the Scavenging Reactions of Hydrogen Sulfide with MEA-triazine**

Romero Logrono, Iveth Alexandra

*DOI (link to publication from Publisher):*  
[10.54337/aau561830543](https://doi.org/10.54337/aau561830543)

*Publication date:*  
2023

*Document Version*  
Publisher's PDF, also known as Version of record

[Link to publication from Aalborg University](#)

*Citation for published version (APA):*  
Romero Logrono, I. A. (2023). *Kinetics of the Scavenging Reactions of Hydrogen Sulfide with MEA-triazine*. Aalborg Universitetsforlag. <https://doi.org/10.54337/aau561830543>

### **General rights**

Copyright and moral rights for the publications made accessible in the public portal are retained by the authors and/or other copyright owners and it is a condition of accessing publications that users recognise and abide by the legal requirements associated with these rights.

- Users may download and print one copy of any publication from the public portal for the purpose of private study or research.
- You may not further distribute the material or use it for any profit-making activity or commercial gain
- You may freely distribute the URL identifying the publication in the public portal -

### **Take down policy**

If you believe that this document breaches copyright please contact us at [vbn@aub.aau.dk](mailto:vbn@aub.aau.dk) providing details, and we will remove access to the work immediately and investigate your claim.



**KINETICS OF THE SCAVENGING REACTIONS  
OF HYDROGEN SULFIDE WITH MEA-TRIAZINE**

**BY  
IVETH ALEXANDRA ROMERO LOGROÑO**

DISSERTATION SUBMITTED 2023



**AALBORG UNIVERSITY**  
DENMARK



# **Kinetics of the Scavenging Reactions of Hydrogen Sulfide With MEA-Triazine**

**PhD DISSERTATION**

by

Iveth Alexandra Romero Logroño



**AALBORG  
UNIVERSITY**

Dissertation submitted August 2023

Dissertation submitted: August 2023

PhD supervisor:: Associate Professor Marco Maschietti,  
Aalborg University, Denmark

Assistant PhD supervisor: Associate Professor Sergey Kucheryavskiy,  
Aalborg University, Denmark

PhD committee: Associate Professor Mads Koustrup Jørgensen  
Aalborg University, Denmark  
Professor Nicolas Von Solms  
Technical University of Denmark, Denmark  
Professor Robert Marriott  
University of Calgary, Canada

PhD Series: Faculty of Engineering and Science, Aalborg University

Department: Department of Chemistry and Bioscience

ISSN (online): 2446-1636  
ISBN (online): 978-87-7573-653-9

Published by:  
Aalborg University Press  
Kroghstræde 3  
DK – 9220 Aalborg Ø  
Phone: +45 99407140  
aauf@forlag.aau.dk  
forlag.aau.dk

© Copyright: Iveth Alexandra Romero Logroño

Printed in Denmark by Stibo Complete, 2023

# ENGLISH SUMMARY

Hydrogen sulfide,  $H_2S$ , is a chemical species naturally present in hydrocarbon reserves. In particular, hydrocarbon fluids produced in the Central and Northern North Sea have significantly high concentrations of  $H_2S$ , with values reaching thousands of ppm, which has a substantial negative impact on oil and gas production due to the extreme toxicity and corrosiveness of  $H_2S$ . Regarding natural gas, the concentration of  $H_2S$  in Denmark must be below 5 ppm, which obliges to treat the gas in topside offshore operations to drastically reduce the  $H_2S$  content before export. Among the methods available for the removal of  $H_2S$  from the gas in offshore processing, the direct injection of liquid  $H_2S$  scavengers stands out for its ease of implementation.  $H_2S$  scavengers are chemicals that react with  $H_2S$  and transform it into substantially less toxic and less corrosive compounds. In some instances, the reaction products (spent scavengers) are discharged into the sea due to the absence of feasible alternatives. The most common  $H_2S$  scavengers used in the industry nowadays are based on 1,3,5-hexahydrotriazines, with 1,3,5-tris(2-hydroxyethyl)-hexahydro-s-triazine (MEA-triazine) largely predominating in the oilfield market. In the treatment of natural gas, aqueous solutions of MEA-triazine are injected into the gas stream. The efficiency of the process depends on both the rate of absorption of  $H_2S$  and the kinetics of the consequent aqueous-phase reaction with the scavenger. Notwithstanding the significance and widespread use of MEA-triazine, the mechanism of the aqueous phase reaction is not fully elucidated and the reaction kinetics at conditions of industrial interest is not available. This is one of the reasons for the empirical design and inefficient operation of the process, causing overdosing of the scavenger that leads to an unnecessary increase of the operating costs and, in some cases, to the discharge of the unreacted scavenger into the sea, which significantly upsurges the environmental impact of offshore oil and gas production.

This PhD thesis presents a study of the kinetics of the reaction between MEA-triazine and bisulfide ( $HS^-$ ), which is the prevailing form of  $H_2S$  in aqueous phase at the pH conditions of interest in industry applications. The measurement of the rate of disappearance of  $HS^-$  in this reaction is particularly challenging by reason of the reaction being very fast under certain conditions, making sampling and off-line analysis problematic. In this work, a methodology based on in-situ Raman spectroscopy and chemometrics was developed and applied for measuring the decrease of  $HS^-$  concentration over time, at different pH values (above 9), temperatures (from 25 to 75 °C), and initial concentration ratio of scavenger to bisulfide (STB) in the range 0.5 to 10.0.

The measurements allowed to quantify the strong decrease of the rate of consumption of  $HS^-$  with increasing pH, as well as its increase with temperature and with the STB ratio. In particular, conditions of excess of scavenger, which are those occurring in the offshore applications, were investigated. The results also showed the possibility

of complete depletion of  $\text{HS}^-$ , provided a sufficient concentration of hydronium is present in solution. In this regard, the results are in line with previous works evidencing the role of the protonation of MEA-triazine in the scavenging reactions.

The reaction between  $\text{HS}^-$  and MEA-triazine was already reported in the literature as occurring via two steps in series, the first one forming thiadiazine and the second one consisting in a further reaction of thiadiazine with  $\text{HS}^-$  forming dithiazine. In addition, the third theoretical substitution of sulfur into the nitrogen of the triazine ring, which would form trithiane, is not observed. Despite this knowledge, the existence of thiadiazine as a long-lived and measurable reaction intermediate, as well as the reasons for the lack of the reaction of dithiazine to trithiane, are still debated in the literature. In this work, nuclear magnetic resonance, NMR, was used to identify thiadiazine and to assess the protonation behavior of MEA-triazine and dithiazine. The experimental results confirmed that thiadiazine is obtained in the scavenging reactions and showed that it is stable enough to be separated and isolated. NMR observations allowed to delimit the pH range of the protonation of MEA-triazine and showed the lack of protonation of dithiazine at the conditions of interest, which is possibly the reason of the absence of the theoretical third scavenging reaction which would lead to trithiane.

Further, a novel kinetic model for the  $\text{H}_2\text{S}$  scavenging reactions with MEA-triazine in aqueous phase was built upon the knowledge gained from the NMR observations and the in-situ Raman spectroscopy measurements. The model includes the protonation equilibrium of MEA-triazine, its irreversible reaction with  $\text{HS}^-$  to form thiadiazine (first scavenging reaction), the protonation equilibrium of thiadiazine and its further irreversible reaction with  $\text{HS}^-$  to form dithiazine (second scavenging reaction), the latter considered as a non-protonating end product. The two scavenging reactions were assumed to be of first order with respect to both the protonated scavenger and  $\text{HS}^-$ . The protonation equilibrium of monoethanolamine, released in the scavenging reactions, was also included in the model. The model was fitted on the experimental data of the scavenging reactions acquired in this work, at temperatures of 25 °C, 50 °C, and 75 °C, initial pH 9 and STB values ranging from 0.5 to 5.0. The optimal values of the regression parameters of the model were determined by a brute-force optimization method. The model provides a satisfactory representation of the rate of disappearance of  $\text{HS}^-$ , with an average relative deviation between experimental and calculated values between 2 to 7%, before acidification. The rate constants of the first and the second scavenging reaction at 25 °C were found to be 0.435 and 0.0004 L mol<sup>-1</sup> s<sup>-1</sup>, respectively. The activation energies of the first and the second scavenging reaction were estimated to be 68 and 57 kJ mol<sup>-1</sup>, respectively.



# DANSK RESUME

Svovlbrinte,  $H_2S$ , er en kemisk forbindelse naturligt til stede i kulbrinte reserver. Specielt kulbrinter produceret i den centrale og nordlige Nordsø indeholder høje koncentrationer af  $H_2S$ , op imod tusinder af ppm, hvilket har en substantiel negativ påvirkning på olie- og gasproduktion grundet den ekstreme toksicitet og høje korrosionsevne af  $H_2S$ . Ifht. naturgas, skal koncentrationen af  $H_2S$  i Danmark være under 5 ppm, hvilket nødvendiggør at gas behandles ved offshore proces-operationer for drastisk at reducere  $H_2S$ -indholdet inden eksport. Blandt metoderne tilgængelig for fjernelse af  $H_2S$  fra gassen i offshore processering fremstår metoden med direkte injektion af flydende  $H_2S$ -scavenger som en bekvem implementering.  $H_2S$ -scavengere er kemikalier der reagerer med  $H_2S$  og omdanner det til substantiel mindre giftige og mindre korrosive forbindelser. I visse tilfælde bliver reaktionsprodukterne (såkaldt spent scavengers) udledt til havet grundet manglen på egnede alternativer. Den mest almindelige  $H_2S$ -scavenger brugt i industrien i dag er baseret på 1,3,5-hexahydrotriazines, med 1,3,5-tris(2-hydroxyethyl)-hexahydro-s-triazine (MEA-triazine) som den dominerende i olieindustrien. Ved behandlingen af naturgas bliver vandige opløsninger af MEA-triazine injiceret i gasstrømmen. Effektivitet af processen afhænger både af absorptionsraten af  $H_2S$  og kinetikken af den deraf følgende vandfasereaktion med  $H_2S$ -scavengeren. Uanset signifikansen og den udbredte brug af MEA-triazine, så er mekanismen for vandfasereaktionen ikke fuldt ud klarlagt og reaktionskinetikkerne ved betingelser interessante for industrien ikke tilgængelige. Dette er en af grundene til det empiriske design og ineffektiv operation af processen, forårsagende overdosering af scavengeren, som dermed leder til en unødvendig forøgelse af operationsomkostninger, og i visse tilfælde, udledning af den ikke-reagerede scavenger til havet, hvilket signifikant øger den miljømæssige påvirkning af offshore olie- og gasproduktion.

Denne Ph.d.-afhandling præsenterer et studie af kinetikken af reaktionen mellem MEA-triazine og bisulfid ( $HS^-$ ), hvilket er den fremherskende form af  $H_2S$  i vandig fase ved de pH-betingelser der er af interesse inden for industriel anvendelse. Målingen af forsvindingsraten af  $HS^-$  i denne reaktion er særlig udfordrende, grundet det at reaktionen er meget hurtig under visse betingelser, hvilket gør prøvetagning og offline analyse problematisk. I denne afhandling, blev en metodik baseret på in-situ Raman spektroskopi og kemometri udviklet og anvendt til måling af faldet af  $HS^-$  koncentration over tid, ved forskellige pH-værdier (over 9), temperaturer (fra 25 til 75 °C), og startkoncentrationsforhold af scavenger til bisulfid (STB) i intervallet 0.5 til 10.0.

Målingerne tillod at kvantificere det kraftige fald af forbrugsraten for  $HS^-$  ved stigende pH, såvel som dens stigning ved øget temperatur og STB-forhold. Særligt, betingelser med overskud af scavenger, hvilket er det som forekommer i offshore

anvendelser, blev undersøgt. Resultaterne viste også muligheden for komplet udtømming af  $\text{HS}^-$ , givet at en tilstrækkelig koncentration af hydronium er til stede i opløsningen. I den henseende er resultaterne i overensstemmelse med tidligere udgivelser som bevisliggør betydningen af protoniseringen af MEA-triazine i scavenging-reaktionerne.

Reaktionen mellem  $\text{HS}^-$  og MEA-triazine var allerede rapporteret i litteraturen som foregående via to trin i serie, den første dannende thiadiazine og den anden bestående af endnu en reaktion af thiadiazine med  $\text{HS}^-$  som danner dithiazine. Ydermere, den tredje teoretiske erstatning af svovl ind i kvælstoffet af triazine-ringen, hvilket ville danne trithiane, er ikke observeret. På trods af denne viden, er eksistensen af thiadiazine som et langlivet og målbart reaktionsmellemed, såvel som årsagerne til den manglende reaktion af dithiazine til trithiane, stadigvæk debatteret i litteraturen. I denne afhandling var kernemagnetisk resonans, NMR, brugt til at identificere thiadiazine og til at vurdere opførelsen af protoniseringen af MEA-triazine og dithiazine. De eksperimentelle resultater bekræftede at thiadiazine fremkommer i scavenging-reaktionerne og viste at det er tilstrækkelig stabilt til at blive separeret og isoleret. NMR-observationer tillod afgrænsning af pH intervallet for protoniseringen af MEA-triazine og viste manglen på protonisering af dithiazine ved interessebetingelserne, hvilket muligvis er grunden til fraværet af den teoretiske tredje scavenging-reaktion som kunne lede til trithiane.

Ydermere, en ny kinetisk model for  $\text{H}_2\text{S}$  scavenging-reaktionerne med MEA-triazine i vandig fase var bygget på viden opnået fra NMR-observationerne og in-situ Raman spektroskopi-målingerne. Modellen inkluderer protoniseringslignevægten af MEA-triazine, dens irreversible reaktion med  $\text{HS}^-$  for at danne thiadiazine (første scavenging-reaktion), protoniseringslignevægten af thiadiazine og den yderligere irreversible reaktion med  $\text{HS}^-$  for at danne dithiazine (anden scavenging-reaktion), det sidste anset som et ikke-protoniserende slut produkt. De to scavenging-reaktioner var antagne som værende førsteordens i forhold til både den protoniserede scavenger og  $\text{HS}^-$ . Protoniseringslignevægten af monoethanolamine, frigjort i scavenging-reaktionerne, var også inkluderet i modellen. Modellen blev tilpasset til det eksperimentelle data for scavenging-reaktionerne erhvervet i dette arbejde, ved temperaturer på 25 °C, 50 °C og 75 °C, oprindelig pH 9 og STB-værdier i intervallet 0.5 til 5.0. De optimale værdier for modellens regressionsparametre blev bestemt via en brute-force optimeringsmetode. Modellen leverer en tilfredsstillende repræsentation af forsvindingsraten af  $\text{HS}^-$ , med en gennemsnitlig relativ afvigelse mellem eksperimentelle og beregnede værdier på mellem 2 til 7%, før forsuring. Ratekonstanterne for den første og anden scavenging-reaktion ved 25 °C blev fundet til at være 0.435 og 0.0004  $\text{L mol}^{-1} \text{s}^{-1}$ , henholdsvis. Aktiveringsenergiene for den første og anden scavenging-reaktion blev estimeret til at være 68 og 57  $\text{kJ mol}^{-1}$ , henholdsvis.

# PREFACE

This thesis is submitted to the Doctoral School of Engineering and Science in partial fulfillment of the requirements for the degree of Doctor of Philosophy at the Department of Chemistry and Bioscience, Aalborg University, Denmark. The PhD project was carried out under the main supervision of Associate Professor Marco Maschietti and co-supervision of Associate Professor Sergey Kucheryavskiy, from August 2019 to July 2023, at the Section of Chemical Engineering at Aalborg University in Esbjerg, Denmark.

The research conducted for this thesis forms part of the EUDP – Energy Technology Development and Demonstration Programme – project Scavenger Optimization (SCAVOP) led by Associate Professor Marco Maschietti. This work aims at providing a deeper insight into the process of reducing  $H_2S$  concentration in gas streams by injection of liquid chemicals –  $H_2S$  scavengers – a process widely used in the offshore oil and gas industry, yet insufficiently understood. Despite the novel interest and focus on alternative energies, optimization of the current processes is necessary to achieve a neat and smooth energy transition, which is why I decided to embark on this challenge.

The fulfilment of this work would not have been possible without the collaboration of people who, either directly or indirectly, helped me during this journey. My sincere appreciation to my supervisors, Marco and Sergey, who constantly guided the work and were always available to give me feedback and suggestions for improvement. To Reinhard Wimmer, who received me at his lab at Aalborg and conducted the NMR experiments that ultimately revealed the hidden truth of this complex system. To Anders Andreasen, for his feedback and collaboration throughout the project. To Fernando Montero, for all the support, valuable discussions, ideas, and insights into the subject throughout the entirety of this project that helped shaping the outcome. To my colleagues at the Section of Chemical Engineering at Aalborg University, for giving a helping hand whenever it was needed. To Jacob Gram Iskov Eriksen for his help with the Danish resume.

Iveth Romero

Aalborg University, August 2023



# THESIS DETAILS

Thesis title: Kinetics of the scavenging reactions of hydrogen sulfide with MEA-triazine

PhD student: Iveth Alexandra Romero Logroño

Supervisors: Marco Maschietti  
Sergey Kucheryavskiy

The main body of this PhD thesis consists of the following articles:

- [A] Iveth Romero, Sergey Kucheryavskiy and Marco Maschietti. Experimental study of the aqueous phase reaction of hydrogen sulfide with MEA-triazine using in situ Raman spectroscopy. *Ind. Eng. Chem. Res.* 2021, 60, 15549-15557. <https://doi.org/10.1021/acs.iecr.1c03833>
- [B] Iveth Romero, Fernando Montero, Sergey Kucheryavskiy, Reinhard Wimmer, Anders Andreasen and Marco Maschietti. Temperature- and pH-dependent kinetics of the aqueous phase hydrogen sulfide scavenging reactions with MEA-triazine. *Ind. Eng. Chem. Res.* 2023, 62, 8569-8580. <https://doi.org/10.1021/acs.iecr.3c00668>

In addition to the main papers, the following contributions were made during the PhD:

Journal articles:

- [C] Anders Andreasen, Iveth Romero, and Marco Maschietti. Validation of an Equilibrium-Stage Model of the Coldfinger Water Exhauster for Enhanced Glycol Regeneration in Natural Gas Dehydration. *Ind. Eng. Chem. Res.* 2020, 59, 44, 19668–19679. <https://doi.org/10.1021/acs.iecr.0c03292>

Conference Contributions:

- [D] Iveth Romero, Sergey Kucheryavskiy and Marco Maschietti. Online monitoring of H<sub>2</sub>S scavenging reactions in aqueous phase using Raman spectroscopy. Oral presentation at the 17<sup>th</sup> Scandinavian Symposium on Chemometrics (SSC17), Aalborg, Denmark, 2021.

- [E] Fernando Montero, Iveth Romero, Sergey Kucheryavskiy, and Marco Maschietti. Online Raman monitoring of H<sub>2</sub>S scavenging reactions using green chemicals. Poster presented at Danish Hydrocarbon Research and Technology Center Technology Conference 2021, Kolding, Denmark.

This thesis has been submitted for assessment in partial fulfillment of the PhD degree. The thesis is based on the published scientific papers, which are listed above. Parts of the papers are used directly or indirectly in the extended summary of the thesis. As part of the assessment, co-author statements have been made available to the assessment committee and are also available at the Faculty of Engineering and Science in Aalborg University.

# TABLE OF CONTENTS

<b>Part I. Extended Summary .....</b>	<b>1</b>
<b>Chapter 1. Introduction.....</b>	<b>3</b>
1.1. Thesis Objectives .....	6
1.2. Thesis Outline .....	7
<b>Chapter 2. Handling of H<sub>2</sub>S in oil and gas facilities .....</b>	<b>9</b>
2.1. Properties of hydrogen sulfide .....	10
2.2. Methods for removal of H <sub>2</sub> S from gas streams .....	11
2.3. Triazine-based H <sub>2</sub> S scavengers .....	14
2.4. H <sub>2</sub> S scavenging process in offshore oil and gas platforms.....	16
2.5. Aqueous-phase H <sub>2</sub> S scavenging reactions with MEA-triazine .....	18
<b>Chapter 3. Analytical methods.....</b>	<b>21</b>
3.1. Raman Spectroscopy.....	21
3.1.1. Quantitative Raman Spectroscopy .....	23
3.1.2. Multivariate Data Analysis.....	26
3.2. Nuclear Magnetic Resonance Spectroscopy .....	29
<b>Chapter 4. Methodology .....</b>	<b>31</b>
4.1. Scavenging Reactions Experiments .....	31
4.1.1. Materials.....	31
4.1.2. Room-Temperature Measurements .....	31
4.1.3. High-Temperature Measurements .....	33
4.2. Method for quantitation of HS <sup>-</sup> in aqueous solutions using Raman Spectroscopy .....	36
4.3. NMR Experiments .....	38
4.3.1. Materials.....	38
4.3.2. Synthesis, purification, and identification of thiadiazine .....	38
4.3.3. pH titration of MEA-triazine and dithiazine .....	39
<b>Chapter 5. Results and Disussion .....</b>	<b>41</b>
5.1. Investigation of the H <sub>2</sub> S Scavenging Reactions with MEA-Triazine in Aqueous Phase .....	41

5.1.1. Parameters influencing the scavenging reactions.....	41
5.1.2. Identification of key species using Raman spectroscopy .....	44
5.1.3. Reaction mechanism between HS <sup>-</sup> and MEA-triazine.....	46
5.2. Development of a Kinetic Model for the Aqueous-Phase H <sub>2</sub> S Scavenging Reactions.....	54
5.2.1. Regression of the Kinetic Model Parameters .....	58
5.3. Discussion of Results .....	62
<b>Chapter 6. Conclusions.....</b>	<b>67</b>
<b>Literature list.....</b>	<b>69</b>
<b>Part II. Publications .....</b>	<b>77</b>



# TABLE OF FIGURES

Figure 1-1. Conventional offshore topside process in the North Sea. Adapted from Bothamley [6].	4
Figure 2-1. Electronic structure of H <sub>2</sub> S.	10
Figure 2-2. pH-dependent distribution of sulfide species in aqueous solutions [31]. Licensed under CC BY 4.0.	11
Figure 2-3. General process flow diagram of gas sweetening with solvent regeneration.	12
Figure 2-4. Formation reaction of MEA-triazine.	14
Figure 2-5. Electronic structure of 1,3,5-tris(2-hydroxyethyl)-hexahydro-s-triazine.	15
Figure 2-6. Point of liquid scavenger injection in gas streams in an offshore oil and gas production platform.	16
Figure 2-7. Hydrogen sulfide scavenging process involving absorption and chemical reaction.	17
Figure 2-8. Reaction mechanism between MEA-triazine and bisulfide in aqueous phase. Paper A. Reprinted with permission from Ind. Eng. Chem. Res. 2021, 60, 43, 15549–15557. Copyright 2023 American Chemical Society.	18
Figure 3-1. Different energy levels and molecular response to incident beams.	22
Figure 3-2. Raman spectra data handling process.	24
Figure 3-3. a) Ideal spectrum. b) Spectrum with baseline variation and noise. Adapted from Zhao et al. [63].	24
Figure 3-4: (A) Raw Raman spectrum. (B) Preprocessed spectrum with ALS baseline correction.	25
Figure 3-5. Formation of an NMR signal [72].	29
Figure 4-1. Setup for acquisition of Raman spectra at room temperature.	32
Figure 4-2. Photo of the experimental setup used for measurements of aqueous-phase scavenging reactions at high temperatures (up to 75 °C). Paper B. Reprinted with permission from Ind. Eng. Chem. Res. 2023, 62, 21, 8269–8280. Copyright 2023 American Chemical Society.	34
Figure 4-3. Scheme of the experimental setup. Paper B. Reprinted with permission from Ind. Eng. Chem. Res. 2023, 62, 21, 8269–8280. Copyright 2023 American Chemical Society.	34
Figure 4-4. Left: Preprocessed and truncated spectra used for the calibration of the PLSR model at room temperature. Right: Predicted vs. measured values of the PLSR model. RMSE expressed in mM. Paper A. Reprinted with permission from Ind. Eng. Chem. Res. 2021, 60, 43, 15549–15557. Copyright 2023 American Chemical Society.	37
Figure 5-1. Influence of scavenger-to-bisulfide concentration ratio on the conversion of HS <sup>-</sup> at pH <sub>0</sub> = 9. The color bar represents the STB ratio: blue: 0.5, green: 1.0, yellow: 5.0, red: 10.0. Paper A. Reprinted with permission from Ind. Eng. Chem. Res. 2021, 60, 43, 15549–15557. Copyright 2023 American Chemical Society.	42

- Figure 5-2. Influence of scavenger-to-bisulfide concentration ratio on the conversion of  $\text{HS}^-$  at  $\text{pH}_0 = 10$ . The color bar represents the STB ratio: blue: 0.5, green: 1.0, yellow: 5.0, red: 10.0. Paper A. Reprinted with permission from Ind. Eng. Chem. Res. 2021, 60, 43, 15549–15557. Copyright 2023 American Chemical Society. .... 42
- Figure 5-3. Influence of scavenger-to-bisulfide concentration ratio on the conversion of  $\text{HS}^-$  at  $\text{pH}_0 = 11$ . The color bar represents the STB ratio: blue: 0.5, green: 1.0, yellow: 5.0, red: 10.0. Paper A. Reprinted with permission from Ind. Eng. Chem. Res. 2021, 60, 43, 15549–15557. Copyright 2023 American Chemical Society. .... 43
- Figure 5-4. Raman spectra of the reaction between  $\text{HS}^-$  and MEA-triazine at room temperature, initial pH 9 and STB concentration ratio 0.5. The color legend shows the reaction times in hours. Selected Raman peaks are shown with gray dashed lines. Adapted from Paper A. Reprinted with permission from Ind. Eng. Chem. Res. 2021, 60, 43, 15549–15557. Copyright 2023 American Chemical Society. .... 45
- Figure 5-5.  $^1\text{H}$ -NMR spectra of solutions of MEA-triazine at pH values between 6.0 and 12.0 at  $25^\circ\text{C}$ . Paper B. Reprinted with permission from Ind. Eng. Chem. Res. 2023, 62, 21, 8269–8280. Copyright 2023 American Chemical Society. .... 47
- Figure 5-6.  $^1\text{H}$ -NMR spectra of solutions of dithiazine at pH values between 3.0 and 12.0 at  $25^\circ\text{C}$ . Paper B. Reprinted with permission from Ind. Eng. Chem. Res. 2023, 62, 21, 8269–8280. Copyright 2023 American Chemical Society. .... 48
- Figure 5-7. NMR of thiadiazine in  $\text{D}_2\text{O}$ ,  $\text{pH}^*=10.0$ , at 298.1 K, with assignment of resonances to atoms. Both MEA-triazine and dithiazine were present as impurities, their signals are labelled accordingly. The residual water signal is labelled HDO. A)  $^1\text{H}$ -NMR spectrum (600 MHz); B) quantitative  $^{13}\text{C}$ -NMR spectrum (150.9 MHz); C) [ $^1\text{H}, ^{13}\text{C}$ ]-HSQC spectrum. Paper B. Reprinted with permission from Ind. Eng. Chem. Res. 2023, 62, 21, 8269–8280. Copyright 2023 American Chemical Society. .... 50
- Figure 5-8.  $^1\text{H}$ -NMR spectra (600 MHz) of A) Thiadiazine, B) MEA-triazine, C) Dithiazine and D) Ethanolamine. Thiadiazine is obtained from in-house synthesis, while the other samples are obtained commercially. All spectra were recorded at pH 10,  $T=298.1\text{ K}$ , and they were all referenced to internal TSP- $\text{d}_4$ . Paper B. Reprinted with permission from Ind. Eng. Chem. Res. 2023, 62, 21, 8269–8280. Copyright 2023 American Chemical Society. .... 51
- Figure 5-9.  $^1\text{H}$ -NMR spectra (600 MHz) of thiadiazine at different temperatures. All spectra are referenced to internal TSP- $\text{d}_4$ . Paper B. Reprinted with permission from Ind. Eng. Chem. Res. 2023, 62, 21, 8269–8280. Copyright 2023 American Chemical Society. .... 52
- Figure 5-10. Reaction mechanism for the scavenging of bisulfide with MEA-triazine in aqueous phase supported by experimental observations. Paper B. Reprinted with permission from Ind. Eng. Chem. Res. 2023, 62, 21, 8269–8280. Copyright 2023 American Chemical Society. .... 53
- Figure 5-11. Experimental (colored dots) and calculated (continuous lines) concentrations of  $\text{HS}^-$  at  $25^\circ\text{C}$  (Plot A),  $50^\circ\text{C}$  (Plot B) and  $75^\circ\text{C}$  (Plot C) at different initial MEA-triazine concentrations: blue 46 mM, green 91 mM, and red 456 mM. System reacidification represented with the dashed vertical line. Duplicate experiments are shown with filled and empty markers. Adapted from Paper B.

Reprinted with permission from Ind. Eng. Chem. Res. 2023, 62, 21, 8269–8280.  
Copyright 2023 American Chemical Society..... 63  
Figure 5-12. Calculated concentrations of thiadiazine and dithiazine for the reactions  
run at 25°C (Row A), 50°C (Row B), and 75°C (Row C) at different initial MEA-  
triazine concentrations: blue 46 mM, green 91 mM, and red 456 mM. System  
reacidification represented with the dashed vertical line. Adapted from Paper B.  
Reprinted with permission from Ind. Eng. Chem. Res. 2023, 62, 21, 8269–8280.  
Copyright 2023 American Chemical Society..... 65



# **PART I. EXTENDED SUMMARY**



# CHAPTER 1. INTRODUCTION

Ever since the production of the first oil field in 1859, the oil and gas industry has played a key role in the global market, for instance the energy sector [1]. By 2019, the world total energy supply (TES) was still dominated by fossil fuels (crude, natural gas, and oil products) with a 54.1% contribution [2]. In Denmark, the contribution of fossil fuels, particularly oil and natural gas, was 53% by 2021 [3]. Even though many countries are establishing plans for reducing the consumption of fossil fuels, with such a high contribution in play, it is still relevant to study ways of optimizing the current procedures for oil and gas production employed in the industry, with the aim of diminishing its impact to the environment.

Oil and natural gas are two of the marketable products obtained from the treatment of the well fluid extracted from the reservoir (field). The well fluid is a multiphase stream (gas, oil, and water) consisting of a complex mixture of hydrocarbons ranging from methane ( $\text{CH}_4$ ) up to paraffin and aromatic hydrocarbons with more than 30 carbon atoms. Natural gas is composed mostly of light alkanes with one to four carbons, i.e., methane - butane, but it also contains non-hydrocarbon components as nitrogen, carbon dioxide ( $\text{CO}_2$ ) and hydrogen sulfide ( $\text{H}_2\text{S}$ ) [4]. Oil is constituted mainly by liquid hydrocarbons with four or more carbon atoms.

The first step in the treatment of the reservoir fluid consists in the separation of the phases constituting it, i.e., oil, gas, and water. Such separation is attained in process equipment at treatment facilities that can be whether onshore (on land) or offshore (on a platform). The main function of the treatment facilities is to stabilize the produced fluids for their export or disposal. The process equipment used for offshore and onshore treatment is alike; rather, physical limitations like weight and vertical clearance between decks in offshore platforms impose the type of equipment to use in the process, for instance, horizontal separators instead of vertical ones [5].

The conventional offshore topside process for treatment of oil and gas in the North Sea is presented in Figure 1-1 [6].

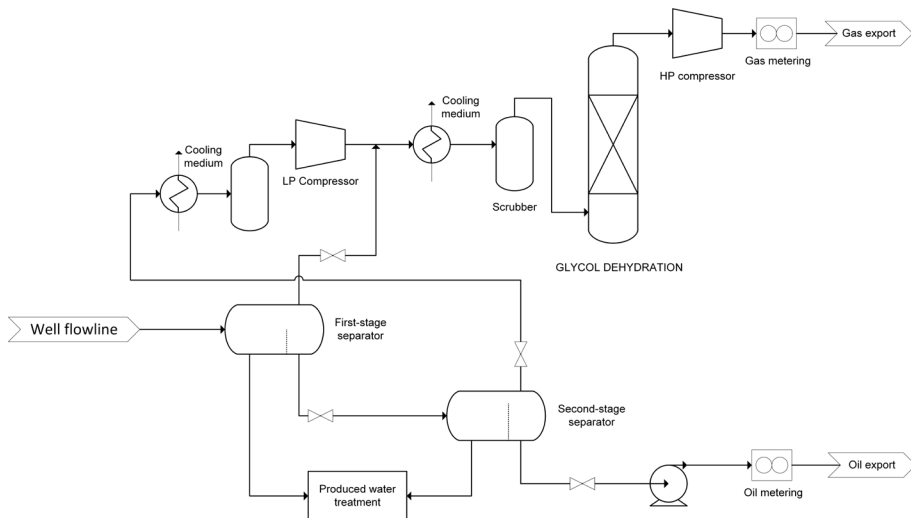


Figure 1-1. Conventional offshore topside process in the North Sea. Adapted from Bothamley [6].

The gas stream coming from the separation train is conditioned to proper water and sour gases content ( $\text{CO}_2$ , and  $\text{H}_2\text{S}$ ) prior to its export to onshore terminals. Typically, the concentration of sour gases in exported natural gas should be below 50 ppmv for  $\text{CO}_2$  and below 4 ppmv for  $\text{H}_2\text{S}$  [7, 8] due to their corrosiveness properties, environmental impact and to the serious health threat posed by  $\text{H}_2\text{S}$ . Hydrogen sulfide scavengers are one kind of production chemicals that are used to reduce the concentration of  $\text{H}_2\text{S}$  in multiphase streams – either at wellbore or before entering the separation process – and in export gas streams [9, 10, 11]. The scavengers react with the  $\text{H}_2\text{S}$  present in the streams, converting it into by far less harmful compounds [10, 12].  $\text{H}_2\text{S}$  scavengers are amongst the most used chemicals during treatment of produced hydrocarbons; in fact, in some installations in the offshore oil and gas sector in the North Sea, the scavengers account for more than 50% of the operational expenditures (OPEX) allotted to production chemicals [13].

Regarding the removal of  $\text{H}_2\text{S}$  in the gas phase in offshore facilities, the most common  $\text{H}_2\text{S}$  scavengers used for this purpose are liquid solutions of triazines that are injected directly into the gas stream, downstream the compression system and upstream the dehydration unit. More specifically, 1,3,5-tris(2-hydroxyethyl)-hexahydro-s-triazine, or simply MEA-triazine, is the most widely used triazine for  $\text{H}_2\text{S}$  scavenging in the oil and gas sector [14]. The removal of  $\text{H}_2\text{S}$  occurs through complex gas-liquid reactions that involve the absorption of hydrogen sulfide from the gas stream into the liquid droplets of the scavenger, where ultimately aqueous-phase reactions between  $\text{H}_2\text{S}$  and the scavenger take place.



The operating conditions of the H<sub>2</sub>S scavenging process are established empirically mainly due to an insufficient knowledge of the absorption-reaction process. Furthermore, the lack of kinetic expressions of the aqueous-phase reactions between H<sub>2</sub>S and MEA-triazine is one of the reasons for the absence of mathematical models that allow to predict the outcome of the injection of scavengers. These aspects together could be the reason of a poorly efficient scavenging process, i.e., overdosing the chemical for reaching the desired H<sub>2</sub>S concentration outcome [15, 16]. For instance, the currently estimated H<sub>2</sub>S scavenger consumption is around 12-20 kg of scavenger (50 wt.% triazine) to remove 1 kg of H<sub>2</sub>S [10], while the stoichiometric requirement to remove the same amount of H<sub>2</sub>S would be ca. 6 kg of MEA-triazine scavenger, meaning that there is a potential excess of approximately 6-12 kg of scavenger. As consequence of such excess, there are large amounts of unreacted MEA-triazine in the aqueous phase – also containing the reaction products – that flow along the process to be finally separated from the gas as effluent. Owing to the characteristic alkaline pH of the effluent and its significant fouling and scaling potential, its reinjection into the wells is often prevented; thus, its discharge into the sea without further treatment is the common procedure, despite the environmental hazard posed by the toxic nature of MEA-triazine [17].

Considering that MEA-triazine scavengers account for over 80% of the worldwide oilfield market [18], a better understanding of the aqueous-phase H<sub>2</sub>S-scavenger reactions are imperative for reaching an optimized scavenging process.

## 1.1. THESIS OBJECTIVES

The research question that this PhD thesis aims at answering is the following:

“Can the kinetic parameters of the aqueous-phase reactions between H<sub>2</sub>S and MEA-triazine be measured under relevant industrial conditions?”

To answer this question, the following specific tasks were performed:

- Development of a suitable experimental setup and procedure for analysis of the scavenging reactions in aqueous phase at room temperature. The experimental setup is detailed in Paper A.
- Definition of a proper analytical method for in-situ monitoring of the concentration of hydrogen sulfide in the aqueous-phase scavenging reactions with MEA-triazine. The analytical methodology developed for this purpose is described in Paper A.
- Analysis of the effect of pH and scavenger concentration on the rate of consumption of hydrogen sulfide in the aqueous-phase scavenging reactions. The results are detailed in Paper A.
- Development of a procedure for acquisition of kinetics data at temperatures over ambient. The methodology for high-temperature experiments is detailed in Paper B.
- Confirmation of the reaction mechanism of the scavenging reactions with MEA-triazine in aqueous phase. The identification of thiadiazine as intermediate product of the reaction and the protonation behavior of MEA-triazine and dithiazine, which confirm the reaction mechanism, are presented in Paper B.
- Development and validation of a kinetic model that accounts for the confirmed reaction mechanism and the protonated forms of MEA-triazine and thiadiazine as actual reactants with bisulfide. The developed model and the kinetic parameters obtained with the model are available in Paper B.

## 1.2. THESIS OUTLINE

This thesis consists of two parts. Part I comprises an extended summary of the main experimental procedures and findings of the PhD work. It also sets the background of the research objective, presents a detailed discussion and description on the main findings of the research, and proposes perspectives for future work within the frame of triazine-based hydrogen sulfide scavengers. Part II presents the scientific publications which represent the outcome of the PhD.

Part I is outlined in 6 chapters:

**Chapter 1** presents an introduction of the oil and gas sector with emphasis in offshore topside processes where triazine-based scavengers are used. It also presents the thesis objectives.

**Chapter 2** focuses on the main characteristics of the two key players of the scavenging reactions: hydrogen sulfide and triazine-based H<sub>2</sub>S scavengers.

**Chapter 3** is a description of the method used for the quantitation of hydrogen sulfide in aqueous solutions by the application of in-situ Raman spectroscopy and chemometrics.

**Chapter 4** presents the materials and the methodology, including the setup, used for the execution of the various experiments of the PhD work. It is divided in two parts pertaining the scavenging reaction experiments and the NMR experiments.

The analysis of the main findings and the outcome of the research are covered in **Chapter 5**, which is divided in two sections. The first section describes the qualitative analysis of the scavenging reactions performed at ambient temperature, which results in the definition of the main parameters influencing the scavenging reactions (pH and scavenger to bisulfide concentration). The second section describes the quantitative investigation of the reactions and presents the kinetic model and the kinetic parameters describing the scavenging reactions in aqueous phase.

Finally, **Chapter 6** compiles the main conclusions of the research work and lays out possibilities for future work.



## CHAPTER 2. HANDLING OF H<sub>2</sub>S IN OIL AND GAS FACILITIES

Hydrogen sulfide (H<sub>2</sub>S) is a component naturally present in oil and gas reservoirs as result of three mechanisms, viz., aquathermolysis, microbial sulfate reduction (MSR), and thermal sulfate reduction (TSR) [19]. Yet, the natural presence of H<sub>2</sub>S can also be induced by processes used to enhance the production of declining reservoirs [19], like steam-assisted oil recovery, where an extreme increase of H<sub>2</sub>S concentrations has been observed in oil fields treated with this method [20], and sea water injection, implemented in mature oil fields in the North Sea for decades, which are currently facing an increased production of H<sub>2</sub>S [21]. The sulfur content in hydrocarbons varies with time and depends on the geological environment, as shown in Table 2-1. In the North Sea, several reservoirs contain natural H<sub>2</sub>S in concentrations above 20,000 ppm [22], representing a serious threat to operators' health, to equipment integrity, and an environmental hazard.

Equipment integrity is severely affected by the presence of hydrogen sulfide in wet streams. It is estimated that 40% of the corrosion issues presented in this industry is attributed to sour corrosion, mainly by H<sub>2</sub>S [23]. In water, H<sub>2</sub>S acts as a weak acid due to its partial dissociation in sulfide species (see Section 2.1), which reportedly exert a significant influence in the corrosion process of steel, specifically through the electrochemical dissolution of iron:  $Fe \rightarrow Fe^{2+} + 2e^{-}$ , and the contribution of sulfide species to cathodic currents [24]. These interactions lead in the long term to undesirable effects, for instance, pitting corrosion in steel.

*Table 2-1. Sulfur content of crude oil depending on the location. Adapted from [12].*

<b>Crude oil name</b>	<b>Location</b>	<b>Sulfur content (wt. %)</b>
Bu Attifel	Libya	0.10
Ekofisk North Sea	Norway	0.18
Arabian light Saudi	Saudi Arabia	1.80
Cyrus	Iran	3.48
Boscan	Venezuela	5.40

## 2.1. PROPERTIES OF HYDROGEN SULFIDE

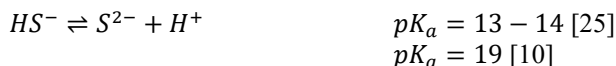
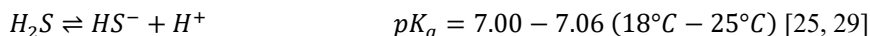
Hydrogen sulfide (CAS No. 7783-06-4), also known as monosulfane, is an inorganic compound present in natural sources such as minerals, ore-bearing deposits, salt and coal mines, flooded grounds, water, and hydrocarbon reserves [25]. H<sub>2</sub>S has a molecular weight of 34.08 g/mol, critical temperature of 100.25°C, and boiling point of -60.28°C at 101.3 kPa [25]; thus, at atmospheric conditions of temperature and pressure, H<sub>2</sub>S is a vapor. It is colorless and heavier than air, with a characteristic *rotten-egg* odor that is only appreciable for the human olfaction at low concentrations of H<sub>2</sub>S in air (5 to 50 ppm [26]). At higher concentrations (50 to 100 ppm), it causes olfactory fatigue and thus inability to detect the distinguishable smell [25]. Exposure to very high concentrations (1,000 to 2,000 ppm) is fatal, causing respiratory failure within seconds, after one or two inspirations [26]. Due to its acute toxic effects, the concentration level of H<sub>2</sub>S in export gas streams in Denmark is limited to 5 mg/Nm<sup>3</sup> [27], equivalent to 3.3 ppmv.

The chemical bonding of hydrogen sulfide is shown in Figure 2-1. H<sub>2</sub>S is a Brønsted-Lowry acid with two hydrogen atoms forming a covalent bond with the sulfur atom.



Figure 2-1. Electronic structure of H<sub>2</sub>S.

In water, hydrogen sulfide is a weak acid that reacts with a base *B* by a proton-transfer reaction that gives as product the bisulfide ion [28]. The reaction has reportedly two dissociation constants:



The existence of the chemical species  $S^{2-}$  is debated in the literature. As shown above, there is a lack of consensus in the value of the second dissociation constant. In fact, some authors [30] claim that  $S^{2-}$  cannot be observed in aqueous solutions even at the most favorable conditions, i.e., highly basic solutions of NaOH (aq.)  $\cong 23 \text{ mol L}^{-1}$ .

Figure 2-2 shows the distribution of the sulfide species as function of pH in aqueous solutions. It is observed that at, when using MEA-triazine, the typical pH values of the aqueous phase in contact with the gas is in the range 9 to 11 (see Section 2.4). In

these conditions, the bisulfide ion is by far the predominant species in relation to the distribution profile shown in Figure 2-2 [31].

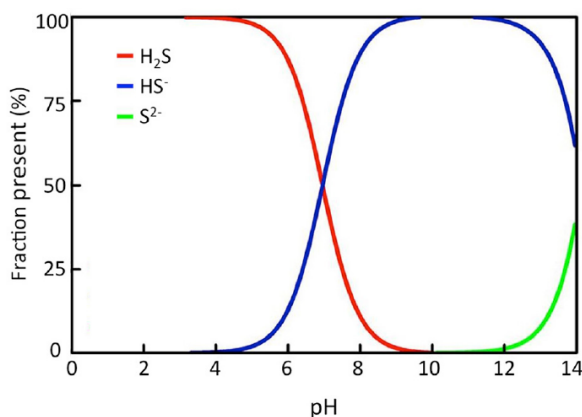


Figure 2-2. pH-dependent distribution of sulfide species in aqueous solutions [31]. Licensed under CC BY 4.0.

The solubility of H<sub>2</sub>S in water is strongly dependent on the pH of the aqueous phase, having a higher dissolution of H<sub>2</sub>S at high pH of the aqueous media. For instance, at pH 10, the dissolution is 12-fold larger than at pH 5 [32].

## 2.2. METHODS FOR REMOVAL OF H<sub>2</sub>S FROM GAS STREAMS

There are two methods for the removal of H<sub>2</sub>S from gas streams applied in the oil and gas industry: regenerative and non-regenerative, which in turn are based on physical absorption, chemical absorption, or physicochemical absorption [4].

### REGENERATIVE METHODS

In large production facilities, regenerative methods such as gas sweetening, or gas scrubbing, can be used for removing sour gases from the gas streams [10]. In these processes, either physical or chemical absorption is applied, which in turn depends on the level of selective removal of H<sub>2</sub>S or CO<sub>2</sub> required.

Figure 2-3 shows the general process used in regenerative methods. The process is generally divided into two sections, the absorption section, and the regeneration section. The process consists in contacting the sour gas with a solvent flowing in countercurrent configuration in a scrubber, absorber or contacting tower in the

absorption section, where the solvent absorbs (physically or chemically) the sour components of the gas. The sour gas enters the scrubber through the bottom section and leaves through the head of the scrubber as sweet gas, whereas the solvent enters the scrubber from the top and leaves from the bottom as a sour-component-rich solvent, from where it is directed to the regeneration section.

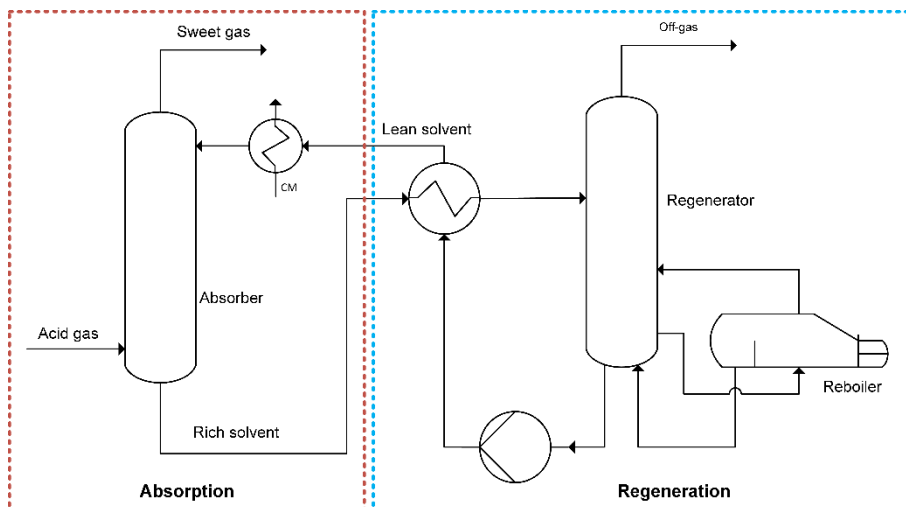


Figure 2-3. General process flow diagram of gas sweetening with solvent regeneration.

Physical absorption is the only method capable of selectively removing sulfur compounds in natural gas streams with high content of sour gases [4]. The solvent is regenerated under strongly reduced pressure instead of heat. Then, the absorbed component is released and reinjected into the reservoir for sequestration, or lack thereof, directed to a sulfur recovery unit (SRU) [33]. One of the solvents used for physical absorption of  $H_2S$  is N-methylpyrrolidone (NMP) [4].

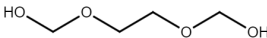
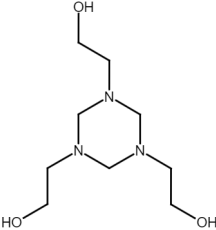
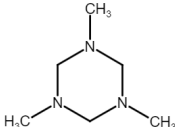
On the other hand, chemical absorption is not selective towards  $H_2S$ , and rather absorbs it together with  $CO_2$ . The most common chemical solvents used for this purpose are alkanolamines, namely, monoethanolamine (MEA), diethanolamine (DEA), diisopropylamine (DIPA), triethanolamine (TEA), 2-amino-2-methyl-1-propanol (AMP) and N-methyldiethanolamine (MDEA). These solvents are also called *sequestrants*, which basically trap  $H_2S$  forming a temporary ammonium salt (hydrosulfide or bicarbonate), that will then release the sequestered  $H_2S$  during the regeneration step [34]. MEA and DEA react with  $H_2S$  and  $CO_2$ , whereas AMP and MDEA tend to react with  $H_2S$  over  $CO_2$  but are mostly less reactive [35]; nonetheless, selective removal of  $H_2S$  is not possible with alkanolamines [4]. Alkanolamines react reversibly with  $H_2S$ , and its regeneration is done by either pH reduction or heating.



## NON-REGENERATIVE METHODS

Non-regenerative methods refer to the chemicals that react irreversibly with H<sub>2</sub>S, transforming it into significantly less-toxic substances [10]. One type of such chemicals are the products of the reaction between alcohols and aldehydes, named hemiacetals; if the aldehyde is specifically formaldehyde the product will be an hemiformal, also called formaldehyde releasers. The most common hemiformal used for H<sub>2</sub>S scavenging is ethylene(dioxy)dimethanol, or EDDM [36]. The other type of chemicals are the products of the reaction between aldehydes and amines, called triazines. The most common triazine used for H<sub>2</sub>S scavenging is the product of ethanolamine and formaldehyde, called MEA-triazine, followed by the product of the reaction between methylamine and formaldehyde, called MMA-triazine [37]. Triazines, more specifically MEA-triazine, is the most used H<sub>2</sub>S scavenger to date, attributed to its low cost and the rapid transformation of H<sub>2</sub>S into sulfides [37]. Both, hemiformals and triazines, undergo an irreversible reaction with H<sub>2</sub>S forming new carbon-sulfur bonds [34, 37]. The structure of the most common scavengers is shown in Table 2-2.

Table 2-2. Structure of the most common non-regenerative hydrogen sulfide scavengers.

EDDM	MEA-triazine	MMA-triazine
		

Liquid scavengers are one type of chemicals used for removing H<sub>2</sub>S from gas streams by direct injection. This is the method commonly used in offshore applications due to the minimal intervention to the facilities required for its operation, without the installation of additional units, due to space and weight limitations in offshore production platforms.

## 2.3. TRIAZINE-BASED H<sub>2</sub>S SCAVENGERS

Triazine-based H<sub>2</sub>S scavengers mostly used in offshore oil and gas topside operations are solutions of 1,3,5-hexahydrotriazines, often simply called triazines, with 1,3,5-tris(2-hydroxyethyl)-hexahydro-s-triazine (MEA-triazine) being largely predominant with at least 80% of the oilfield market [18].

Triazines are heterocyclic compounds consisting of three carbons and three nitrogen atoms disposed in alternated manner forming a symmetrical structure. Triazines are obtained from the reaction between a primary amine and an aldehyde. If the primary amine is monoethanolamine and the aldehyde an aqueous solution of formaldehyde, the resulting triazine will be 1,3,5-tris(2-hydroxyethyl)-hexahydro-s-triazine, as shown in Figure 2-4.

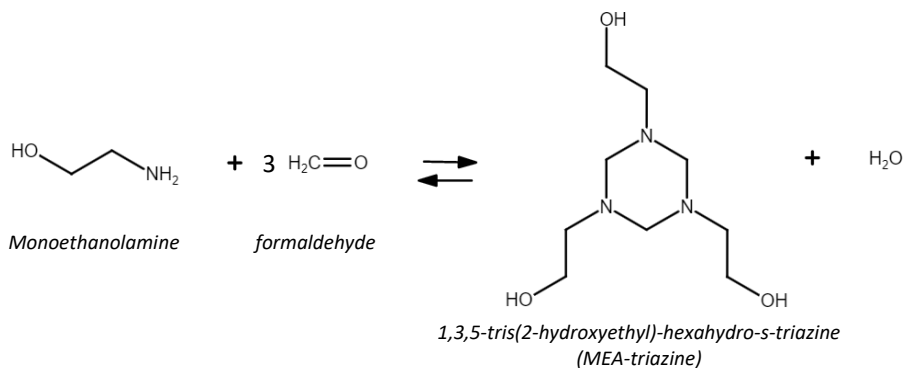


Figure 2-4. Formation reaction of MEA-triazine.

The side group attached to the nitrogen atoms in triazine can be selected to modify the properties of the triazines, such as solubility [38]. Figure 2-5 shows the chemical structure of MEA-triazine, where it is observed that three 2-hydroxyethyl radicals are attached to the ring nitrogen atoms, hence its name. In addition, the presence of the hydroxyl groups on the side chains of the nitrogen atoms increases the hydrophilic properties of the molecule [38]. The nitrogen atoms present in MEA-triazine are Brønsted-Lowry bases due to their lone pair. In fact, the selective action of MEA-triazine towards H<sub>2</sub>S is attributed to the tertiary nitrogen atoms, which act as hydrogen bond acceptors only.

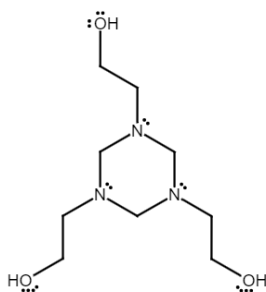


Figure 2-5. Electronic structure of 1,3,5-tris(2-hydroxyethyl)-hexahydro-s-triazine.

The main physical-chemical data of MEA-triazine is summarized in Table 2-3.

Table 2-3. Physical-chemical properties of 1,3,5-tris(2-hydroxyethyl)-hexahydro-s-triazine.

Property	Value
CAS number	4719-04-4
Molecular weight	219.28
Boiling point	80 °C, at 16.67 Pa [39]
Density	1.1787 g/cm <sup>3</sup> at 20 °C [39]
Solubility	Water, ≥10 mg/mL at 24°C [40]

Commercial aqueous solutions of MEA-triazine (ca. 50 wt.%) generally have a pH around 10.5-11.0.

MEA-triazine is highly susceptible to hydrolysis in aqueous solutions at pH values ≤ 8 [41]. Its rate of hydrolysis depends greatly on pH, presenting a negligible rate at pH values indicatively above 9 [41].

Triazine-based scavengers are not listed within the OSPAR list of substances/preparations used and discharged offshore which are considered to pose little or no risk to the environment (PLONOR) [42]; however, the discharge of the unspent scavenger together with the products of the scavenging reaction is reportedly accepted [17]. Moreover, according to the European Chemicals Agency (ECHA), the scavenging reaction product, monoethanolamine (MEA), is “harmful to aquatic life with long lasting effects” [43]. Besides its widespread use as hydrogen sulfide

scavenger in gas streams, MEA-triazine is also used as biocide to control bacterial contamination in well stimulation fluids [44].

## 2.4. H<sub>2</sub>S SCAVENGING PROCESS IN OFFSHORE OIL AND GAS PLATFORMS

As aforementioned, hydrogen sulfide scavengers are injected directly into the gas stream, downstream the compressor discharge. A zoom in to the typical process with the injection point is depicted in Figure 2-6.

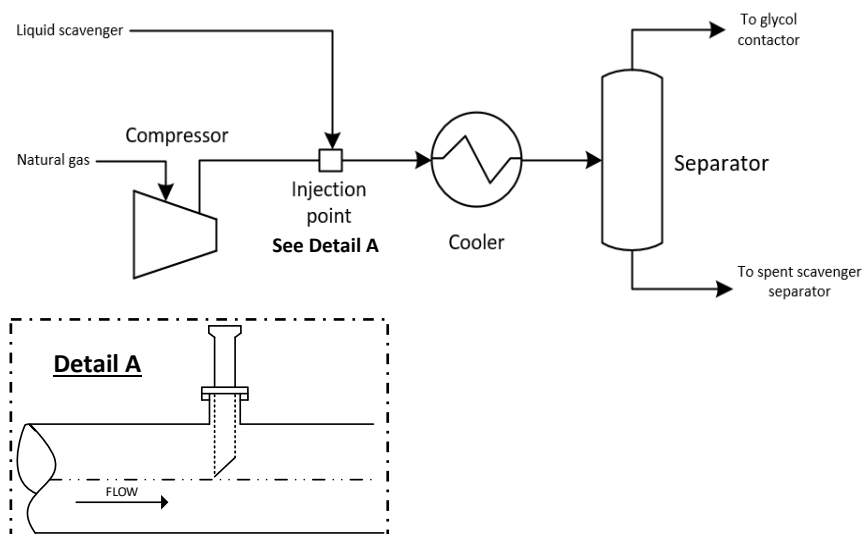


Figure 2-6. Point of liquid scavenger injection in gas streams in an offshore oil and gas production platform.

The injection point usually consists of a quill inserted in the pipeline through which the liquid scavenger is dispersed into the flow stream. The angle of insertion of the quill as its orientation are reportedly determining parameters in the efficiency of the scavenger injection process [45].

Based on the injection point of the scavenger shown in Figure 2-6, the H<sub>2</sub>S scavenging process of gas streams by injection of liquid scavengers in offshore oil and gas platforms takes place in a broad temperature range, from ambient up to 160°C. Furthermore, considering the typical pH values of commercial aqueous solutions of MEA-triazine (~10.5 – 11.0) and the reported pH values of spent scavenger streams

being around 8.9 – 9.4 [15, 17, 46], it is fair to conclude that the pH of the aqueous phase dispersed in the gas stream is in the range 9.0 – 11.0.

The scavenging of hydrogen sulfide in a hydrocarbon gas stream takes place in a multiple-step continuous process involving absorption and chemical reaction. Figure 2-7 depicts the steps of the process: i) diffusion of the gaseous hydrogen sulfide through the bulk gas-phase to the surface of the liquid droplets of scavenger; ii) absorption of H<sub>2</sub>S (g) into the liquid scavenger, and iii) reaction between H<sub>2</sub>S and the scavenger inside the liquid droplets, i.e., the aqueous phase.

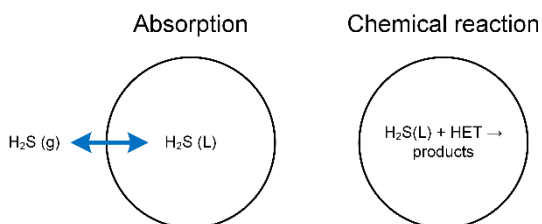


Figure 2-7. Hydrogen sulfide scavenging process involving absorption and chemical reaction.

The parameters influencing the absorption of H<sub>2</sub>S gas in the liquid scavenger are known to be the pH and the concentration of the scavenger solution, the temperature of the gas stream and the scavenger, the surface area for mass transfer available for the absorption to occur, viz., the surface of the liquid droplets of the injected scavenger, and the pressure of the gas-liquid system, which has a direct effect on the absorption process [47]. Considering the H<sub>2</sub>S pH-dependent solubility mentioned in Section 2.1, and the pH of commercial aqueous solutions of MEA-triazine, the H<sub>2</sub>S absorbed in the liquid droplets of scavenger is present as bisulfide (HS<sup>-</sup>), which reacts with MEA-triazine in the aqueous phase through the mechanism further explained in Section 2.5.

The aqueous-phase reaction between hydrogen sulfide and MEA-triazine is scarcely addressed to in existing open literature and a full understanding of it is essential for reaching an optimization of the scavenging process and reduce the amount of unreacted scavenger in effluents and exported streams.

## 2.5. AQUEOUS-PHASE H<sub>2</sub>S SCAVENGING REACTIONS WITH MEA-TRIAZINE

The generally accepted mechanism for the hydrogen sulfide scavenging reaction with MEA-triazine in aqueous phase involves a multiple reaction pathway, shown in Figure 2-8.

The first step involves the protonation of MEA-triazine. The protonated form of MEA-triazine is thus the actual reactant in the scavenging reaction [38]. Although MEA-triazine has three Lewis-base nitrogen atoms, the first step involves the protonation of one nitrogen atom only [48]. The protonated MEA-triazine then reacts with HS<sup>-</sup> through a nucleophilic substitution S<sub>N</sub>2 reaction [48, 49], where the ring structure opens, neutral monoethanolamine is released from the structure, and the nitrogen atom is substituted by a sulfur atom, producing a molecule of 3,5-di-(2-hydroxyethyl)-hexahydro-1,3,5-thiadiazine, hereafter thiadiazine or TDZ [38, 49]. In the next step, the thiadiazine molecule also undergoes protonation of one nitrogen atom to then react with HS<sup>-</sup> in a S<sub>N</sub>2 reaction, obtaining in this step another molecule of monoethanolamine and one molecule of 5-(2-hydroxyethyl)-hexahydro-1,3,5-dithiazine, hereafter dithiazine or DTZ.

The final step would involve the protonation of dithiazine for reaction with bisulfide and the substitution of a third sulfur atom into the ring, obtaining 1,3,5-trithiane; however, the latter has reportedly not been observed, leading to consider dithiazine as the final product of the scavenging reaction [34, 38, 41, 48-53]. In fact, Bakke et al. [41] observed that the reaction of thiadiazine with bisulfide was slower than the reaction of MEA-triazine with bisulfide, while dithiazine did not react with HS<sup>-</sup> in a pH range of 10 to 2. Yet, to the author's knowledge, there is a lack of experimental evidence in the literature explaining the reasons for the absence of trithiane. Paper B provides such evidence, contributing to the state of the art of the aqueous-phase hydrogen sulfide scavenging reactions with MEA-triazine.

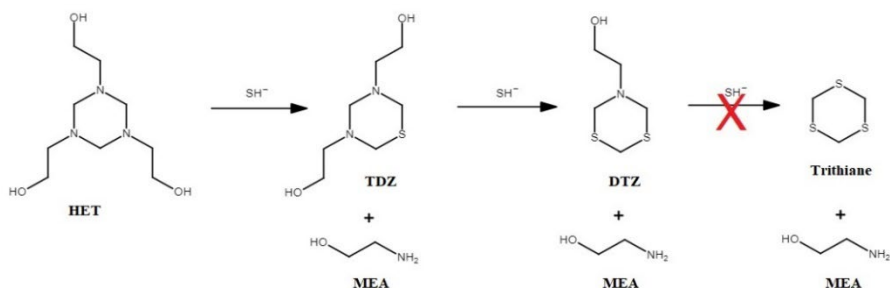


Figure 2-8. Reaction mechanism between MEA-triazine and bisulfide in aqueous phase. Paper A. Reprinted with permission from *Ind. Eng. Chem. Res.* 2021, 60, 43, 15549–15557. Copyright 2023 American Chemical Society.

To date, the only rate equation reported in the literature for the aqueous-phase reaction between bisulfide and MEA-triazine is the one expressed in Equation 2-1 and proposed by Bakke and Buhaug [38]:

$$(-r_{HET}) = k'[HET] \quad \text{Eq. 2-1}$$

where  $(-r_{HET})$  is the rate of disappearance of moles of MEA-triazine per unit volume,  $k'$  is a *pseudo* rate constant, and the squared brackets represent molar concentrations.

Such expression assumes a constant concentration of hydronium ions and a constant concentration of bisulfide by reason of the claimed constant pH during the scavenging experiments for the former and the presence of excess HS<sup>-</sup> for the latter. In addition, the rate law of Equation 2-1 can be reached by considering solely the first scavenging reaction. Thus, the *pseudo* rate constant  $k'$  incorporates the actual rate constant of the first scavenging reaction ( $k$ ), the protonation equilibrium constant of MEA-triazine ( $K_a$ ), the concentration of hydronium ( $[H_3O^+]$ ), and the concentration of bisulfide ( $[HS^-]$ ), as shown in Eq. 2-2:

$$k' = \frac{k}{K_a} [H_3O^+][HS^-] \quad \text{Eq. 2-2}$$

As stated in Chapter 1, MEA-triazine is typically used in excess in oil and gas topside processes. Furthermore, the H<sub>2</sub>S that is absorbed from the gas phase into the liquid droplets of scavenger reacts fast with MEA-triazine; thus, the only rate equation reported in the literature does not refer to the conditions occurring in the installations, which are characterized by excess of scavenger rather than excess of sulfide.

Another characteristic of the aqueous-phase scavenging reactions of bisulfide with MEA-triazine is the fast consumption of bisulfide. Other authors [38] have reported failed attempts in monitoring the concentration of bisulfide in aqueous-phase scavenging reactions experiments via sulfide sensitive-electrodes. This PhD work presents a methodology for monitoring in situ the concentration of bisulfide in aqueous-phase scavenging reactions with MEA-triazine, which is detailed in Chapter 4.

A debated aspect in the literature is the identification of the intermediate component, thiadiazine. Different analytical techniques have been used for this purpose, reaching to contrasting outcomes. For instance, Bakke et al. [41] reported the detection of thiadiazine through <sup>1</sup>H and <sup>13</sup>C NMR spectroscopy and was identified as a product of the aqueous phase reaction of MEA-triazine and HS<sup>-</sup> when starting with an equimolar concentration of reactants at room temperature. Madsen and Sogaard [49] also reported the identification of thiadiazine through electrospray ionization mass

spectrometry (ESI-MS) as the main product of the gas-liquid reaction between H<sub>2</sub>S and MEA-triazine at room temperature in a 2:1 initial concentration ratio. Finally, Perez Pineiro et al. [54], reported the identification of thiadiazine using Raman spectroscopy in spent scavenger samples resulting from the gas-liquid reaction of aqueous solutions of MEA-triazine with gaseous H<sub>2</sub>S at room temperature. In all cases the results refer to laboratory reaction experiments. On the other hand, Taylor and Matherly [50] and Wylde et al. [34] reported the absence of thiadiazine in partially spent scavenger samples and attributed such absence to a higher reactivity of thiadiazine, compared to MEA-triazine, with H<sub>2</sub>S, contrarily to the findings of Bakke et al. [41]. Considering the unclear perspectives towards thiadiazine, this aspect is investigated in Paper B.



## CHAPTER 3. ANALYTICAL METHODS

### 3.1. RAMAN SPECTROSCOPY

Raman spectroscopy is a branch of vibrational spectroscopy that uses inelastic scattered light to measure the vibrational energy modes (or types) of a sample [55]. In Raman spectroscopy, the sample is irradiated with a beam in the UV-visible or near infrared (NIR) region and the light is scattered in a direction perpendicular to the incident beam [55, 56]. Essentially, matter interacts with electromagnetic radiation in two ways: 1) absorption, where the incident photons disappear (absorbed) in a certain degree after contact with matter and 2) scattering, where the photons change their direction after contact with matter [57]. In both cases, the intensity of the transmitted or reflected radiation decreases in an exponential function with the thickness of the material being analyzed.

There are two types of scattering effects: Rayleigh scattering (or elastic scattering), when the scattered photons have the same energy (and hence frequency) as the incident ones, and Raman scattering (or inelastic scattering), when the scattered photons have a frequency higher or smaller than the frequency of the incident photons ( $\nu_0$ ) by the vibrational frequency of the molecule ( $\nu_m$ ). When the frequency of Raman scattering is higher than the frequency of the incident beam, i.e.,  $\nu_0 + \nu_m$ , it is called anti-Stokes Raman scattering. On the contrary, if the frequency of Raman scattering is smaller than the frequency of the incident beam, i.e.,  $\nu_0 - \nu_m$ , it is called Stokes Raman scattering [56]. In general, Rayleigh scattering exists predominantly over Raman scattering; however, when Raman scattering occurs, Stokes Raman scatter is more intense than anti-Stokes Raman scatter and the former is measured in Raman spectroscopy [55]. Moreover, the overall intensity of the inelastic scattered radiation depends (among other factors) on the number of molecules present in a sample which makes Raman spectroscopy an efficient tool for quantitative analyses.

Figure 3-1 shows an energy level diagram with the different types of molecule response to incident beams. When a molecule is excited by an incident photon (black arrow), the molecule reaches an instantaneous virtual energy state until the photon is emitted. If the energy of the emitted photon is higher than the energy of the incident photon, it gives rise to anti-Stokes Raman scattering (red arrow); else, it results in Stokes Raman scattering (cyan arrow). If the energy of the incident and emitted photon is the same, then it is obtained Rayleigh scattering (black arrow). After Raman scattering, the sample reaches a different vibrational state.

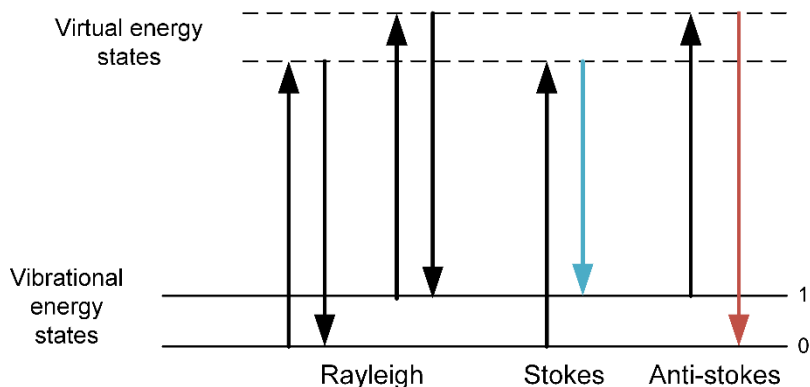


Figure 3-1. Different energy levels and molecular response to incident beams.

### RAMAN-ACTIVE MOLECULES

When a laser beam irradiates a molecule, the electric field creates a separation of the charges of the molecule with the positively charged part attracted toward the negative pole and the electrons attracted toward the positive pole. Such separation of charges produces an induced dipole moment ( $\mu$ ) which is directly proportional to the strength of the electric field ( $E$ ). The proportionality constant ( $\alpha$ ) is known as polarizability [56]:

$$\mu = \alpha E$$

Raman spectroscopy detects vibrations in the molecules only when their polarizability changes during the molecule movement. In consequence, a vibration is called Raman-active if the rate of change of the polarizability with the vibration is different from zero. For instance, the symmetric stretching vibration of a molecule - the movement of atoms in opposite directions as the bonds shrink or stretch with respect to the central atom - increases the size of its electron cloud, making it Raman active [58].

### RAMAN EXCITATION WAVELENGTHS

One of the main interferences for performing analytical measurements using Raman spectroscopy is the potential auto fluorescence of the material, which can easily obscure the Raman signal. Another limitation is the Raman signal per se since it is weak in comparison to elastic scattering [59]. In this way, to perform measurements with Raman spectroscopy it is important to select an appropriate laser wavelength, depending on the properties of the material and the purpose of the analysis. There are four common laser excitation wavelengths commercially available: 532, 638, 785 and 1064 nm, with 785 nm being the most common selection since it offers good spectral

coverage and resolution and at the same time gives smaller autofluorescence effect compared to excitation sources with smaller wavelength [59].

### 3.1.1. QUANTITATIVE RAMAN SPECTROSCOPY

The basis for quantitative analysis using Raman spectroscopy is the proportional relationship existing between the intensity of the Raman scattered radiation,  $I_R$ , and the number of scattering molecules in a state  $\nu$  ( $N$ ), as shown in the following expression [59]:

$$I_R \propto I_0 N \nu^4 \left( \frac{\partial \alpha}{\partial Q} \right)^2$$

Where  $I_0$  is the incident laser intensity,  $\nu$  is the frequency of the excitation light,  $\alpha$  is the polarizability of the molecules,  $Q$  their vibrational amplitude, and  $(\partial \alpha / \partial Q)$  is the Raman cross section, which measures the likelihood of a molecule to undergo Raman scattering when it is illuminated with a specific frequency of light [59].

$I_R$  represents the intensity integrated over the width of a Raman band [60], and is proportional to the concentration of the analyte in the sample.

A single Raman spectrum contains substantial information about a sample, for instance, the Raman band(s) that can be used for determining the amount of analyte in a sample, called signal; however, the same Raman spectrum also contains unwanted information (noise) which, if not removed, will significantly affect the results of the quantitative analysis. Noise in a Raman spectrum comes from different sources like the instrument, digitization of the detector data into the “raw” spectrum presented to the operator, the sample itself due to changes in temperature or fluorescence, and external interferences not related with the instrument nor the sample, like interference of external light in the optical path of the instrument [60].

The noise in a Raman spectrum can be separated from the signal by applying preprocessing methods. In general, preprocessing refers to any set of algorithms used to reduce or eliminate unwanted variations (artifacts) in a spectrum before applying a mathematical model for quantitation purposes [60, 61]. Figure 3-2 represents a typical process for Raman spectral analysis.

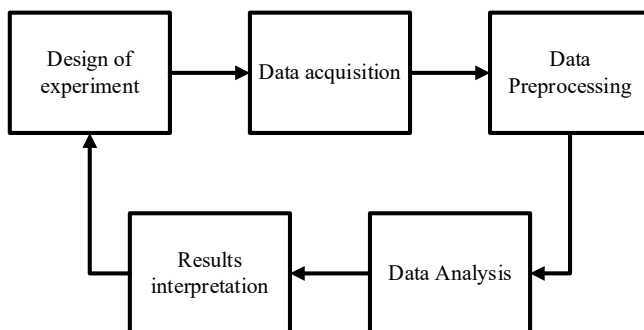


Figure 3-2. Raman spectra data handling process.

Other artifacts, i.e., unwanted variations in Raman spectra, are baseline variations that arise from changes to the background due to fluorescence of impurities in the sample or luminescence, and changes in spectral intensity due to heterogeneity in the sample and instrumental effects [62].

Figure 3-3 depicts the common artifacts encountered in Raman spectra.

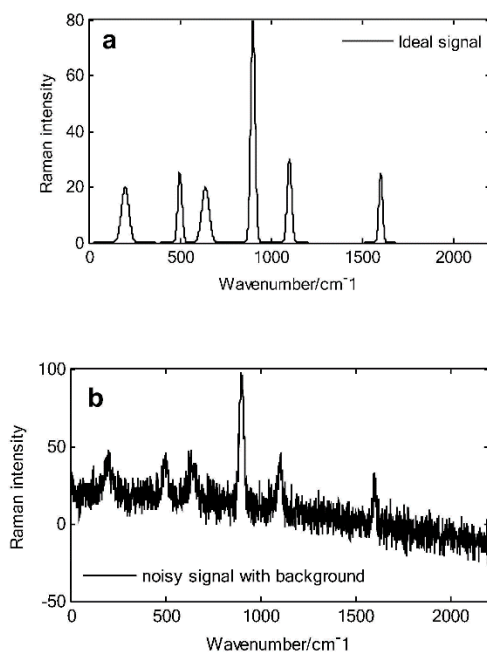


Figure 3-3. a) Ideal spectrum. b) Spectrum with baseline variation and noise. Adapted from Zhao et al. [63].

The spectral regions useful for quantitative analysis can be identified by acquiring the Raman spectra of a set of samples with different analyte concentration, where the spectral regions relevant for predicting analyte concentration must vary with analyte concentration [60].

## PREPROCESSING

A feasible quantitative Raman analysis is typically obtained with two basic preprocessing steps: baseline correction and normalization, the latter used to remove global intensity effects from position of probe, variation of laser power among others [64].

A description of the most used techniques from the two steps follows.

### ASYMMETRIC LEAST SQUARES (ALS)

ALS is used for correction of baseline problems (shifts, drifts, and curvatures), which consists in setting the baseline at zero intensity. Figure 3-4 shows the difference in a spectral plot after baseline correction with ALS technique.

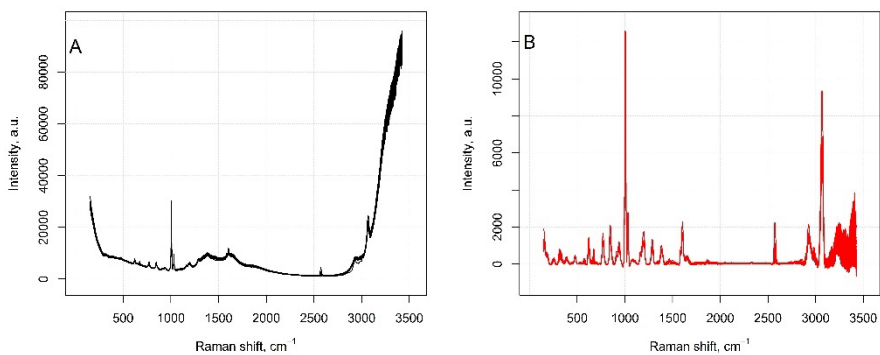


Figure 3-4: (A) Raw Raman spectrum. (B) Preprocessed spectrum with ALS baseline correction.

The main objective of ALS is to find a function that fits the curve that represents the original spectrum but penalize it if subsequent points have a low fitting. The principle of ALS is to divide the spectral points into several intervals, fit a low order polynomial through the first interval, keep the fitted value in the middle of the interval and shift

one interval to the right to repeat the procedure until all smoothed variables of the intervals are defined. The challenge of any baseline correction technique is reaching a balance between fidelity to the data ( $S$ ) and roughness of the smoothed function ( $R$ ), the latter expressed as the sum of the squared differences between the values of the smoothed function ( $z_i$ ). The lack of fit between the smoothed function and the original data ( $y_i$ ) can be expressed as the sum of the squared differences [65]. Thus, the balance ( $Q$ ) between fidelity to the data (lack of fit) and roughness can be expressed as:

$$Q = S + \lambda R$$

where,  $\lambda$  is an arbitrary number that will alter the effect of  $R$  on  $Q$ , and consequently affect the degree of fit to the data [65].  $\lambda$  is also called *penalty*.

In addition,

$$S = \sum_i (y_i - z_i)^2$$

$$R = \sum_i (\Delta z_i)^2$$

The objective of ALS is to find  $z$  such that  $Q$  is minimized, obtaining the corrected baseline.

## NORMALIZATION

Normalization is another preprocessing technique whose objective is to remove the influence from intensity variation or changes in the focusing of the instrument laser [66]. It consists in dividing the intensity of the spectrum by the length, area, or the Euclidean norm of a specific region of the spectra [66], which can be the whole spectrum or the Raman band of an internal standard, the latter by definition being an intensity value that remains constant among all the samples [66, 67].

### 3.1.2. MULTIVARIATE DATA ANALYSIS

Multivariate data analysis (MDA) is the set of mathematical methods used to analyze presumably wide datasets — where number of objects (individual measurements) is smaller than the number of variables (measured characteristics of the objects) [68]. Many MDA methods utilize dimensionality reduction by projecting data points into a smaller number of latent variables, oriented in the original variable space according to pre-defined criteria.

One of the most widely used methods is Principal Component Analysis (PCA). PCA finds latent variables which are oriented along directions of biggest variation of the

data points and are mutually orthogonal. It often makes possible to reduce the original data dimension without significant loss of information [60].

The latent variables (in terms of PCA: *principal components*, *PCs*) are linear combinations of the variables constituting the original data. Each principal component is oriented to minimize the orthogonal distance between the data points and the PC. Every PC explains a part of data points variation, which can be computed by projecting the data points to the PC and estimating variance of the projected points. Principal components are arranged as function of the variance; for instance, the first principal component has the largest explained variance, the second principal component has the next largest, and so on [69].

Considering a dataset as a matrix  $\mathbf{X}$ , where rows correspond to the objects and columns to the measured characteristics (e.g., wavelength), then PCA can be considered as matrix decomposition [67]:

$$\mathbf{X} = \mathbf{TP}^T + \mathbf{E}$$

where,

- matrix  $\mathbf{T}$  represents the *scores* and has the same number of rows as the original data matrix ( $\mathbf{X}$ ),
- matrix  $\mathbf{P}$  represents the *loadings* and has the same number of columns as the original data matrix ( $\mathbf{X}$ ),
- matrix  $\mathbf{E}$  represents the *residuals* and has the same dimension as the original data matrix ( $\mathbf{X}$ ).

The number of columns in the matrix  $\mathbf{T}$  equals the number of rows in the matrix  $\mathbf{P}$  (both corresponds to the number of principal components); thus, the decomposition of  $\mathbf{X}$  considers the transpose of matrix  $\mathbf{P}$  ( $\mathbf{P}^T$ ) [69].

*Loadings* are the unit vectors defining the orientation of the principal components in original variable space; thus, the matrix  $\mathbf{P}$  is a matrix of unit vectors. *Scores*, on the other hand, are the coordinates of the projections of the original data onto the principal components. Each score gives information on the extent that a particular data point contributes to that specific principal component. Thus, if a data point has a high score on the first principal component, it means that it aligns strongly with the main pattern captured by that component [67, 69].

### PARTIAL LEAST SQUARES REGRESSION (PLSR)

PLSR is a linear regression method based on similar principles as PCA. PLSR is used to predict or explain the relationship between a set of independent variables (matrix of predictors,  $\mathbf{X}$ ) and a set of dependent variables (matrix of responses,  $\mathbf{Y}$ ). Each of

those matrices is decomposed into scores, loadings, and residuals by using *latent variables*, the latter equivalent to the principal components of PCA. However, in contrast to PCA, the latent variables in PLSR are selected to maximize the covariance between **X**- and **Y**-scores, i.e., the latent variables will capture the part of **X** that is related to **Y** and the part of **Y** that is related to **X**. Since PLSR is a linear model, the response value is a linear combination of predictors, with the main outcome being a vector with regression coefficients [67].

In simplest cases, matrix **Y** contains only one column (one response variable, e.g., concentration) and can be considered as a column vector **y**.

### CROSS VALIDATION

Validation is used to estimate the performance of a model for predicting response values of new data points. It can be also used for model optimization, e.g., for selecting an optimal number of latent variables in the model. Usually, validation requires a new set of samples comprising the same population as the data used to train the model. However, in many cases, it can be replaced by cross-validation — a technique based on resampling.

The most common cross validation method is called *leave one out (LOO)* in which one sample is removed from the data at the time to evaluate the performance of the model in predicting the response value of the excluded sample [69]. This method is specifically useful when the amount of data available is relatively small. In case of larger datasets several samples are removed simultaneously using random or systematic selection.

The metrics used to assess the cross-validation results are root mean squared error for cross validation (RMSECV), used for evaluating the validity of the developed model, and coefficient of determination,  $R^2$ , that indicates the relative variance of response values explained by the model [70].

The following equations show how to compute both statistics:

$$RMSECV = \sqrt{\frac{1}{n} \sum (y_i - y_{pi})^2}$$

$$R^2 = 1 - \frac{\sum (y_i - y_{pi})^2}{\sum (y_i - \bar{y})^2}$$

Here  $y_i$  is an  $i$ -th element of a vector with reference  $y$ -values (**y**),  $y_{pi}$  is an element of a vector with predicted values (**y<sub>p</sub>**), obtained by applying the model to the excluded



samples,  $\bar{y}$  is the mean of the reference  $y$ -values, and  $n$  is the total number of samples in the training set.

### 3.2. NUCLEAR MAGNETIC RESONANCE SPECTROSCOPY

In general terms, Nuclear Magnetic Resonance (NMR) spectroscopy is an analytical technique used to assess the chemical structure of materials based on the behavior of atomic nuclei, specifically their spin property and magnetic moment, in the presence of a strong magnetic field. When an external magnetic field is applied, the magnetic moment of atomic nuclei tends to align either parallel (alpha spin state) or antiparallel (beta spin state) to the magnetic field, giving rise to an energy difference between the two states. The two spin states have different energy, with the alpha spin state being at a lower energy than the beta spin state [71].

Depending on the energy of the magnetic field applied, the nuclei in the alpha spin state absorb energy and shift to the higher energy spin state, i.e., the nuclei are in resonance with the applied magnetic field. The energy at which such resonance occurs is related to a certain frequency, through Planck's constant, and falls within the radio wave region of the electromagnetic spectrum. When the nuclei return to their original spin state, the absorbed energy is released, detected by the NMR spectrometer, and presented as a signal on the NMR spectrum [72]. Figure 3-5 depicts the process of obtaining an NMR signal.

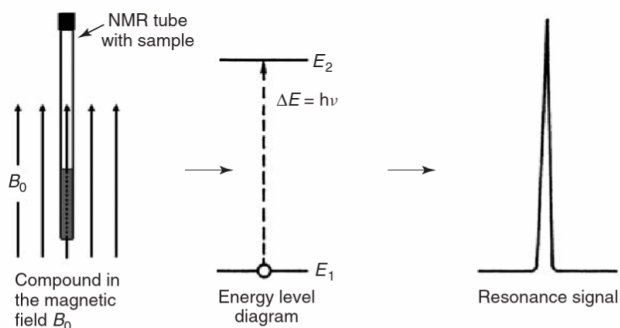


Figure 3-5. Formation of an NMR signal [72].

The atoms whose nuclei have non-zero magnetic moments can be subjected to NMR spectroscopy to generate spectra like the one shown in Figure 3-5; for instance,  $^1\text{H}$ ,  $^{19}\text{F}$ , nitrogen isotopes  $^{14}\text{N}$  and  $^{15}\text{N}$ , and  $^{13}\text{C}$ , which is the stable isotope of the carbon nucleus [72].

Proton nuclear magnetic resonance ( $^1\text{H-NMR}$ ) and carbon nuclear magnetic resonance ( $^{13}\text{C-NMR}$ ) are used to study the number and types of molecular connections in materials. Due to the natural abundance of the proton, and its higher gyromagnetic ratio with respect to  $^{13}\text{C}$ , out of the two methods,  $^1\text{H-NMR}$  has a higher spectral sensitivity, whereas  $^{13}\text{C-NMR}$  has a higher selectivity allowing a more detailed characterization [73].

#### HETERONUCLEAR TWO-DIMENSIONAL $^1\text{H},^{13}\text{C}$ CHEMICAL SHIFT CORRELATION

This technique allows the assignment of signals to individual positions in a chemical structure [72]. It is based on the correlation existing between resonance frequencies of scalar-coupled nuclei, which occurs between magnetic nuclei chemically bonded to each other [74], in this case  $^1\text{H}$  and  $^{13}\text{C}$ . As result, cross peaks with coordinates referring to the frequency of  $^1\text{H}$ ,  $\delta(^1\text{H})$ , and  $^{13}\text{C}$ ,  $\delta(^{13}\text{C})$ , are obtained, meaning that those nuclei are direct neighbors in the molecule [72].

Among the pulse sequences used for two-dimensional heteronuclear shift correlations is HSQC, heteronuclear single quantum correlation, which shows  $^{13}\text{C-}^1\text{H}$  direct relationships, i.e., it shows the specific carbon to which a specific hydrogen is attached. This technique is used to unequivocally identify molecules of similar structure [72].

## CHAPTER 4. METHODOLOGY

### 4.1. SCAVENGING REACTIONS EXPERIMENTS

Based on the fast consumption of bisulfide in aqueous-phase scavenging reactions, as detailed in Section 2.5, the development of a method for the in-situ monitoring of the reactions was imperative for acquiring relevant information on the aqueous-phase reactions. The fast response and non-invasive and non-destructive characteristics of Raman spectroscopy made it the optimal technique to use for acquisition of data of the scavenging reactions at conditions closer to the ones observed in field applications.

#### 4.1.1. MATERIALS

A commercial aqueous solution of 1,3,5-tris(2-hydroxyethyl)-hexahydro-s-triazine (MEA-triazine, HET), containing 30-60 wt.% of MEA-triazine, <2 wt.% of monoethanolamine and <1 wt.% of formaldehyde, was used as hydrogen sulfide scavenger in aqueous-phase reactions in Paper A and Paper B. Such solution will be hereinafter referred to as technical MEA-triazine. The pH of the technical MEA-triazine solution at room temperature was 10.6 and the density 1.11 g/mL.

Disodium sulfide about trihydrate ( $\text{Na}_2\text{S}\cdot 3\text{H}_2\text{O}$ ) was used as source of  $\text{H}_2\text{S}$  - present as bisulfide ( $\text{HS}^-$ ) in basic aqueous solutions. The water content of the salt was determined by Karl Fischer titration (KF) as described in Paper A.

High-purity standards of MEA-triazine, 5-(2-hydroxyethyl)-hexahydro-1,3,5-dithiazine (dithiazine, DTZ) and monoethanolamine (MEA) were used for identification of the respective Raman characteristic bands, as described in Paper A.

The scavenging reactions were studied via in-situ Raman spectroscopy using either acetonitrile (ACN) or phenylacetic acid (PAA) as the internal standard; the former for reactions at room temperature and the latter for reactions at higher temperatures i.e.,  $25^\circ\text{C} \leq T \leq 75^\circ\text{C}$ .

#### 4.1.2. ROOM-TEMPERATURE MEASUREMENTS

Aqueous-phase scavenging reactions were studied at room temperature ( $22^\circ\text{C}$ ) via in-situ Raman spectroscopy with the setup shown in Figure 4-1.

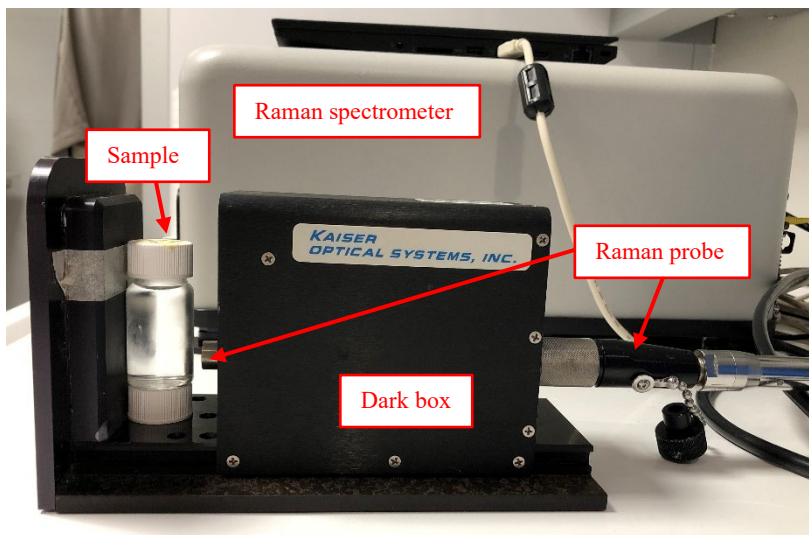


Figure 4-1. Setup for acquisition of Raman spectra at room temperature.

The setup consisted of a Raman spectrometer (Rxn1-785, Kaiser Optical Systems) equipped with a 785 nm laser as the source of excitation light with a non-contact probe, a dark box and a glass vial containing the reacting solution. The glass vial and the probe were located inside the dark box to avoid the interference of external light during acquisition of Raman spectra. The probe was placed laterally to the vial at approximately 1 cm distance.

Using the aforementioned setup, the study of the aqueous-phase scavenging reactions at room temperature encompassed the analysis of the influence of pH and scavenger-to-bisulfide (STB) molar concentration ratio on the rate of disappearance of bisulfide in a reacting phase volume of 20 mL. The STB ratio was varied in a way that the reactions would be run under stoichiometric ratio of reactants to excess of scavenger, i.e., STB from 0.5 to 10.0, following the expectations of the presence of excess MEA-triazine in field  $\text{H}_2\text{S}$  scavenger operations. Batch-reaction experiments were designed fitted to this purpose and are explained in detail in Paper A; therefore, a simplified description follows.

The experimental conditions of the scavenging reactions are summarized in Table 4-1.

*Table 4-1. Experimental conditions for batch-reaction experiments at room temperature.*

<b>Initial H<sub>2</sub>S concentration, mM</b>	<b>Initial Scavenger concentration, mM</b>	<b>STB ratio</b>	<b>Initial pH</b>
100	50	0.5	9
	100	1.0	10
	500	5.0	11
	1000	10.0	

All possible combinations of the experimental conditions detailed in Table 4-1 were investigated, with duplicates of each combination, which resulted in 24 experimental executions carried out in random order. Independent solutions of each reactant, i.e., H<sub>2</sub>S + ACN (the internal standard) and MEA-triazine, were prepared in water at the desired initial pH, which was adjusted by dropwise addition of concentrated hydrochloric acid (HCl, 6M). Then, both solutions were vigorously mixed and the glass vial containing the resulting solution was placed inside the dark box. The initial time of the reaction was set at the instant of mixture of both solutions. The reaction was monitored by taking a Raman spectrum every 30 seconds during a first period of 3 hours. At the end of the first period, the scavenging reaction was reactivated by lowering its pH as close as possible to its initial value through acid injection (HCl, 6M) and monitored for another 3 hours. For reactions with STB ratios of 0.5, two additional acid injections were performed after 4 and 5 hours of reaction yet keeping the total reaction/monitoring time to 6 hours. The concentration of HS<sup>-</sup> over time was then calculated from the Raman spectra of the monitored reactions through a partial least squares regression model (PLSR), as detailed in Section 4.2.

#### 4.1.3. HIGH-TEMPERATURE MEASUREMENTS

The aqueous-phase scavenging reactions were studied at temperatures in the range 25 to 75°C via in-situ Raman spectroscopy using a custom setup specifically designed for these experiments. The setup is shown in Figure 4-2 and Figure 4-3.



Figure 4-2. Photo of the experimental setup used for measurements of aqueous-phase scavenging reactions at high temperatures (up to 75 °C). Paper B. Reprinted with permission from *Ind. Eng. Chem. Res.* 2023, 62, 21, 8269–8280. Copyright 2023 American Chemical Society.

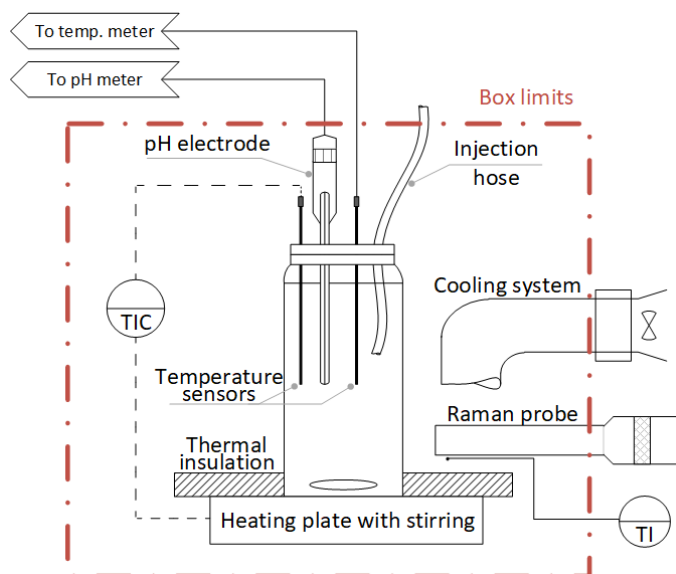


Figure 4-3. Scheme of the experimental setup. Paper B. Reprinted with permission from *Ind. Eng. Chem. Res.* 2023, 62, 21, 8269–8280. Copyright 2023 American Chemical Society.

The setup consists of a dark box enclosing a hot plate with magnetic stirrer, over which the reactor (45 mL glass vial) is placed. The reactor is provided with a magnetic stir bar for constant agitation and a lid with nozzles for insertion of a micro pH-electrode, a thermometer, and two hoses: one for injection of acid for pH adjustment and the other for injection of the scavenger to start the reaction. The Raman probe is located laterally to the vial at 11 mm distance. This setup grants the great advantage of heating and stirring the solution while monitoring in situ the concentration of bisulfide, pH, and temperature throughout the duration of the scavenging reaction. In addition, the temperature limitation of 30°C of the Raman probe was overcome with the cooling system placed directly over the probe, allowing the acquisition of high-quality spectra even at temperatures above its temperature limit.

The study focused on measuring the time-variation of the concentration of  $\text{HS}^-$  at pH, temperature, and STB ratio conditions that, while relevant to industrial applications, would also provide a better understanding of the behavior of scavenging reactions with MEA-triazine, built upon the knowledge gained from reactions at room temperature. The experimental conditions of the scavenging reactions are summarized in Table 4-2.

*Table 4-2. Experimental conditions for batch-reaction experiments at high temperature*

<b>Initial H<sub>2</sub>S concentration, mM</b>	<b>Initial scavenger concentration, mM</b>	<b>STB ratio</b>	<b>Initial pH</b>	<b>Temperature, °C</b>
100	46	0.46	9	25
	91	0.91		50
	456	4.56		75

All possible combinations of the experimental conditions of Table 4-2 were investigated, with duplicates of each combination, resulting in 18 experimental executions. All runs were carried out in random order. Independent solutions of each reactant, i.e.,  $\text{H}_2\text{S} + \text{PAA}$  (the internal standard) and MEA-triazine, were prepared in water at initial pH 9. Then, the vial containing 20 mL of the bisulfide was placed inside the dark camera, with all accessories in place, heating and stirring was started and the box closed. Once at the desired temperature, the Raman acquisition started and after 15 seconds of spectral acquisition, 10 mL of the scavenger solution was injected into the reactor through the dedicated hose, stating the initial time of the reaction. The total volume of the reacting phase was thus 30 mL. The reaction was monitored for a total of 3.5 hours, and the reaction was reactivated by lowering its pH as close as possible to its initial value with acid injection (HCl, 6M) after 3 hours of monitoring. Further details on the methodology are given in Paper B.

## 4.2. METHOD FOR QUANTITATION OF HS<sup>-</sup> IN AQUEOUS SOLUTIONS USING RAMAN SPECTROSCOPY

A partial least squares regression model (PLSR) was developed for each value of experimental temperature, viz., ambient (22 °C), 25, 50, and 75°C, for measuring the concentration of bisulfide in aqueous solutions. The models were calibrated using Raman spectra of aqueous solutions at pH 9 measured at each experimental temperature, containing bisulfide released from disodium sulfide about trihydrate (Na<sub>2</sub>S~3H<sub>2</sub>O) in concentrations ranging from 0 mM to 100 mM, in a step size of 10 mM, and an inert compound not taking part in the reactions as internal standard. For the room-temperature scavenging reaction experiments, the internal standard was acetonitrile (ACN, 100 mM), whereas phenylacetic acid (PAA, 200 mM) was used for the experiments at high temperature. Both components are suitable internal standards since they are Raman-active and have a stable response in the pH range of the scavenging reactions. The normal boiling point of acetonitrile (82 °C, at 1.013 bar) prevented its use as internal standard for high temperature experiments due to extensive evaporation. Two independent solutions for each HS<sup>-</sup> concentration level were prepared, i.e., 33 aqueous solutions for each experimental temperature, totaling 132 solutions for calibration of the PLSR models.

The preprocessing of the spectra for the calibration of the PLSR models was done in a two-step procedure, where first the baseline was corrected using the asymmetric least squares method with lambda of 10<sup>5</sup> and an asymmetry ratio of 0.025 (Paper A), and then the spectra were normalized to the sum of the intensities related to the wavenumbers for the area around the Raman peak of the internal standard, identified at 2261 cm<sup>-1</sup> for acetonitrile and at 1004 cm<sup>-1</sup> for phenylacetic acid. Then, the preprocessed spectra were truncated around the characteristic peak for bisulfide, identified at 2575 cm<sup>-1</sup>. Figure 4-4 shows the preprocessed and truncated spectra used for calibration of the PLSR model for experiments at room temperature.



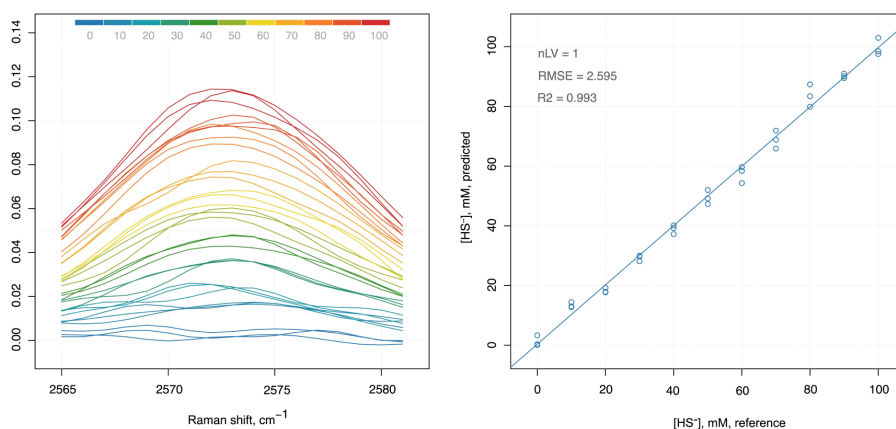


Figure 4-4. Left: Preprocessed and truncated spectra used for the calibration of the PLSR model at room temperature. Right: Predicted vs. measured values of the PLSR model. RMSE expressed in mM. Paper A. Reprinted with permission from *Ind. Eng. Chem. Res.* 2021, 60, 43, 15549–15557. Copyright 2023 American Chemical Society.

The preprocessing conditions were selected from the results of the cross-validation using PLSR models with one component. One PLSR model was calibrated for each value of temperature of the scavenging reaction experiments. The prediction performance of the four PLSR models for the quantitation of  $\text{HS}^-$  is shown in Table 4-3. The table shows the root mean squared error for the cross-validation, RMSECV, used for evaluating the validity of the developed model, and the coefficient of determination,  $R^2$ , that indicates the variance in the data explained by the model. It is observed that the four PLSR models developed for the quantitation of  $\text{HS}^-$  have a high  $R^2$  and a low RMSECV, which indicate the accuracy of the model for predicting new data.

Table 4-3. Prediction performance of the PLSR models used for quantitation of bisulfide in aqueous solutions at pH 9.

Temperature, °C	Internal Standard	$R^2$	RMSECV, mM
Ambient (22°C)	ACN	0.993	2.595
25	PAA	0.995	2.269
50	PAA	0.996	2.014
75	PAA	0.995	2.300

The final and calibrated PLSR models were then used for the in-situ measurement of the concentration of  $\text{HS}^-$  during the scavenging reactions. Neither the characteristic peak of bisulfide nor the peak of the internal standard overlap with the Raman peaks of the reaction components; thus, the final PLSR models can be used for predicting the concentration of bisulfide in the reacting mixtures of the scavenging reactions.

### 4.3. NMR EXPERIMENTS

#### 4.3.1. MATERIALS

The technical solution of MEA-triazine, described in Section 4.1.1, and the aqueous solutions of disodium sulfide about trihydrate were used as reactants for the in-house synthesis of thiadiazine.

In addition, high-purity MEA-triazine (purity  $\geq 95$  wt.%) and aqueous solutions of disodium sulfide about trihydrate were also used in experiments aimed at confirming the generation of thiadiazine in the scavenging reactions.

High purity dithiazine (purity  $> 98$  wt.%) and the technical solution of MEA-triazine were used to study the protonation behavior of these species via  $^1\text{H-NMR}$ .

Deuterium oxide was used as solvent of the thiadiazine-identification scavenging reactions, and deuterium oxide with 0.75 wt.% 3-(trimethylsilyl)-propionic-2,2,3,3-d<sub>4</sub> acid sodium salt ( $\text{D}_2\text{O}$  with TSP-d<sub>4</sub>) was used as reference for the identification of chemical shifts in NMR studies.

Water (LC-MS grade) supplemented with 0.05% diethylamine, and acetonitrile (LC-MS grade) supplemented with 0.05% diethylamine were used for LC-MS analyses related to the identification of thiadiazine via NMR.

#### 4.3.2. SYNTHESIS, PURIFICATION, AND IDENTIFICATION OF THIADIAZINE

In one experiment, 1.5 g of  $\text{Na}_2\text{S}\cdot 3\text{H}_2\text{O}$  was added to 5 mL of the technical MEA-triazine solution in water. To promote the production of thiadiazine, the pH of the solution was continuously reduced by dropwise addition of 37% HCl in water. (Paper B). The reacting solution was used for purification of thiadiazine via preparative high performance liquid chromatography (HPLC). Then, the fractions of purified thiadiazine were prepared for collection of NMR spectra.

In another experiment, an aqueous-phase reaction of high-purity MEA-triazine and  $\text{HS}^-$  in equimolar concentrations (50 mM each) at initial pH 8 was run at room temperature as basis of identification of TDZ via  $^1\text{H-NMR}$  and  $[^1\text{H},^{13}\text{C}]\text{-HSQC}$  recorded at 298.1 K. 23 mg of high-purity MEA-triazine was dissolved in 450  $\mu\text{L}$  of pure  $\text{D}_2\text{O}$  and 50  $\mu\text{L}$  of  $\text{D}_2\text{O}$  with TSP-d4, and pH adjusted to 8 at room temperature. After pH adjustment, the sample was taken to 1 mL with further addition of pure  $\text{D}_2\text{O}$ . The final pH of the MEA-triazine solution was 8.44 at room temperature. The same procedure was followed for the preparation of the bisulfide solution, using 13 mg of  $\text{Na}_2\text{S}\cdot 3\text{H}_2\text{O}$ . The final pH of the bisulfide solution was 8.03 at room temperature. An aliquot of 500  $\mu\text{L}$  of the HET solution was transferred to a micro centrifuge tube, mixed with an aliquot of 500  $\mu\text{L}$  of the bisulfide solution, stirred and heated to 50  $^\circ\text{C}$  for 2 hours. After this time, the reacting mixture was left at room temperature overnight and NMR spectra recorded.

The purification and identification of thiadiazine was developed and performed by Prof. Reinhard Wimmer in the Section of Bioscience and Engineering of Aalborg University. A detailed description of the procedure is available in Paper B.

#### 4.3.3. pH TITRATION OF MEA-TRIAZINE AND DITHIAZINE

The pH titration of MEA-triazine and dithiazine was done via  $^1\text{H-NMR}$  spectroscopy to analyze the protonation behavior of these compounds as a function of pH.

Single-component stock solutions of the technical solution of MEA-triazine (24 mM) and dithiazine (86 mM) were prepared in milli-Q water and 5% (v/v)  $\text{D}_2\text{O}$  with TSP-d4. Aliquots of 600  $\mu\text{L}$  were transferred from each stock solution to 11 micro centrifuge tubes (22 tubes in total) and heated to 25 $^\circ\text{C}$ . At this temperature, the pH of the sample in each tube was adjusted to one value in the range 7 to 12 with a step size of ca. 0.5 between each sample. For the dithiazine stock solution, two additional samples were conditions to pH 3 and 5. After pH adjustment, each sample was transferred to an NMR tube for the acquisition  $^1\text{H-NMR}$  spectra at 25 $^\circ\text{C}$ .



# CHAPTER 5. RESULTS AND DISUSSION

## 5.1. INVESTIGATION OF THE H<sub>2</sub>S SCAVENGING REACTIONS WITH MEA-TRIAZINE IN AQUEOUS PHASE

### 5.1.1. PARAMETERS INFLUENCING THE SCAVENGING REACTIONS

The in-situ monitoring of the scavenging reactions at room temperature allowed the analysis of the extent of the influence of the concentration of reagents and pH on the rate of the reaction between bisulfide and MEA-triazine in aqueous phase. The reaction system in all experimental executions was always a transparent homogenous phase, with no signs of solid precipitation.

Figure 5-1 to Figure 5-3 show the trend of the concentration of bisulfide with the reaction time. Each plot depicts the influence of the STB ratio in reactions at room temperature for different initial pH values, viz., 9, 10 and 11. The colored numbers shown over the bisulfide concentration curves refer to the value of pH reached by the system after 3 and 6 hours. The dashed line at the third hour of reaction marks the moment when acid was injected to all reacting solutions, whereas the dotted lines represent the moment of acid injection at 4 and 5 hours for the reactions with STB 0.5 only.

For the three values of initial pH analyzed, it is clearly observed a larger bisulfide consumption for high STB ratios along the entirety of the reaction time, i.e., 6 hours. It is noted that all the bisulfide concentration curves have a steep slope in the first minutes of the reaction, and that such slope is sharper in reactions with higher STB ratios and low pH<sub>0</sub>, indicating that the scavenger concentration influences on the rate of the scavenging reactions; that is, at higher initial scavenger concentration, higher initial reaction rate.

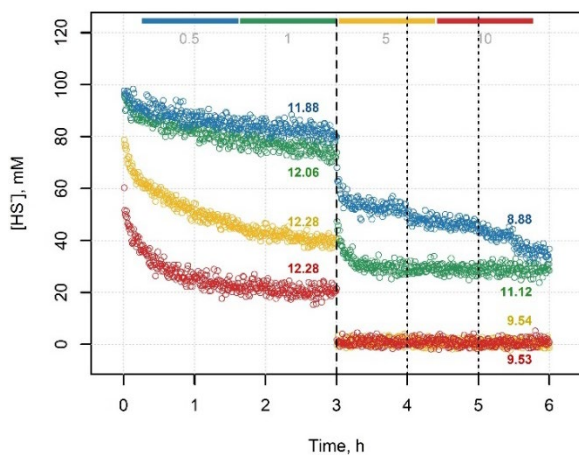


Figure 5-1. Influence of scavenger-to-bisulfide concentration ratio on the conversion of  $HS^-$  at  $pH_0 = 9$ . The color bar represents the STB ratio: blue: 0.5, green: 1.0, yellow: 5.0, red: 10.0. Paper A. Reprinted with permission from *Ind. Eng. Chem. Res.* 2021, 60, 43, 15549–15557. Copyright 2023 American Chemical Society.

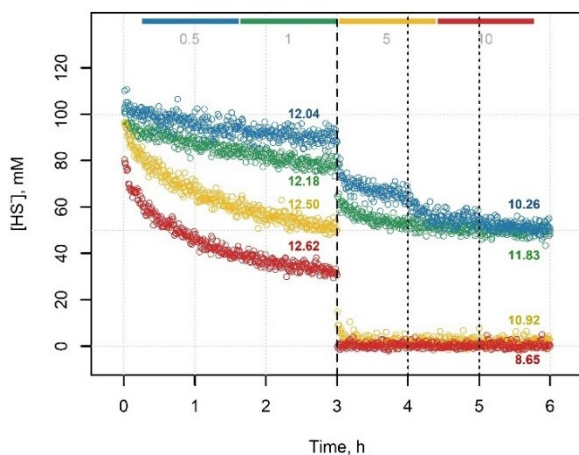


Figure 5-2. Influence of scavenger-to-bisulfide concentration ratio on the conversion of  $HS^-$  at  $pH_0 = 10$ . The color bar represents the STB ratio: blue: 0.5, green: 1.0, yellow: 5.0, red: 10.0. Paper A. Reprinted with permission from *Ind. Eng. Chem. Res.* 2021, 60, 43, 15549–15557. Copyright 2023 American Chemical Society.

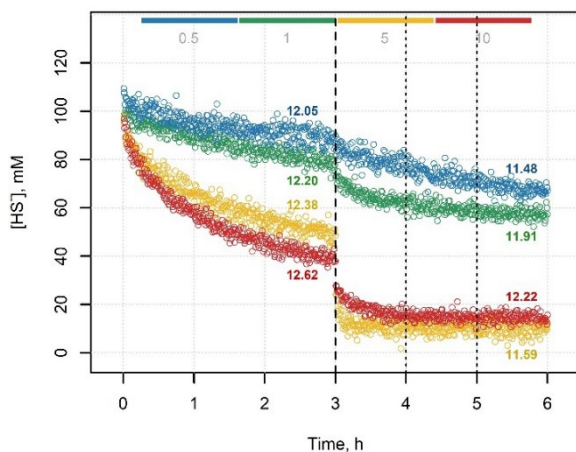


Figure 5-3. Influence of scavenger-to-bisulfide concentration ratio on the conversion of  $\text{HS}^-$  at  $\text{pH}_0 = 11$ . The color bar represents the STB ratio: blue: 0.5, green: 1.0, yellow: 5.0, red: 10.0. Paper A. Reprinted with permission from *Ind. Eng. Chem. Res.* 2021, 60, 43, 15549–15557. Copyright 2023 American Chemical Society.

Such effect can also be noted in the value of the first point of bisulfide concentration detected in the experiments, summarized in Table 5-1.

Table 5-1. Average concentration of  $\text{HS}^-$  at  $t = 30$  s in duplicate experiments at room temperature

STB	$\text{pH}_0 = 9$	$\text{pH}_0 = 10$	$\text{pH}_0 = 11$
0.5	95.6 mM	105.3 mM*	110.4 mM*
1.0	94.7 mM	102.0 mM*	106.9 mM*
5.0	79.5 mM	95.2 mM	99.0 mM
10.0	59.1 mM	81.0 mM	95.0 mM

\* Experimental inaccuracies of the quantitation method.

As per Table 5-1, the available concentration of bisulfide after 30 seconds of reaction is affected by both, STB ratio and  $\text{pH}_0$ , having a bisulfide conversion of 40.9% for STB ratio 10 and  $\text{pH}_0$  9. Analyzing the results for the same STB ratio, it is observed how higher values of  $\text{pH}_0$ , i.e., 11, significantly decrease the conversion of bisulfide with only 5% of the initial  $\text{HS}^-$  converted in 30 seconds of reaction.

Further analysis of Figure 5-1 to Figure 5-3 shows that the bisulfide concentration curves flatten out by the end of the first monitoring period (3 hours) and tend to constant values of bisulfide concentration, in all cases well above 0 mM, suggesting an apparent completion of the scavenging reaction even in the presence of large amounts of scavenger still available. Such decrease in the reaction rate is more evident in reactions at the highest STB ratio, which is to say, reactions under excess of scavenger. At the same time, the results show that in all the reactions run, the pH increased to values above 11.8 after 3 hours. According to the reaction mechanism for the scavenging of H<sub>2</sub>S with MEA-triazine in aqueous phase shown in Figure 2-8, the protonation of the triazine compounds, MEA-triazine and thiadiazine, is required for the reactions to occur. The protonation of such compounds implies the consumption of available hydronium ions which increases the pH of the solution.

On the other hand, high pH values reduce the availability of the protonated forms of MEA-triazine and thiadiazine leading to a reduction of the rate of the scavenging reactions as pH increases, explaining the flattening of the bisulfide curves observed by the end of the first 3 hours of reaction. Moreover, the injection of acid after 3 hours of reaction led to a further consumption of bisulfide, as depicted in Figure 5-1 to Figure 5-3, and in the cases of STB ratio 5 and 10, and pH<sub>0</sub> 9 and 10, the available bisulfide was completely depleted after injection of acid. These results are a strong indicator that the reactions' halt was caused by the high pH reached by the system rather than by a reduction in the concentration of bisulfide or scavenger. These results also suggest that the reaction between protonated MEA-triazine/thiadiazine and HS<sup>-</sup> are irreversible as they seem to proceed to completion provided that the pH of the reacting volume is kept low enough, indicatively at pH 9.

### **5.1.2. IDENTIFICATION OF KEY SPECIES USING RAMAN SPECTROSCOPY**

The Raman spectra of the scavenging reactions served further for performing a qualitative analysis of the existence/development of the reactants/products of the reactions, by identification of the Raman characteristic peaks of the components of interest. Such peak identification was done by juxtaposition of the spectra of single-component solutions, selecting the peaks that had little to none overlapping with neighboring peaks. The Raman peaks selected for the identification and monitoring of the key components in the scavenging reactions are summarized in Table 5-2 (Paper A and Paper B).



Table 5-2. Selected Raman peaks for the main components of the scavenging reactions in aqueous phase.

Component	Raman peak, $\text{cm}^{-1}$
MEA-triazine	923
Dithiazine	675
Monoethanolamine	840
Bisulfide	2574
Acetonitrile	2261
Phenylacetic acid	1004

Figure 5-4 shows the Raman spectra for one experimental execution run at initial pH 9, STB concentration ratio of 0.5 and room temperature, acquired between hour 3 and 6 of reaction phase.

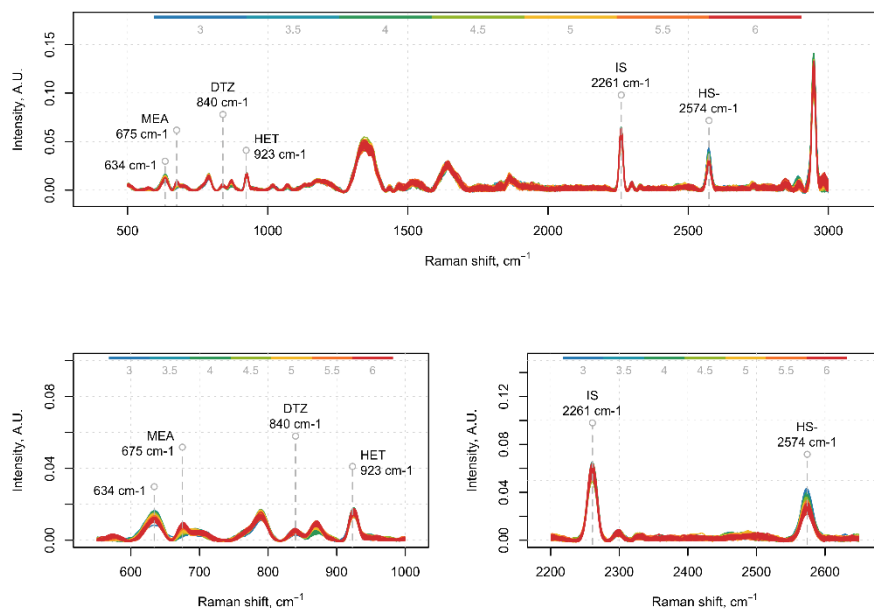


Figure 5-4. Raman spectra of the reaction between  $\text{HS}^-$  and MEA-triazine at room temperature, initial pH 9 and STB concentration ratio 0.5. The color legend shows the reaction times in hours. Selected Raman peaks are shown with gray dashed lines. Adapted from Paper A. Reprinted with permission from *Ind. Eng. Chem. Res.* 2021, 60, 43, 15549–15557. Copyright 2023 American Chemical Society.

The spectra clearly show the time-development of the peaks selected for each component of the scavenging reactions. It is observed that the peaks for bisulfide and MEA-triazine decrease in time while the peaks for monoethanolamine (MEA) and dithiazine (DTZ) increase during the reaction time; on the other hand, the peak of acetonitrile (IS) stays invariable. These results evidence the occurrence of the scavenging reactions.

### 5.1.3. REACTION MECHANISM BETWEEN HS<sup>-</sup> AND MEA-TRIAZINE

There are two essential aspects of the reaction mechanism between bisulfide and MEA-triazine required for the occurrence of the scavenging reactions: 1) protonation of the triazine species involved, and 2) formation of thiadiazine as intermediate compound of the reactions. The former has been addressed in the literature to some extent [38] whilst the latter has been a debated subject with contrasting perspectives, as discussed in Chapter 2. The investigation of both aspects is explained in detail in Paper B; thus, a summary follows.

#### PROTONATION OF TRIAZINE SPECIES

The pH titration of the triazine species involved in the scavenging reactions by means of NMR spectroscopy was attempted with the objective of defining their pK<sub>a</sub> value, parameter required for a proper assessment of the protonation behavior of such species in the operating pH range of the scavenging reactions. Despite its relevance, the pK<sub>a</sub> of the triazine species was not reported in the literature; the determination of the pK<sub>a</sub> values of the species involved in the scavenging reactions was therefore deemed of high relevance for this project.

The result of the pH titration of MEA-triazine analyzed by <sup>1</sup>H-NMR at 25°C is shown in Figure 5-5.

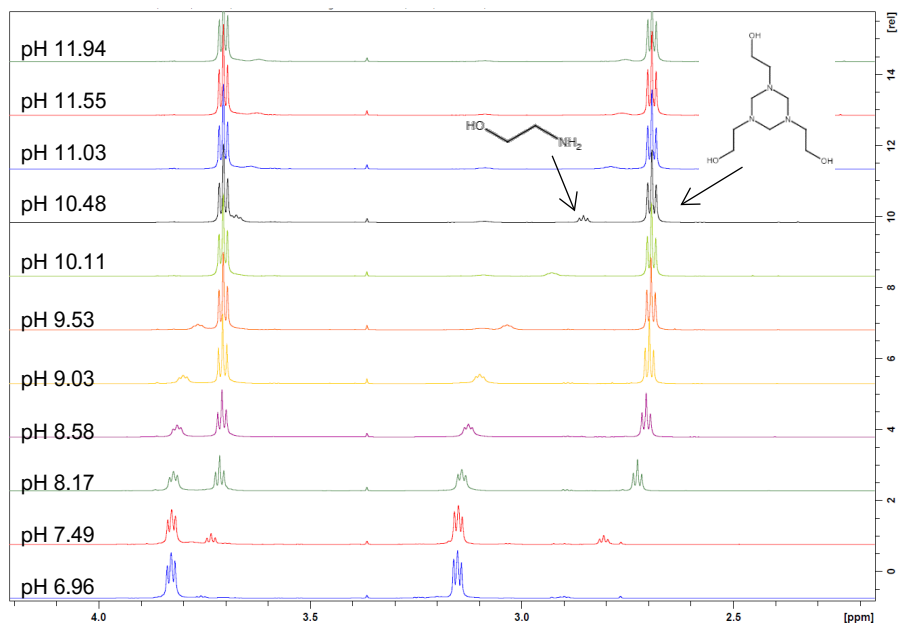


Figure 5-5.  $^1\text{H-NMR}$  spectra of solutions of MEA-triazine at pH values between 6.0 and 12.0 at  $25^\circ\text{C}$ . Paper B. Reprinted with permission from *Ind. Eng. Chem. Res.* 2023, 62, 21, 8269–8280. Copyright 2023 American Chemical Society.

In Figure 5-5, two triplets associated to the side chains of MEA-triazine were identified, one corresponding to the  $\text{CH}_2$  group bound to the nitrogen, located at around 2.7 ppm, and the other corresponding to the  $\text{CH}_2$  group bound to the oxygen, located at around 3.7 ppm. Both triplets were invariant at pH above 9 and only a very small amount of monoethanolamine was detectable at this pH range. At lower pH values, four observations occurred concomitantly: i) the shift of the  $\text{NH}_2\text{-CH}_2$  group varied towards higher ppm values, ii) the detected small amount of ethanolamine increased steadily, iii) the shift of the  $\text{CH}_2\text{-OH}$  group kept its positioning while observable, and iv) both the triplets of MEA-triazine decreased considerably until becoming barely detectable while the triplets for ethanolamine increased significantly. At the lowest pH of the analysis, there was practically only ethanolamine present in the solution, as result of the acid-catalyzed hydrolysis of MEA-triazine [41]. Considering that the position of the signals in the NMR spectra corresponds to the weighted average of the neutral and the protonated forms of the molecule, the observed shift variation can be associated with the occurrence of molecule protonation. Altogether, these observations revealed a protonation/deprotonation equilibrium of MEA-triazine yet, the decomposition of MEA-triazine prevented from deriving an exact  $\text{pK}_a$  value for this molecule. Nonetheless, the  $^1\text{H-NMR}$  observations

for MEA-triazine do not indicate detectable protonation/deprotonation of this compound at pH above 9.

The result of the pH titration of dithiazine analyzed by  $^1\text{H-NMR}$  at  $25^\circ\text{C}$  is shown in Figure 5-6.

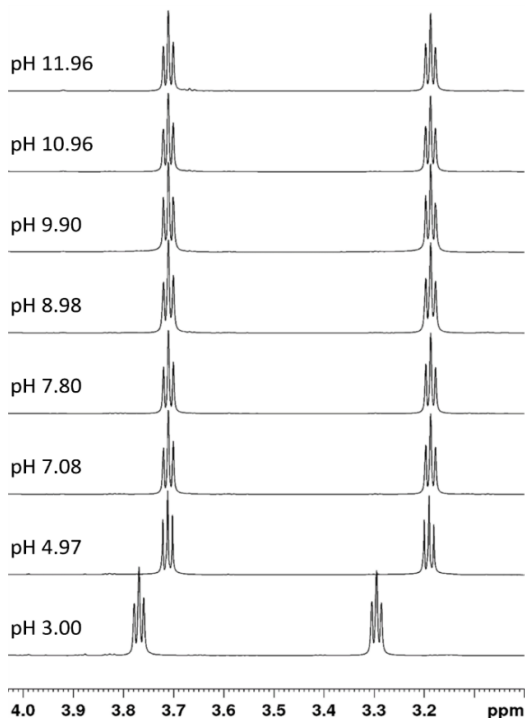


Figure 5-6.  $^1\text{H-NMR}$  spectra of solutions of dithiazine at pH values between 3.0 and 12.0 at  $25^\circ\text{C}$ . Paper B. Reprinted with permission from *Ind. Eng. Chem. Res.* 2023, 62, 21, 8269–8280. Copyright 2023 American Chemical Society.

In the case of dithiazine, the two triplets associated to the side chains of the molecule are also observed, one corresponding to the  $\text{CH}_2$  group bound to the nitrogen, located at around 3.2 ppm, and the other corresponding to the  $\text{CH}_2$  group bound to the oxygen, located at around 3.7 ppm. Both triplets were invariant in a large range of pH, even at acid pH values. Only at a pH as low as 3.0, both triplets changed position. These observations allowed to conclude that dithiazine does not protonate at pH values typical of the scavenging reactions, i.e.,  $\text{pH} > 9$ . These results could explain the nonoccurrence of the third scavenging reaction, which would lead to the formation of 1,3,5-trithiane.

## IDENTIFICATION OF THIADIAZINE

In-house synthesized thiadiazine, starting from  $\text{HS}^-$  and MEA-triazine, was analyzed by means of NMR spectra, obtaining the spectra shown in Figure 5-7.

Figure 5-7 A shows the proton NMR spectrum of TDZ, where the triplet corresponding to the  $\text{CH}_2$  bound to the oxygen (8,10) is slightly shifted towards ppm values lower than 3.7 ppm, which was identified in the MEA-triazine and dithiazine spectra of Figure 5-5 and Figure 5-6. This slight shift is probably attributed to a ring inversion of the ring hydrogen atoms. In addition, the  $\text{CH}_2$  bound to the nitrogen (7,9) is severely broadened, suggesting an influence of the ring inversion. The  $[\text{}^1\text{H}, \text{}^{13}\text{C}]$ -HSQC spectrum shown in Figure 5-7 C reveals the expected correlations between the protons in thiadiazine with their directly attached carbons, confirming the identification of TDZ in the scavenging reactions.

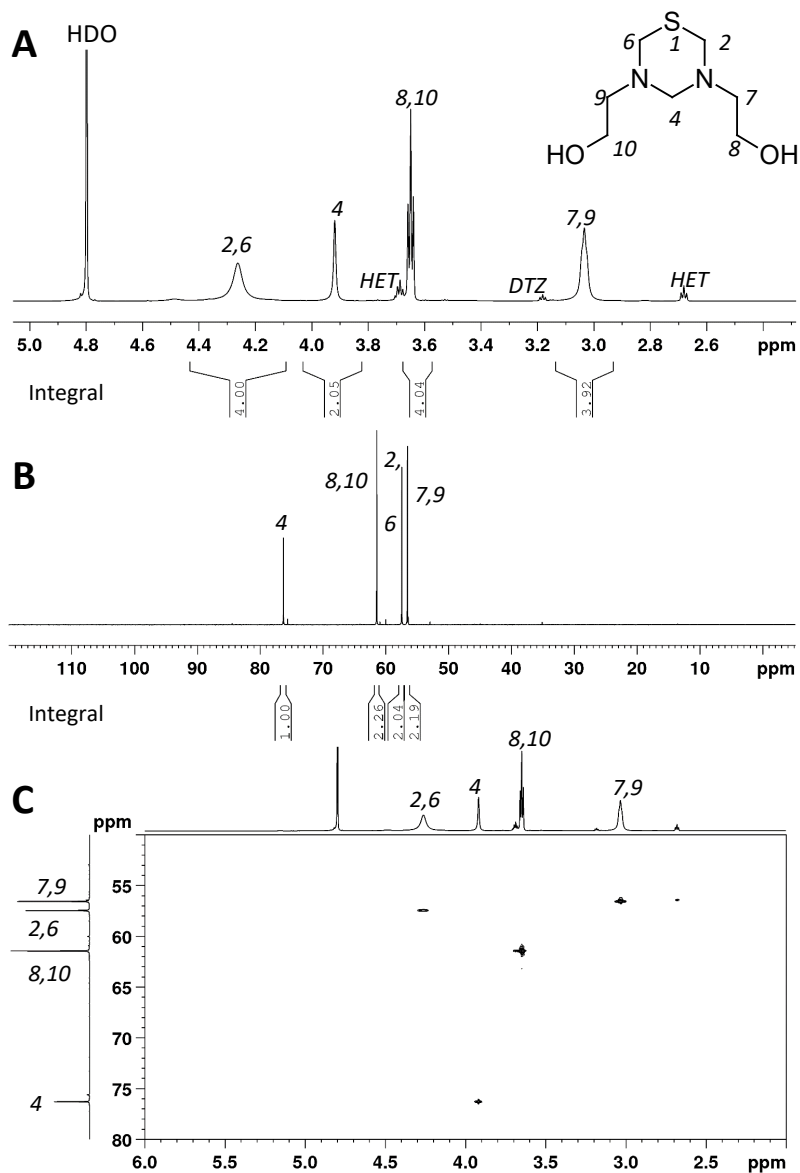


Figure 5-7. NMR of thiadiazine in  $\text{D}_2\text{O}$ ,  $\text{pH}^*=10.0$ , at 298.1 K, with assignment of resonances to atoms. Both MEA-triazine and dithiazine were present as impurities, their signals are labelled accordingly. The residual water signal is labelled HDO. A)  $^1\text{H}$ -NMR spectrum (600 MHz); B) quantitative  $^{13}\text{C}$ -NMR spectrum (150.9 MHz); C)  $[^1\text{H},^{13}\text{C}]$ -HSQC spectrum. Paper B. Reprinted with permission from *Ind. Eng. Chem. Res.* 2023, 62, 21, 8269–8280. Copyright 2023 American Chemical Society.

Figure 5-8 shows the  $^1\text{H-NMR}$  spectrum of the thiadiazine sample (A) and its comparison with the spectra of the other triazine-containing species: MEA-triazine (B) and dithiazine (C), and ethanolamine (D), all recorded at  $25^\circ\text{C}$ . As observed, spectrum A is very different to spectra B, C and D. The broader peaks attributed to a ring inversion can be corroborated with Figure 5-9.

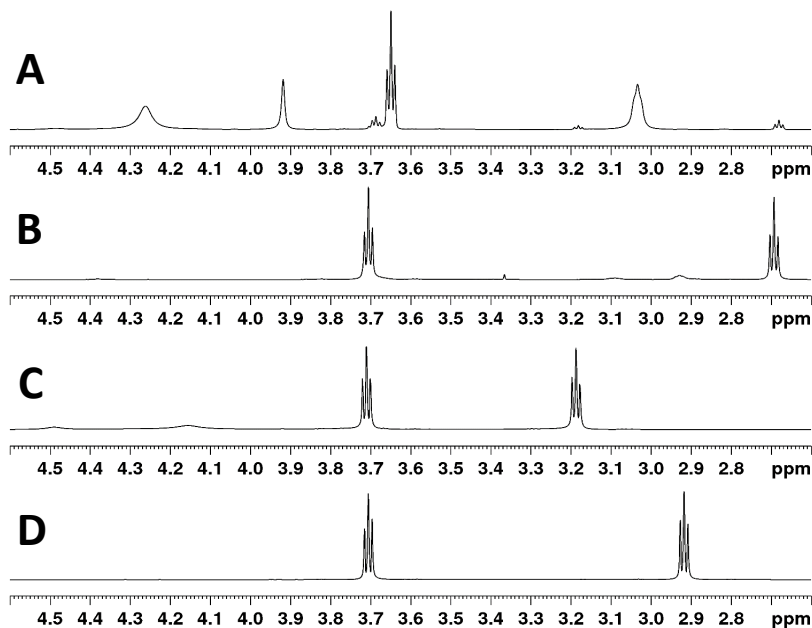


Figure 5-8.  $^1\text{H-NMR}$  spectra (600 MHz) of A) Thiadiazine, B) MEA-triazine, C) Dithiazine and D) Ethanolamine. Thiadiazine is obtained from in-house synthesis, while the other samples are obtained commercially. All spectra were recorded at  $\text{pH } 10$ ,  $T=298.1 \text{ K}$ , and they were all referenced to internal TSP- $d_4$ . Paper B. Reprinted with permission from *Ind. Eng. Chem. Res.* 2023, 62, 21, 8269–8280. Copyright 2023 American Chemical Society.

Figure 5-9 shows the spectra of thiadiazine at different temperatures. From this figure it is possible to notice how the set of lines for thiadiazine gets sharper with increasing temperature, confirming the suspected influence of the ring inversion in the  $\text{NH}_2\text{-CH}_2$  group in the thiadiazine spectrum at  $25^\circ\text{C}$ .

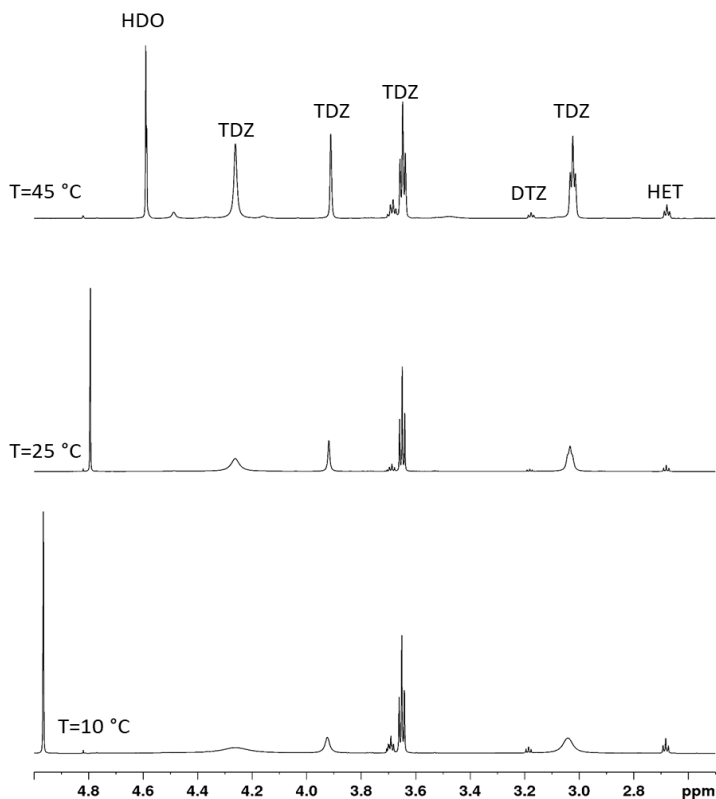


Figure 5-9.  $^1\text{H-NMR}$  spectra (600 MHz) of thiadiazine at different temperatures. All spectra are referenced to internal TSP- $d_4$ . Paper B. Reprinted with permission from *Ind. Eng. Chem. Res.* 2023, 62, 21, 8269–8280. Copyright 2023 American Chemical Society.

Ultimately, the NMR observations confirmed that thiadiazine is an intermediate compound of the scavenging reactions, is stable at room temperature and pH above 10 for several days, enough to be detected and measured by spectroscopic methods. Further, the pH titration of MEA-triazine and dithiazine confirmed the protonation/deprotonation behavior of the former on one hand, and the lack of protonation of the latter on the other hand, both under values of pH typical for the scavenging reactions, i.e.,  $\text{pH} > 9$ . Such lack of protonation of dithiazine could explain why the scavenging reactions do not proceed to form trithiane, the hypothesized last compound of the series of reactions, and instead stop at the formation of dithiazine. Thus, the experimental observations support the confirmation of the reaction mechanism of the scavenging reactions between bisulfide and MEA-triazine in aqueous phase as the one shown in Figure 5-10.



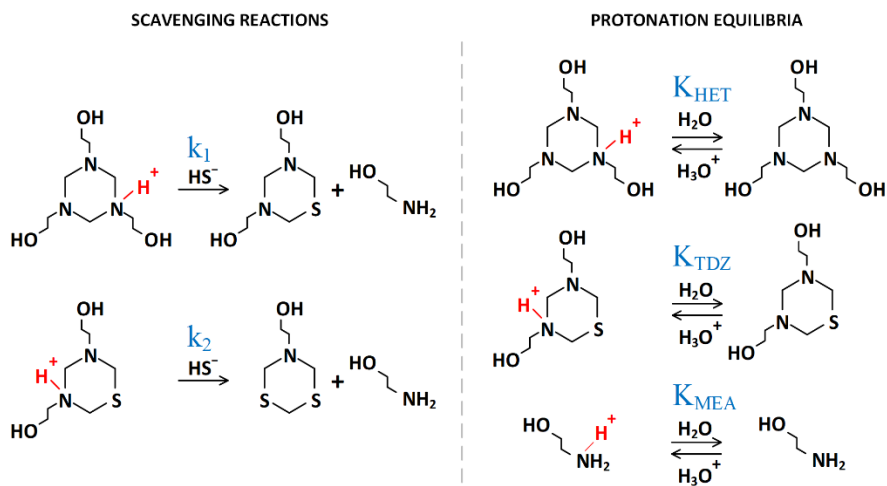


Figure 5-10. Reaction mechanism for the scavenging of bisulfide with MEA-triazine in aqueous phase supported by experimental observations. Paper B. Reprinted with permission from *Ind. Eng. Chem. Res.* 2023, 62, 21, 8269–8280. Copyright 2023 American Chemical Society.

## 5.2. DEVELOPMENT OF A KINETIC MODEL FOR THE AQUEOUS-PHASE H<sub>2</sub>S SCAVENGING REACTIONS

In this section, it is presented the kinetic model developed to best describe the scavenging process under conditions of interest, i.e., pH values in the range of 9 to 11, temperatures above ambient, and presence of excess of bisulfide.

A five-reaction scheme, as per Table 5-3, has been developed upon the qualitative investigation of the scavenging reactions detailed in Section 5.1. Firstly, the model considers the reaction scheme confirmed by means of NMR spectroscopy: a multiple reaction scheme in series with respect to the scavenger and in parallel with respect to bisulfide (Reactions 1 and 2). Further, the observation of increasing pH in the development of the scavenging reactions led to assume that the reactants of this reaction scheme are the protonated forms of the scavenger, i.e., protonated MEA-triazine in the first scavenging reaction and protonated thiadiazine in the second scavenging reaction. Then, the model considers the protonation equilibrium of the species involved in the scavenging system which were observed to protonate at the pH range of interest, MEA-triazine, thiadiazine and ethanolamine, by Reactions 3 to 5.

The kinetic model was built upon the following hypotheses, which are described in Paper B:

- i) HS<sup>-</sup> is the only species from the ionization equilibrium of H<sub>2</sub>S that is present in the system, considering that the pK<sub>a</sub> value of H<sub>2</sub>S is around 7 at room temperature [25, 29].
- ii) Protonated MEA-triazine and protonated thiadiazine are the actual species reacting with HS<sup>-</sup>.
- iii) The protonation reactions of MEA-triazine and thiadiazine are always at equilibrium.
- iv) The protonation reaction of monoethanolamine is included, and this reaction is also always at equilibrium.
- v) Dithiazine does not undergo protonation in the pH range of interest and does not undergo any scavenging reaction with HS<sup>-</sup>.
- vi) The first and second scavenging reactions are irreversible.
- vii) The hydrolysis of MEA-triazine is negligible at the pH range of interest [41].

Table 5-3. Set of reactions forming the reaction scheme for development of the kinetic model.

Description	Reaction	Reaction No.
First scavenging reaction	$HET^+ + HS^- \rightarrow TDZ + MEA$	1
Second scavenging reaction	$TDZ^+ + HS^- \rightarrow DTZ + MEA$	2
Protonation equilibrium of MEA-triazine	$HET^+ + H_2O \rightleftharpoons HET + H_3O^+$	3
Protonation equilibrium of thiadiazine	$TDZ^+ + H_2O \rightleftharpoons TDZ + H_3O^+$	4
Protonation equilibrium of ethanolamine	$MEA^+ + H_2O \rightleftharpoons MEA + H_3O^+$	5

Assuming Reactions 1 and 2 are irreversible and of first order with respect to their respective reactants, the rate of consumption of bisulfide can be written as:

$$(-r_{HS^-}) = k_1[HET^+][HS^-] + k_2[TDZ^+][HS^-] \quad (1)$$

In addition, the protonation equilibrium of MEA-triazine, thiadiazine and monoethanolamine can be written as:

$$K_{HET} = \frac{[HET][H_3O^+]}{[HET^+]} \quad (2)$$

$$K_{TDZ} = \frac{[TDZ][H_3O^+]}{[TDZ^+]} \quad (3)$$

$$K_{MEA} = \frac{[MEA][H_3O^+]}{[MEA^+]} \quad (4)$$

At all points in time, there will exist a balance between the neutral and the protonated species of these compounds, which means that their total concentration – denoted here with a star – will be the result of the addition of the concentration of the neutral and the protonated species. Therefore, equations 5 to 7 hold:

$$[HET^*] = [HET^+] + [HET] \quad (5)$$

$$[TDZ^*] = [TDZ^+] + [TDZ] \quad (6)$$

$$[MEA^*] = [MEA^+] + [MEA] \quad (7)$$

The extent of reaction,  $x_k$ , defined in equation 8, correlates the variation in the number of moles of species  $i$  in the reaction  $k$  with the stoichiometry of reaction  $k$ , providing thus a measure of the degree of progress of the reactions.

$$x_k = \frac{\Delta N_{k_i}}{\nu_{k_i}} \quad (8)$$

Where,  $\nu_{k_i}$  is the stoichiometric coefficient of species  $i$  in reaction  $k$ , which is positive for products and negative for reactants. Also,  $\Delta N_{k_i} > 0$  for products and  $\Delta N_{k_i} < 0$  for reactants.

Thus, the molar balance for the all the species present in the system, represented by the set of reactions 1 to 5, can be expressed in terms of the extent of reactions, yielding the following system of equations:

$$[HS^-] = [HS^-]_0 - x_1 - x_2 \quad (9)$$

$$[HET^+] = [HET^+]_0 - x_1 - x_3 \quad (10)$$

$$[HET] = [HET]_0 + x_3 \quad (11)$$

$$[TDZ^+] = [TDZ^+]_0 - x_2 - x_4 \quad (12)$$

$$[TDZ] = [TDZ]_0 + x_1 + x_4 \quad (13)$$

$$[DTZ] = x_2 \quad (14)$$

$$[MEA^+] = [MEA^+]_0 - x_5 \quad (15)$$

$$[MEA] = [MEA]_0 + x_1 + x_2 + x_5 \quad (16)$$

$$[H_3O^+] = [H_3O^+]_0 + x_3 + x_4 + x_5 \quad (17)$$

Assuming constant density of the reacting mixture and an ideal behavior of the batch reactor, i.e., ideal mixing, based on the intense stirring imposed during the development of the kinetic experiments of Paper B, it is possible to express the design equation of an ideal BSTR, shown in equation 18, in terms of the concentration of any species in the reaction.

$$r_i = \frac{dC_i}{dt}, \text{ where } i \text{ represents any species in the reactor} \quad (18)$$

Considering the total rate of consumption of bisulfide (Eq.1) and Eq.18, it holds that:

$$-\frac{d[HS^-]}{dt} = k_1[HET^+][HS^-] + k_2[TDZ^+][HS^-] \quad (19)$$

For MEA-triazine, it is necessary to consider the contribution of both the protonated and the neutral forms of the compound. Adding Eq. 11 to Eq. 10 one obtains Eq. 20, which shows that the total concentration of MEA-triazine only depends on the first scavenging reaction (Reaction 1) and that the protonation equilibrium of MEA-triazine (Reaction 3) does not affect the total amount of triazine.

$$[HET^*] = [HET^*]_0 - x_1 \quad (20)$$

Thus, the design equation of the ideal BSTR in terms of the total concentration of MEA-triazine can be expressed as:

$$-\frac{d([HET^+] + [HET])}{dt} = k_1[HET^+][HS^-] \quad (21)$$

Furthermore, the design equations 19 and 21 can be expressed in terms of the extent of reactions by considering the molar balances written in equations 9 to 17, as follows:

$$\begin{aligned} -\frac{d([HS^-]_0 - x_1 - x_2)}{dt} &= \dots \\ \dots k_1([HET^+]_0 - x_1 - x_3)([HS^-]_0 - x_1 - x_2) &+ \dots \\ \dots k_2([TDZ^+]_0 - x_2 - x_4)([HS^-]_0 - x_1 - x_2) & \end{aligned}$$

And

$$\begin{aligned} -\frac{d([HET^+]_0 - x_1 - x_3 + [HET]_0 + x_3)}{dt} &= \dots \\ \dots k_1([HET^+]_0 - x_1 - x_3)([HS^-]_0 - x_1 - x_2) & \end{aligned}$$

Which yield to Equations 22 and 23 that represent the design equations for the ideal batch reactor:

$$\frac{dx_1}{dt} = k_1([HET^+]_0 - x_1 - x_3)([HS^-]_0 - x_1 - x_2) \quad (22)$$

$$\frac{dx_2}{dt} = k_2([TDZ^+]_0 - x_2 - x_4)([HS^-]_0 - x_1 - x_2) \quad (23)$$

Similarly, the protonation equilibria for MEA-triazine, thiadiazine and ethanolamine written in Eqs. 2 to 4 can also be expressed in terms of the extent of reactions:

$$K_{HET} = \frac{([HET]_0 + x_3)([H_3O^+]_0 + x_3 + x_4 + x_5)}{([HET^+]_0 - x_1 - x_3)} \quad (24)$$

$$K_{TDZ} = \frac{([TDZ]_0 + x_1 + x_4)([H_3O^+]_0 + x_3 + x_4 + x_5)}{([TDZ^+]_0 - x_2 - x_4)} \quad (25)$$

$$K_{MEA} = \frac{([MEA]_0 + x_1 + x_2 + x_5)([H_3O^+]_0 + x_3 + x_4 + x_5)}{([MEA^+]_0 - x_5)} \quad (26)$$

The system of differential and algebraic equations (DAE) formed by equations 22 to 26 constitute the kinetic model for the H<sub>2</sub>S scavenging reactions with MEA-triazine in aqueous phase.

### 5.2.1. REGRESSION OF THE KINETIC MODEL PARAMETERS

The kinetic parameters of the reaction rate are the rate constant for the first and the second scavenging reactions, the order of both reactions with respect to each component, and the protonation equilibrium constants for MEA-triazine and thiadiazine based on the high relevance of the protonation of such species for the reaction occurrence. The order of the scavenging reactions has been assumed to be equal to one, as explained in Section 0; thus, the determination of the rate and equilibrium constants will allow to fully define the rate law of the scavenging reactions.

In the DAE system, the protonation equilibrium constant of ethanolamine ( $K_{MEA}$ ) at different temperatures was taken from the literature [75]; hence,  $K_{MEA}$  was set as a fixed parameter in the kinetic model with the values:  $10^{-9.45}$  at 25 °C,  $10^{-8.72}$  at 50 °C, and  $10^{-8.22}$  at 75 °C.

To solve the DAE system, five regression parameters were set. The regression parameters along with their constraints are summarized in Table 5-4.

Table 5-4. Regression parameters and constraint values for solving the kinetic model.

Regression Parameter	Description	Constraint
$k_1$	Rate constant of the first scavenging reaction	$k_1 > 0$
$k_2$	Rate constant of the second scavenging reaction	$k_2 > 0$
$K_{HET}$	Concentration-based protonation equilibrium constant for MEA-triazine	$10^{-5} > K_{HET} > 10^{-9.5}$
$K_{TDZ}$	Concentration-based protonation equilibrium constant for thiadiazine	$10^{-5} > K_{TDZ} > 10^{-9.5}$
$pH_0$	Initial pH	$9 > pH_0 > 10.6$

For the reasons stated in Section 4.3.3, the experimental determination of  $K_{HET}$  and  $K_{TDZ}$  was not possible thus, they have been considered as the third and fourth regression parameters.

The fifth parameter,  $pH_0$ , on the other hand, has been considered a regression parameter for practical reasons. Based on the significant and rapid increase of pH observed after the injection of MEA-triazine during the development of the kinetic experiments, which did not give the pH-meter enough time for providing a stable reading, it was impractical to obtain a reliable measure of pH at the start of the reaction, i.e., the moment of the injection of MEA-triazine. For instance, one experimental execution reached a pH value of 10.6 after 15 seconds of the injection of MEA-triazine to the batch reactor, whereas the second execution at the same conditions of STB ratio and temperature reached a pH value of 10.2 after the same time. This behavior led to set the initial pH as another regression parameter of the kinetic model, constraint based on the experimental observations.

The rate constants are known to depend only on temperature and their values must be developed from experimental data; hence, it is not possible to predict *a priori* an approximate value of these parameters.

Regarding the constraint for the protonation equilibrium of MEA-triazine and thiadiazine, it was considered the pKa values typically found for amines,  $pK_a > 5$  [75],

and the NMR observations for the shift of MEA-triazine, which did not show any noticeable protonation above pH 9.5. In addition, it was assumed that thiadiazine behaves similarly to MEA-triazine, thus maintaining the same constraints for the pKa of both species.

#### DEFINITION OF INITIAL CONDITIONS

The concentration of bisulfide at the start of the reaction,  $[HS^-]_0$ , was calculated from the first Raman spectral acquisition.

The starting total concentration of MEA-triazine and ethanolamine were calculated based on the assumption that the second scavenging reaction did not occur in the first 30 seconds of mixing the bisulfide with the injected scavenger. Hence, the following stoichiometric relations are valid:

$$[HET^*]_0 = [HET^*]_n + [HS^-]_0 - [HS^-]_n$$

$$[MEA^*]_0 = [MEA^*]_n + [HS^-]_n - [HS^-]_0$$

where the subscript  $n$  indicates the nominal concentration (calculated from the solution preparation) and  $0$  indicates the starting concentration.

#### OPTIMIZATION STRATEGY

The optimal values of the regression parameters shown in Table 5-4 were found by a two-stage brute force optimization. The optimization grid for each stage is defined in Table 5-5.

Table 5-5. Optimization grid for the regression parameters of the kinetic model. Adapted from Paper B.

Regression parameter	Optimization grid	Optimization grid	Units
	Stage 1	Stage 2	
$10^{-1} \leq k_1 \leq 10^2$	step $10^{0.1}$	step 0.001	$L \text{ mol}^{-1} \text{ s}^{-1}$
$10^{-2} \leq k_2 \leq 10^1$	step $10^{0.1}$	step 0.001	$L \text{ mol}^{-1} \text{ s}^{-1}$
$5 \leq pK_{HET} \leq 9.5$	step 0.1	step 0.01	-
$5 \leq pK_{TDZ} \leq 9.5$	step 0.1	step 0.01	-



All the experimental data at the same temperature was regressed simultaneously, obeying in this way the single dependence on temperature for the rate constants. In addition, the data before and after acidification was treated separately. The algorithm for finding the optimal regression parameters consisted of the following steps:

Stage  
1

- a. Select one value for  $k_1$ ,  $k_2$ ,  $pK_{\text{HET}}$ , and  $pK_{\text{TDZ}}$  from the optimization grid 1.
- b. Find the value for  $pH_{0b}$  that gives the smallest mean squared error (MSE) by fitting the experimental data from the kinetic experiments **before** acidification at a given value of temperature.
- c. Find the value for  $pH_{0c}$  that gives the smallest MSE by fitting the experimental data from the kinetic experiments **after** acidification at a given value of temperature.
- d. Find the MSE value for this combination of regression parameters as the average between  $MSE_b$  and  $MSE_c$ .
- e. Repeat steps *a* to *d* for all the combinations of  $k_1$ ,  $k_2$ ,  $pK_{\text{HET}}$ , and  $pK_{\text{TDZ}}$  from the optimization grid 1.
- f. Select the regression parameters with the smallest MSE for stage 1, namely:  $k_{11}$ ,  $k_{21}$ ,  $pK_{\text{HET}1}$ , and  $pK_{\text{TDZ}1}$ , where the second subscript represents the optimization stage.

Stage  
2

- g. Create a finer optimization grid around the regression parameters from stage 1 and repeat steps *a* to *e*.
- h. Select the regression parameters with the smallest MSE for stage 2, which will represent the optimal regression parameters.

### 5.3. DISCUSSION OF RESULTS

The optimal regression parameters obtained for the kinetic model are summarized in Table 5-6.

Table 5-6. Optimal regression parameters for the aqueous-phase scavenging reactions. Adapted from Paper B.

Temperature, °C	$k_1$ , L mol <sup>-1</sup> s <sup>-1</sup>	$k_2$ , L mol <sup>-1</sup> s <sup>-1</sup>	$K_{HET}$ , L mol <sup>-1</sup>	$K_{TDZ}$ , L mol <sup>-1</sup>	Initial pH
25	0.435	0.004	$10^{-7.58}$	$10^{-9.04}$	9.3 – 10.1
50	3.260	0.018	$10^{-7.50}$	$10^{-9.10}$	9.0 – 10.1
75	22.200	0.110	$10^{-7.05}$	$10^{-9.05}$	9.0 – 9.8

Figure 5-11 illustrates the calculated concentration of bisulfide obtained with the optimal parameters shown in Table 5-6 and their satisfactory fitting with the experimental data. Simultaneously, Figure 5-11 exhibits high reproducibility between executions at the same experimental conditions, and the validity of its use for kinetic studies.

From Figure 5-11 it is also evident the influence of temperature in the rate of the scavenging reactions, observing a drastic change in the slope of the bisulfide concentration curves at 75°C, where practically most of the consumption takes place in approximately the first 20 minutes of the reaction. From that point onwards, the curves present the same behavior as the one observed at room temperature experiments: they flatten at a constant value of HS<sup>-</sup> concentration ( $[HS^-] > 0$ ) up until the acid injection, even in the presence of large excess of scavenger. Such decrease in the reaction rate is also observed at the other two temperatures in discussion, and it is attributed to the rapid increment of pH displayed right after the injection of the scavenging solution, viz., the start of the scavenging reactions, which reached values of ca. 10-11 within a few minutes. Despite such complexity, the developed kinetic model is able to reproduce this behavior of the scavenging reactions, as can be seen in Figure 5-11.

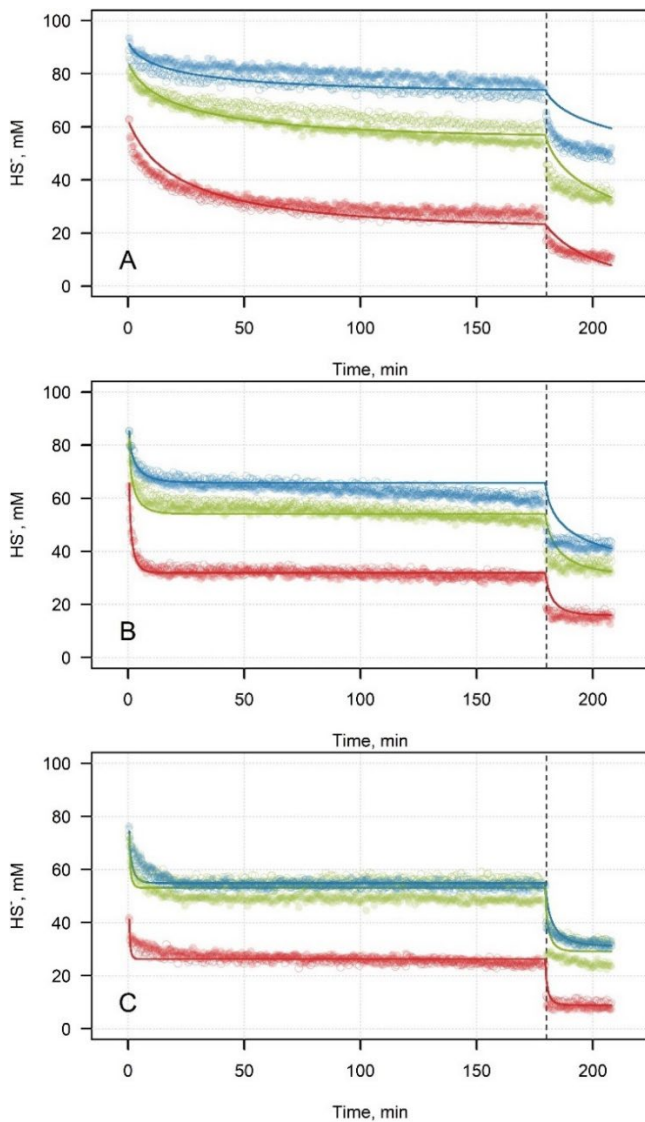


Figure 5-11. Experimental (colored dots) and calculated (continuous lines) concentrations of  $\text{HS}^-$  at 25°C (Plot A), 50°C (Plot B) and 75°C (Plot C) at different initial MEA-triazine concentrations: blue 46 mM, green 91 mM, and red 456 mM. System reacidification represented with the dashed vertical line. Duplicate experiments are shown with filled and empty markers. Adapted from Paper B. Reprinted with permission from *Ind. Eng. Chem. Res.* 2023, 62, 21, 8269–8280. Copyright 2023 American Chemical Society.

The accuracy in the representation of the experimental data by the kinetic model can further be verified with the average relative deviation (ARD) between experimental and calculated values, which falls within the range of 2% to 7% before acidification and 3% to 22% after acidification. The latter wider range for ARD is attributed to the higher uncertainty associated with the acidification during experimental executions, detailed in Paper B.

The mentioned decrease of the rate of disappearance of bisulfide can be explained by the reduced availability of protonated MEA-triazine and thiadiazine because of the increase in pH, which was correctly captured by the kinetic model through the consideration of the protonated forms of MEA-triazine and thiadiazine as reactants of the scavenging reactions and their protonation equilibria.

Moreover, Table 5-6 shows that the rate constants,  $k_1$  and  $k_2$ , increase with temperature, and that the rate constant for the second scavenging reaction is two orders of magnitude smaller than that for the first scavenging reaction. This behavior suggests that the consumption of bisulfide is mainly attributed to the occurrence of the first scavenging reaction, i.e., the action of the scavenger of MEA-triazine.

The dependence of the rate constants,  $k_1$  and  $k_2$ , with temperature can be explained through the Arrhenius relationship, from which the estimated values of activation energy for the first and second scavenging reactions are 68 kJ/mol and 57 kJ/mol, respectively, denoting a significant dependence of both scavenging reactions on temperature. The only kinetic data available in the literature for this reacting system was reported by Bakke and Buhaug [38] for the first scavenging reaction as function of the protonation equilibrium constant for MEA-triazine. In the cited work, it was estimated the parameter  $k_1/K_{HET}$  equal to  $9.1 \times 10^7 \text{ M}^2\text{s}^{-1}$ . Considering the data reported in Table 5-6, this parameter is estimated to be  $1.65 \times 10^7 \text{ M}^2\text{s}^{-1}$ , which is in the same order of magnitude.

Further evidence of the soundness of the kinetic model is found in the values of the protonation equilibrium constants for MEA-triazine and thiadiazine obtained by regression of the experimental data. The optimal values reported in Table 5-6 are in good agreement with the values of acid dissociation constants reported in literature for amines, between 7 to 11 [75], and the observed protonation of MEA-triazine by NMR spectroscopy at  $\text{pH} < 9.5$ .

The optimal regression parameters and the kinetic model were used to estimate the concentration of the main components of the reaction: MEA-triazine, thiadiazine, dithiazine and ethanolamine. Detailed plots are available in Paper B; hence, the hereby presented analysis focuses on the intermediate and final product of the scavenging reactions, thiadiazine and dithiazine, for being considered key components in the evaluation of the kinetic model.

Figure 5-12 presents the calculated concentrations of thiadiazine and dithiazine for the three studied temperatures, where the behavior of both compounds under stoichiometric conditions of reaction, i.e., initial concentration of 46 mM of MEA-triazine, is particularly highlighted.

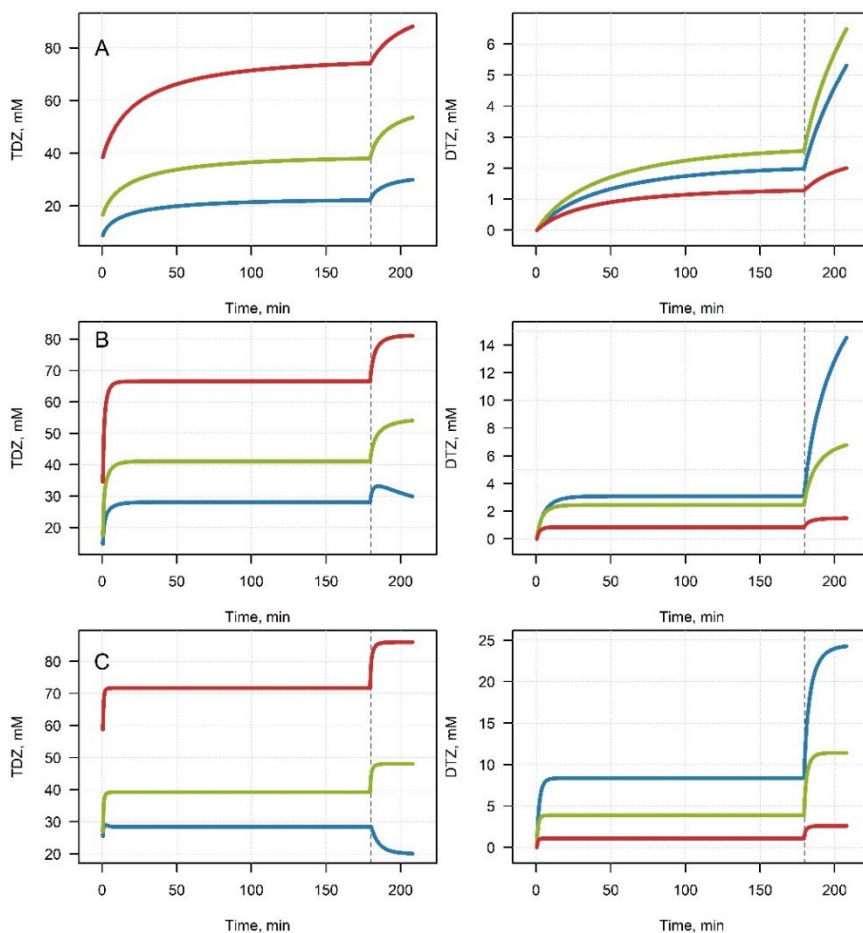


Figure 5-12. Calculated concentrations of thiadiazine and dithiazine for the reactions run at 25°C (Row A), 50°C (Row B), and 75°C (Row C) at different initial MEA-triazine concentrations: blue 46 mM, green 91 mM, and red 456 mM. System reacidification represented with the dashed vertical line. Adapted from Paper B. Reprinted with permission from *Ind. Eng. Chem. Res.* 2023, 62, 21, 8269–8280. Copyright 2023 American Chemical Society.

At 25°C (Row A), the highest calculated concentration of thiadiazine is observed for conditions of excess of scavenger whereas, for the same initial scavenger concentration, the lowest calculated concentration is obtained for dithiazine. This behavior explains the predominance of the first scavenging reaction, given that thiadiazine is produced via the first reaction at a higher rate than it is consumed by the second reaction to get dithiazine as product. At 50°C (Row B), the highest calculated concentration of thiadiazine is again obtained for the conditions of excess of scavenger; however, at the lowest initial scavenger concentration, i.e., stoichiometric conditions of reactants, it is noted that after acidification, thiadiazine reaches a maximum concentration while the concentration of dithiazine increases sharply, denoting that the second scavenging reaction is favored after the reacidification. Similar behavior is evidenced at 75°C (Row C), where the concentration of thiadiazine decreases after acidification while the concentration of dithiazine increases. Overall, these results confirm the general predominance of the first scavenging reaction in the consumption of bisulfide in aqueous-phase reactions with MEA-triazine, and that the second scavenging reaction becomes predominant after prolonged reaction times, provided that the pH of the system does not increase to a point of hindering the scavenging reactions.

## CHAPTER 6. CONCLUSIONS

The method developed for the in-situ measurement of the concentration of bisulfide in the aqueous-phase scavenging reactions with MEA-triazine using Raman spectroscopy is robust and adequate for its application to fast chemical reactions.

The investigation of the aqueous-phase hydrogen sulfide scavenging reactions with MEA-triazine confirmed the influence of the pH and the initial concentration of scavenger solution in the rate of consumption of bisulfide. A higher consumption of  $\text{HS}^-$  is obtained at pH values of 9, while high pH values in the order of 12, inhibit the scavenging reactions. On the other hand, higher initial concentrations of scavenger solution promote a significantly faster consumption of bisulfide compared with the consumption attained with a concentration 20 times smaller.

The experimental observations of this work at the laboratory conditions of the study support that thiadiazine is a measurable intermediate product of the scavenging reactions at pH values above 9 and temperatures ranging from 25°C up to 50°C. It has been shown that thiadiazine can be synthesized starting from MEA-triazine and  $\text{HS}^-$ , purified by HPLC, and identified via NMR spectroscopy.

The experimental observations at the laboratory conditions of this study also reveal dithiazine as the final product of the aqueous-phase scavenging reactions and the nonoccurrence of a third scavenging reaction. Further, the NMR observations showed that dithiazine does not undergo protonation in a pH range of 3 to 12 which could explain its lack of reaction with bisulfide in the scavenging process.

The presented kinetic model developed based on protonation/deprotonation equilibria of MEA-triazine, thiadiazine, and monoethanolamine, and two second-order bisulfide scavenging reactions (first order with respect to the protonated species and first order with respect to bisulfide) represents satisfactorily the reaction kinetics of the aqueous-phase scavenging reactions with MEA-triazine. The optimal regression parameters suggest that the rate constant of the first scavenging reaction is two orders of magnitude higher than the constant for the second reaction. The activation energies of the first and second scavenging reactions were estimated to be 68 and 57 kJ/mol, respectively, evidencing a significant dependency on temperature.

Conclusively, the hereby presented kinetic model can be used in the development of physicochemical models aimed at representing the overall scavenging process of hydrogen sulfide in gas streams via the injection of aqueous solutions of MEA-triazine through gas-liquid reactions, which will allow the optimization of the process currently used in offshore oil and gas installations.





# LITERATURE LIST

- [1] A. Inkpen and M. Moffet, *The Global Oil & Gas Industry: Management, Strategy & Finance*, Tulsa: Pennwell, 2011.
- [2] International Energy Agency - IEA, "Total primary energy supply by fuel, 1971 and 2019," 26 October 2022. [Online]. Available: <https://www.iea.org/data-and-statistics/charts/total-primary-energy-supply-by-fuel-1971-and-2019>. [Accessed 23 January 2023].
- [3] IEA Bioenergy Technology Collaboration Program, "Country Reports: Implementation of bioenergy in Denmark - 2021 update," October 2021. [Online]. [Accessed 23 January 2023].
- [4] G. Hammer, T. Lübcke, R. Kettner, M. Pillarella, H. Recknagel, A. Commichau, H.-J. Neumann and B. Paczynska-Lahme, "Natural Gas," in *Ullmann's Encyclopedia of Industrial Chemistry*, Weinheim, Wiley-VCH GmbH, 2012, pp. 740-792.
- [5] H. Bradley, *Petroleum Engineering Handbook*, Texas: Society of Petroleum Engineers, 1987.
- [6] M. Bothamley, "Offshore processing options vary widely," *Oil & Gas Journal*, vol. 102, no. 45, pp. 47-55, 2004.
- [7] F. Manning and R. Thompson, *Oilfield Processing of Petroleum. Volume One: Natural Gas*, Tulsa: PennWell Books, 1991.
- [8] K. Koczko, M. Leatherman and J. J. Wylde, "Foam Control," in *Surface Process, Transportation, and Storage. Volume 4 in Oil and Gas Chemistry Management Series*, Cambridge, Gulf Professional Publishing, 2023, pp. 153-226.
- [9] R. Horton, R. Stoker and P. Davis, "Process for Preventing or Remediating Trithiazine Deposition in High H<sub>2</sub>S Wells". United States of America Patent US 8,596,364 B2, 3 December 2013.
- [10] M. A. Kelland, *Production Chemicals for the Oil and Gas Industry*, Boca Raton: Taylor & Francis Group, 2009.

- [11] R. Garret, R. Clark, L. Carney and C. Grantham, "Chemical scavengers for sulfides in water-base drilling fluids," *Journal of Petroleum Technology*, vol. 31, no. 06, pp. 787-796, 1979.
- [12] O. Agbroko, K. Piler and T. Benson, "A comprehensive review of H<sub>2</sub>S scavenger technologies from oil and gas streams," *ChemBioEng Reviews*, vol. 4, no. 6, pp. 339-359, 2017.
- [13] M. Maschietti, "Oral Presentation: Towards zero discharge of H<sub>2</sub>S spent and unspent scavengers," in *Danish Hydrocarbon Research and Technology Center Technology Conference 2021*, Kolding, 2021.
- [14] G. Taylor, J. Wylde, T. Müller, S. Murison and F. Schneider, "Fresh insight into the H<sub>2</sub>S scavenging mechanism of MEA-triazine vs. MMA-triazine," in *SPE International Conference on Oilfield Chemistry*, Montgomery - Texas, 2017, doi: 10.2118/184529-MS.
- [15] M. N. Fini, N. Montesantos, M. Maschietti and J. Muff, "Performance evaluation of membrane filtration for treatment of H<sub>2</sub>S scavenging wastewater from offshore oil and gas production," *Separation and Purification Technology*, vol. 277, p. 119641, 2021.
- [16] X. Wang, Y. Zheng, J. Shi, X. Gong, Y. Ji, W. Han, Y. Jiang, D. E. Austin, X. Fang and Z. Zhang, "Elucidating the reaction mechanisms between triazine and hydrogen sulfide with pH variation using mass spectrometry," *Analytical Chemistry*, vol. 90, pp. 11138-11145, 2018.
- [17] N. Montesantos, M. Fini, J. Muff and M. Maschietti, "Proof of concept of hydrothermal oxidation for treatment of triazine-based spent and unspent H<sub>2</sub>S scavengers from offshore oil and gas production," *Chemical Engineering Journal*, vol. 427, no. 131020, 2022, doi: 10.1016/j.cej.2021.131020.
- [18] G. Taylor, M. Smith-Gonzalez, J. Wylde and A. Oliveira, "H<sub>2</sub>S Scavenger Development During the Oil and Gas Industry Search for an MEA triazine replacement in hydrogen sulfide mitigation and enhanced monitoring techniques employed during their evaluation," in *SPE International Conference on Oilfield Chemistry*, Galveston, 2019, doi: 10.2118/193536-MS.
- [19] R. A. Marriot, P. Pirzadeh, J. J. Marrugo-Hernandez and S. Raval, "Hydrogen sulfide formation in oil and gas," *Canadian Journal of Chemistry*, vol. 94, pp. 406-413, 2016.

- [20] Q. Ma, Z. Yang, L. Zhang, R. Lin and X. Wang, "Generation of hydrogen sulfide during the thermal enhanced oil recovery process under superheated steam conditions," *RSC Advances*, vol. 9, p. 33990, 2019.
- [21] I. Skjevraak, D. Standnes, U. Thomsen, J. Xu, K. Håland, A. Kjølhamar and P. Munkerud, "Field observations of reservoir souring development and implications for the Extended Growth Zone (EGZ) souring model," *Journal of Petroleum Science and Engineering*, vol. 204, p. 108721, 2021.
- [22] R. Worden, P. Smalley and S. Barclay, "H<sub>2</sub>S and diagenic pyrite in North Sea sandstones: due to TSR or organic sulfur compound cracking?," *Journal of Geochemical Exploration*, Vols. 78-79, pp. 487-491, 2003.
- [23] K. Sotoodeh, *Subsea Valves and Actuators for the Oil and Gas Industry*, Gulf Professional Publishing, 2021.
- [24] A. Kahyarian, B. Brown and S. Nestic, "Fundamental mechanisms of mild steel corrosion in H<sub>2</sub>S containing environments," in *NACE Corrosion Conference & Expo 2019*, Nashville, 2019.
- [25] F. Pouliquen, C. Blanc, E. Arretz, I. Labat, J. Tournier-Lasserve, A. Ladousse, J. Nougayrede, G. Savin, R. Ivaldi, M. Nicolas, J. Fialaire, R. Millischer, C. Azema, L. Espagno, H. Hemmer and J. Perrot, "Hydrogen Sulfide," in *Ullmann's Encyclopedia of Industrial Chemistry*, Wiley-VCH, 2000, pp. 429-449.
- [26] Australian Department of Climate Change, Energy, the Environment and Water, "Hydrogen Sulfide," 30 June 2022. [Online]. Available: <https://www.dcceew.gov.au/environment/protection/npi/substances/fact-sheets/hydrogen-sulfide>. [Accessed 09 April 2023].
- [27] Retsinformation, "Gasreglementet - BEK nr 4009," 16 October 1981. [Online]. Available: <https://www.retsinformation.dk/eli/retsinfo/1981/4009>. [Accessed 9 April 2023].
- [28] G. Astarita, D. Savage and A. Bisio, *Gas Treating with Chemical Solvents*, New York: John Wiley & Sons, 1983.
- [29] H. Loy and D. Himmelblau, "The first ionization constant of hydrogen sulfide in water," *Journal of Physical Chemistry*, vol. 65, no. 2, pp. 264-267, 1961.

- [30] P. M. May, D. Batka, G. Hefter, E. Königsberger and D. Rowland, "Goodbye to S<sup>2-</sup> in aqueous solution," *Chemical Communications*, vol. 54, pp. 1980-1983, 2018.
- [31] M. Holmer and H. Hasler-Sheetal, "Sulfide intrusion in seagrasses assessed by stable sulfur isotopes - a synthesis of current results," *Frontiers in Marine Science*, vol. 1, no. 64, pp. 1-13, 2014.
- [32] J. Spedding and M. Vujcich, "Exchange of H<sub>2</sub>S between air and water," *Journal of Geophysical Research*, vol. 87, no. 11, pp. 8853-8856, 1982.
- [33] S. Mokhatab, W. A. Poe and J. Y. Mak, *Handbook of Natural Gas Transmission and Processing. Principles and Practices*, Gulf Professional Publishing, 2019.
- [34] J. Wylde, G. Taylor, K. Sorbie and W. Samaniego, "Formation, chemical characterization and oxidative dissolution of amorphous polymeric dithiazine (apDTZ) during the use of the H<sub>2</sub>S scavenger monoethanolamine-triazine," *Energy & Fuels*, vol. 34, pp. 9923-9931, 2020, doi: <https://doi.org/10.1021/acs.energyfuels.0c01402>.
- [35] A. Pudi, M. Rezaei, V. Signorini, M. P. Andersson, M. G. Baschetti and S. S. Mansouri, "Hydrogen sulfide capture and removal technologies: a comprehensive review of recent developments and emerging trends," *Separation and Purification Technology*, vol. 298, p. 121448, 2022.
- [36] J. Wylde, G. Taylor, K. Sorbie and W. Samaniego, "Synthesis and reaction byproduct characterization and mechanistic understanding of hemiformal based hydrogen sulfide scavengers," *Energy & Fuels*, vol. 34, pp. 4808-4821, 2020.
- [37] T. Owens and P. Clark, "Triazine chemistry: Removing H<sub>2</sub>S and mercaptans," *ASRL Quaterly Bulletin No. 155*, vol. 47, no. 3, pp. 1-21, 2010.
- [38] J. Bakke and J. Buhaug, "Hydrogen sulfide scavenging by 1,3,5-triazinanes. Comparison of the rates of reaction," *Industrial & Engineering Chemistry Research*, vol. 43, no. 9, pp. 1962-1965, 2004.
- [39] Elsevier Information Systems GmbH, "Reaxys," 2023. [Online]. Available: [https://www.reaxys.com/#/results/substances/0/RX001\\_5320172163092741256/UlgwMDE9UyNIMDEwPUMjSDAwOD1S/list/240edd93-78b4-458f-890a-e04e107730e2/1/desc/IDE.NUMREF///](https://www.reaxys.com/#/results/substances/0/RX001_5320172163092741256/UlgwMDE9UyNIMDEwPUMjSDAwOD1S/list/240edd93-78b4-458f-890a-e04e107730e2/1/desc/IDE.NUMREF///). [Accessed 23 June 2023].

- [40] National Oceanic and Atmospheric Administration - U.S. Department of Commerce, "CAMEO Chemicals - Hexahydro-1,3,5-tris(hydroxyethyl)-5-triazine," version 2.8.0 rev 2. [Online]. Available: <https://cameochemicals.noaa.gov/chemical/20473>. [Accessed 11 July 2023].
- [41] J. Bakke, J. Buhaug and J. Riha, "Hydrolysis of 1,3,5-Tris(2-hydroxyethyl)hexahydro-s-triazine and its reaction with H<sub>2</sub>S," *Industrial & Engineering Chemistry Research*, vol. 40, pp. 6051-6054, 2001.
- [42] OSPAR Commission, "Offshore Chemicals," [Online]. Available: <https://www.ospar.org/work-areas/oic/chemicals>. [Accessed 9 April 2023].
- [43] European Chemicals Agency, "Substance Infocard - 2,2',2''-(hexahydro-1,3,5-triazine-1,3,5-triyl)triethanol," [Online]. Available: <https://echa.europa.eu/substance-information/-/substanceinfo/100.022.916>. [Accessed 9 April 2023].
- [44] J. Fink, *Petroleum Engineer's Guide to Oil Field Chemicals and Fluids*, Saint Louis: Elsevier Science & Technology, 2011.
- [45] M. G. Lioliou, C. B. Jenssen, K. Øvsthus, A.-M. Brurås and Ø. L. Aasen, "Design principles for H<sub>2</sub>S scavenger injection systems," in *Oilfield Chemistry Symposium*, Geilo, Norway, 2018.
- [46] N. Montesantos, L. Skjolding, A. Baun, J. Muff and M. Maschietti, "Reducing the environmental impact of offshore H<sub>2</sub>S scavenging wastewater via hydrothermal oxidation," *Water Research*, vol. 230, p. 119507, 2023; <https://doi.org/10.1016/j.watres.2022.119507>.
- [47] O. Maile, H. Tesfagiorgis and E. Muzenda, "Factors influencing chemical absorption of CO<sub>2</sub> and H<sub>2</sub>S in biogas purification: a review," in *World Congress on Engineering and Computer Science*, San Francisco, 2015.
- [48] R. Fiorot and J. de M. Carneiro, "The mechanism for H<sub>2</sub>S scavenging by 1,3,5-hexahydrotriazines explored by DFT," *Tetrahedron*, vol. 76, p. 131112, 2020, doi: 10.1016/j.tet.2020.131112.
- [49] H. Madsen and E. Søgaaard, "Use of ESI-MS to determine the reaction pathway for hydrogen sulphide scavenging with 1,3,5-tri-(2-hydroxyethyl)-hexahydro-s-triazine," *European Journal of Mass Spectrometry*, vol. 18, no. 4, pp. 377-383, 2012.

- [50] G. Taylor and R. Matherly, "Gas chromatographic - mass spectrometric analysis of chemically derivatized hexahydrotriazine-based hydrogen sulfide scavengers: Part II," *Industrial & Engineering Chemistry Research*, vol. 49, pp. 6267-6269, 2010, doi: 10.1021/ie1001247.
- [51] G. Taylor and R. Matherly, "Structural elucidation of the solid byproduct from the use of 1,3,5-tris(hydroxyalkyl)hexahydro-s-triazine based hydrogen sulfide scavengers," *Industrial & Engineering Chemistry Research*, vol. 50, pp. 735-740, 2011, doi: 10.1021/ie101985v.
- [52] G. Taylor, P. Prince, R. Matherly, R. Ponnappati, R. Tompkins and P. Vaithilingam, "Identification of the molecular species responsible for the initiation of amorphous dithiazine formation in laboratory studies of 1,3,5-tris(hydroxyethyl)-hexahydro-s-triazine as a hydrogen sulfide scavenger," *Industrial & Engineering Chemistry Research*, vol. 51, pp. 11613-11617, 2012, doi: 10.1021/ie301288t.
- [53] H. Madsen and E. Sogaard, "Fouling formation during hydrogen sulfide scavenging with 1,3,5-tri-(hydroxyethyl)-hexahydro-s-triazine," *Petroleum Science and Technology*, vol. 32, no. 18, pp. 2230-2238, 2014, doi: 10.1080/10916466.2013.783066.
- [54] R. Perez Pineiro, C. A. Peeples, H. Hendry, J. Hoshowski, G. Hanna and A. Jenkins, "Raman and DFT Study of the H<sub>2</sub>S Scavenger Reaction of HET-TRZ under Simulated Contactor Tower Conditions," *Industrial & Engineering Chemistry Research*, vol. 60, no. 15, pp. 5394-5402, 2021.
- [55] Edinburgh Instruments, "What is Raman Spectroscopy?," Edinburgh Instruments Ltd., 2023. [Online]. Available: <https://www.edinst.com/us/blog/what-is-raman-spectroscopy/>. [Accessed 16 April 2023].
- [56] J. Ferraro, K. Nakamoto and C. Brown, *Introductory Raman Spectroscopy*, Elsevier, 2003.
- [57] L. Øgendal, *Light Scattering. A brief introduction. Lecture Notes*, University of Copenhagen, 2019.
- [58] E. Smith and G. Dent, *Modern Raman Spectroscopy - A Practical Approach*, West Sussex: John Wiley & Sons Ltd, 2005.

- [59] P. Larkin, *Infrared and Raman Spectroscopy. Principles and Spectral Interpretation*, Stanford: Elsevier, 2011.
- [60] M. Pelletier, "Quantitative analysis using Raman Spectrometry," *Applied Spectroscopy - Focal Point*, vol. 57, no. 1, pp. 20A-42AA, 2003.
- [61] B. Barton, J. Thomson, E. Lozano Diz and R. Portela, "Chemometrics for Raman Spectroscopy Harmonization," *Applied Spectroscopy*, vol. 76, no. 9, pp. 1021-1041, 2022.
- [62] E. Caballero, *Webinar: How to pre-process your spectra for research (SNV, MSC, Derivatives)*, Center for Chemical Sensors-Chemical Imaging and Surface Analysis Center - University of Puerto Rico Mayagüez, 2022.
- [63] X. Zhao, G. Liu, Y. Sui, M. Xu and L. Tong, "Denoising method for Raman spectra with low signal-to-noise ratio based on feature extraction," *Spectrochimica Acta Part A: Molecular and Biomolecular Spectroscopy*, vol. 250, p. 119374, 2021.
- [64] K. H. Liland, A. Kohler and N. K. Afseth, "Model-based pre-processing in Raman spectroscopy of biological samples," *Journal of Raman Spectroscopy*, vol. 47, pp. 643-650, 2016.
- [65] P. H. C. Eilers, "A perfect smoother," *Analytical Chemistry*, vol. 75, pp. 3631-3636, 2003.
- [66] S. Guo, J. Popp and T. Bocklitz, "Chemometric analysis in Raman spectroscopy from experimental design to machine learning-based model," *Nature Protocols*, vol. 16, pp. 5426-5459, 2021.
- [67] S. Kucheryavskiy, "Getting started with mdatools for R," 31 March 2023. [Online]. Available: <https://mdatools.com/docs/index.html>. [Accessed 15 June 2023].
- [68] J. Hair, W. Black, B. Babin and R. Anderson, *Multivariate Data Analysis*, Seventh ed., Pearson, 2009.
- [69] R. Brereton, *Chemometrics: Data Driven Extraction for Science*, John Wiley & Sons Ltd., 2018.

- [70] B. Wise, "Evaluating Models: Hating on R-squared," Eigenvector Research Incorporated, 16 June 2022. [Online]. Available: <https://eigenvector.com/%EF%BF%BCevaluating-models-hating-on-r-squared/>. [Accessed 24 June 2023].
- [71] Chemistry and Biochemistry Department of University of Colorado, Boulder, "Spin states, magnetic fields, and electromagnetic radiation," 2011. [Online]. Available: <https://www.orgchemboulder.com/Spectroscopy/nmrtheory/nmrtheory.shtml>. [Accessed 16 June 2023].
- [72] H. Günther, "NMR Spectroscopy: Basic Principles, Concepts and Applications in Chemistry," John Wiley & Sons, Incorporated, 2013.
- [73] J. Koenig, *Spectroscopy of Polymers*, Elsevier, 1999.
- [74] S. Bagby, "J Coupling," in *Encyclopedia of Biophysics*, Berlin, Springer, 2013.
- [75] A. Rayer, K. Sumon, L. Jaffari and A. Henni, "Dissociation constants (pKa) of tertiary and cyclic amines: structural and temperature dependences," *Journal of Chemical & Engineering Data*, vol. 59, no. 11, pp. 3805-3813, 2014.



## **PART II. PUBLICATIONS**



## PAPER A

Experimental study of the aqueous phase reaction of hydrogen sulfide with  
MEA-triazine using in situ Raman spectroscopy

Iveth Romero, Sergey Kucheryavskiy, Marco Maschietti

The manuscript has been published in the journal

*Industrial & Engineering Chemistry Research*, Volume 60, Pages 15549-15557,  
2021



# Experimental Study of the Aqueous Phase Reaction of Hydrogen Sulfide with MEA-Triazine Using In Situ Raman Spectroscopy

Iveth Romero, Sergey Kucheryavskiy, and Marco Maschietti\*

Cite This: *Ind. Eng. Chem. Res.* 2021, 60, 15549–15557

Read Online

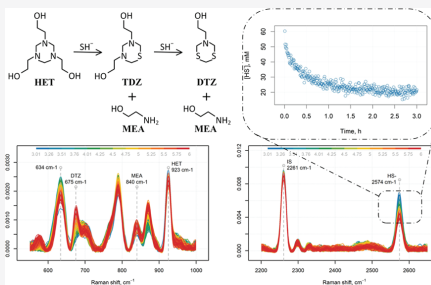
ACCESS |

Metrics & More

Article Recommendations

Supporting Information

**ABSTRACT:** A method for quantitation of bisulfide in the aqueous phase reactions of  $H_2S$  scavenging with MEA-triazine is proposed. The method is based on time-resolved in situ Raman spectroscopy, thus allowing in situ monitoring of the reactions. The method is applied to obtain the kinetic data of the reactions in batch configuration at room temperature for initial pH values of 9, 10, and 11 and MEA-triazine/bisulfide initial concentration ratios in the range of 0.5–10. The pH increases remarkably during the reactions, causing a substantial decrease in the rate of disappearance of bisulfide. If the system is reacidified, complete depletion of bisulfide can be achieved, evidencing the irreversibility of the scavenging reactions. The results are also supported by a qualitative analysis of the trends of the characteristic Raman peaks of MEA-triazine, dithiazine, and monoethanolamine. These trends are in line with the currently accepted reaction scheme, consisting of two scavenging reactions in series.



## 1. INTRODUCTION

Hydrogen sulfide ( $H_2S$ ) is a sour gas that is naturally encountered in exploration and production of hydrocarbons. It is highly corrosive to metals and poses a serious health and environmental threat because of its high toxicity. Its concentration in export oil and gas streams must be within allowable limits, which often requires its removal from the produced fluids at the oil and gas separation facilities near the wellheads.<sup>1</sup> With regard to natural gas, export specifications typically require a maximum concentration below 4 ppm.<sup>2</sup>

One of the methods available for the removal of  $H_2S$  from natural gas streams is the direct injection of  $H_2S$  scavengers, which are chemicals reacting with  $H_2S$  and transforming it into substantially less toxic and corrosive species.<sup>2</sup> The applicability of  $H_2S$  scavenging is limited to  $H_2S$  concentrations in the gas typically up to approximately 5000 ppmv due to the process economics.<sup>1</sup> The most common  $H_2S$  scavengers used nowadays are 1,3,5-hexahydrotriazines, often simply called triazines, with 1,3,5-tris(2-hydroxyethyl)-hexahydro-*s*-triazine (HET) being largely predominant (at least 80% of the oilfield market<sup>3</sup>) due to its high scavenging efficiency, high solubility in water, and high solubility of its byproducts in water.<sup>2,4</sup> In particular, the injection of HET into gas streams is the preferred  $H_2S$  scavenging method in topside process units in offshore oil and gas production due to the low footprint and simplicity of implementation. The process consists of injecting and dispersing a basic aqueous solution of HET in the wet gas, inducing the absorption of  $H_2S$  in the dispersed liquid phase where the scavenging reaction actually takes place, thus enhancing the absorption itself.

To date, it is accepted that the aqueous phase reaction of  $H_2S$  with HET occurs through a multiple reaction scheme, which is reported in a simplified form in Figure 1. The first step involves the protonation of HET and its reaction with  $HS^-$ , producing 3,5-bis(2-hydroxyethyl)hexahydro-1,3,5-thiadiazine (thiadiazine, TDZ) and monoethanolamine (MEA). TDZ, in turn, can also undergo protonation and reaction with  $HS^-$ , leading to 5-(2-hydroxyethyl)hexahydro-1,3,5-dithiazine (dithiazine, DTZ) and another molecule of MEA. The substitution of a third sulfur atom into the triazine ring, which would give trithiane, is instead typically not observed.<sup>1,5–12</sup> This is presumably attributed to the absence of a nucleophilic carbon center in DTZ susceptible to an attack by  $HS^-$ , as opposed to TDZ.<sup>1</sup> Thus, from a stoichiometric standpoint, 2 mol of sulfur from  $H_2S$  can be converted into DTZ using 1 mol of HET, with the liberation of 2 mol of MEA. The production of MEA in the scavenging reaction with HET is the reason for the common name of this scavenger in the oil and gas industry, where it is typically referred to as MEA-triazine.

Typical field values of injection of triazine-based commercial scavengers (40–50 wt % aqueous solutions) are in the range of

Received: September 23, 2021

Revised: October 4, 2021

Accepted: October 12, 2021

Published: October 22, 2021



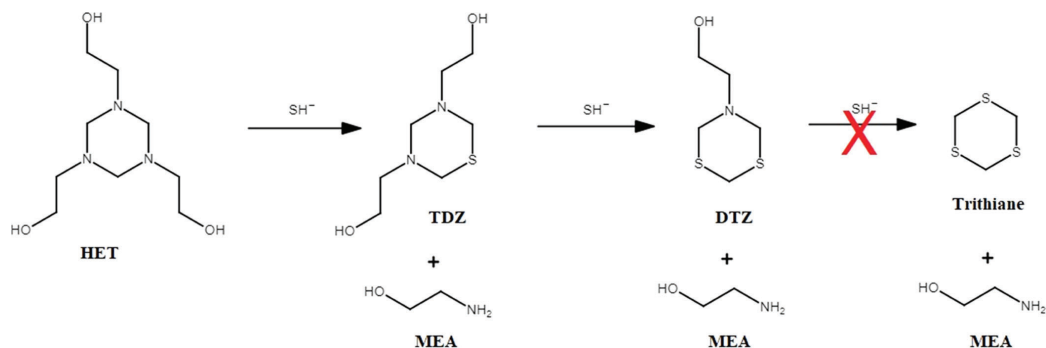


**Figure 1.** Simplified reaction scheme reporting the stoichiometry of the aqueous phase H<sub>2</sub>S scavenging reactions using MEA-triazine (HET).

12–20 kg of the commercial product for the removal of 1 kg of H<sub>2</sub>S.<sup>2</sup> The stoichiometric requirement that can be calculated from the abovementioned stoichiometry gives 6–8 kg of the commercial MEA-triazine-based scavenger per 1 kg of H<sub>2</sub>S. Thus, a large stoichiometric excess of HET is actually used by offshore oil and gas operators, which is detrimental to the environment, due to the discharge of relatively large amounts of unspent scavengers into the sea, and to the operating expenditures since a large part of the injected HET is actually not reacting with H<sub>2</sub>S.<sup>13</sup> The application of a large excess of MEA-triazine is a conservative measure owing to the insufficient fundamental physicochemical knowledge of the absorption–reaction process and consequent lack of predictability of the outcome of the operation as a function of design variables (e.g., injector type, gas velocity, temperature, and partial pressures).<sup>2,14</sup> The lack of experimental quantitative data on the rate of the H<sub>2</sub>S scavenging reaction with HET is one of the factors hindering the development of physicochemical models of the absorption–reaction process, which could allow a rational design of this operation.

To the best of our knowledge, quantitative experimental data on the rate of the aqueous phase reaction of HS<sup>-</sup> with HET have not been reported in the literature, except for the work of Bakke and Buhaug.<sup>6</sup> However, in their work, the authors focused on operating conditions under excess of HS<sup>-</sup>, which are unrealistic in field operation due to the employed excess of HET and to the concurrence of the H<sub>2</sub>S absorption and its reaction with HET in the aqueous phase. It is noted that the authors alleged that their attempts in measuring the concentration of HS<sup>-</sup> by means of a sulfide-sensitive electrode failed to provide reproducible results. Their kinetic study was thus focused on the variation of the HET concentration over time under excess of HS<sup>-</sup> with the reaction observed to be of first order with respect to HET.

A few studies recently reported in the literature proposed the use of Raman spectroscopy as a tool for monitoring H<sub>2</sub>S scavenging reactions with HET.<sup>15–17</sup> More specifically, Perez Pineiro et al.<sup>16</sup> reported the use of Raman spectroscopy for quantitation of HET and DTZ in spent scavenger samples. Furthermore, OndaVia has made available cartridges and instrumentation for the assay of HET and DTZ by Raman spectroscopy.<sup>18</sup> In a previous work from our research group,<sup>17</sup> it was shown that it is possible to online monitor the decrease of HS<sup>-</sup> over time in the scavenging reaction with HET and to detect the appearance of the characteristic Raman bands

associated with the carbon–sulfur bonds of the reaction products. However, no internal standard was used, which made the results merely qualitative. The reaction rate was however observed to depend strongly on the pH.

The objective of this work is twofold: (i) to develop a method for in situ accurate quantitative measurement of the HS<sup>-</sup> concentration during the aqueous phase reaction between HET and HS<sup>-</sup> based on Raman spectroscopy and chemometric methods for spectral preprocessing and analysis and (ii) to generate novel experimental data for the rate of disappearance of HS<sup>-</sup> in the aqueous phase scavenging reactions with HET under relevant conditions for industrial applications (i.e., excess of HET). The study is based on batch-reaction experiments carried out at room temperature for three different values of the initial pH (9, 10, and 11) and four different HET-to-HS<sup>-</sup> initial concentration ratios (in the range of 0.5–10). In addition, the methodology allows a qualitative analysis of the development of the main scavenging reaction products over time.

## 2. MATERIALS AND METHODS

**2.1. Materials.** Aqueous solutions of 1,3,5-tris(2-hydroxyethyl)hexahydro-s-triazine (HET; CAS 4719-04-4) of technical purity, hereinafter termed technical triazine solution, were used as H<sub>2</sub>S scavengers. Monoethanolamine (MEA) is the main impurity of this solution. The concentrations of HET and MEA were determined by means of GC-FID analysis, according to a method reported elsewhere,<sup>13</sup> and were found to be 2.60 ± 0.06 and 2.06 ± 0.39 M, respectively. The density of the triazine solution was measured by weighing accurately measured volumes of the solution by means of an analytical balance (Sartorius 1702, accuracy 0.1 mg). The volumes were measured by means of a precision pipette (Finn F2, 0.5–5 mL, Thermo Scientific, accuracy 0.03 mL) previously calibrated with distilled water at 20 °C. Measurements were performed in quintuplicate. The density of the triazine solution at 20 °C resulted to be 1.11 ± 0.01 g/mL. The pH of the solution was 10.9. All pH values reported in this work were measured with a pH meter (Metrohm, 914 pH/conductometer) and a microelectrode (Metrohm, 6.0234.110) calibrated prior to the execution of each experimental run with two-point calibration between pH 7.0 and 10.0 at 22 °C.

Disodium sulfide about trihydrate (Na<sub>2</sub>S·~3H<sub>2</sub>O; CAS 27610-45-3) from VWR Chemicals (product ID 83756.230) was used to prepare aqueous bisulfide solutions that were used

as both reactants and standard solutions for the determination of Raman calibration curves. The declared impurities in the product, on a water-free basis, were limited to nitrogen (max. 0.0125 wt %), sulfur trioxide (SO<sub>3</sub>, max. 0.6 wt %), and thiosulfate (S<sub>2</sub>O<sub>3</sub>, max. 0.5 wt %). The actual degree of hydration of sodium sulfide (grams of water per gram of wet solid) used for preparing the samples was measured by means of Karl Fischer (KF) titration (870 KF Titrino plus, Metrohm AG), equipped with an oven (860 KF Thermoprep, Metrohm AG) in which the sample was thermally prepared at 210 °C. KF titrations were carried out in triplicate. The degree of hydration was found to be 38.2 wt % with a relative standard deviation (RSD) equal to 1.79%.

Aqueous solutions of hydrochloric acid (HCl, 6 M) were used for pH adjustment and prepared from fuming hydrochloric acid from Merck Chemicals (product ID 1.00317, HCl ≥37 wt %). MEA from Sigma-Aldrich (product ID 02400, purity ≥99 wt %), HET from Santa Cruz Biotechnology (CAS 4719-04-4; product ID sc-474806; purity ≥95 wt %), and DTZ from Toronto Research Chemicals (CAS 88891-55-8; product ID D493850, purity >98 wt %) were used as analytical standards. Analytical grade acetonitrile from VWR Chemicals (product ID 83640.290, purity ≥99.9 wt %) was used as an internal standard (IS) for calibration and determination of HS<sup>-</sup> concentrations in the reaction experiments.

The aqueous solutions of reactants used in the present work were prepared with distilled water previously stripped with nitrogen for the removal of dissolved oxygen to a final concentration between 0.01 and 0.02 mg/L at 22 °C, measured with a portable oxygen meter (OxyGuard, Handy Polaris 2, measuring range 0–60 ppm, 0–600% saturation).

**2.2. Reaction Experiments.** All experiments were carried out in batch mode at room temperature (21–22 °C) with an initial concentration of HS<sup>-</sup> of 100 mM. One experimental campaign was based on a full factorial design with two factors: the initial concentration of HET (three levels: 100, 500, and 1000 mM) and the initial pH (pH<sub>0</sub>, three levels: 9, 10, and 11). For each combination, two solutions were prepared independently, which resulted in 18 reaction runs. All runs were carried out in a randomized order. Each reaction was monitored for 3 h. Subsequently, the aqueous reacting phase was acidified back to a value as close as possible to pH<sub>0</sub> and then monitored for three additional hours to allow verifying the possibility of completing the reaction.

The experimental data provided by Bakke et al.<sup>5</sup> indicate that the hydrolysis of HET at high pH values is slow enough to be neglected. The actual pH established in the aqueous phase in contact with the sour gas stream in field operational use depends on the balance between the H<sub>2</sub>S absorption, which tends to decrease the pH of the aqueous phase, and the scavenging reactions, which tend to increase it. Technical solutions of HET have a pH of around 11 (see Section 2.1), while spent scavenger samples are seen with a pH of around 9.<sup>13</sup> The pH of the aqueous phase in contact with the sour gas is expected to be in the range from 8–9 to 11–12. Based on the rate constants determined by Bakke et al.,<sup>5</sup> the expected loss of HET due to hydrolysis in our experiments should not be above 0.22%. Therefore, the initial pH values applied in this work allow neglecting the hydrolysis of HET as a side reaction. In addition, the reacidifications allowed restoring pH values within the ranges of interest in field operation, while restarting the reactions in the presence of unconverted bisulfide and HET and therefore acquiring additional experimental data.

A second experimental campaign was carried out with an initial concentration of HET of 50 mM, at three levels of pH<sub>0</sub>: 9, 10, and 11. Also in this case, experiments for each combination of the two factors were carried out in duplicate with independent preparation of the solutions charged to the reactor. This experimental campaign was planned after analyzing the data of the first experimental campaign with the aim of analyzing the reacting system at high fractional conversions of HET and high yields of DTZ. In all of the experiments of the second campaign, the reacting system was monitored for a total time of 6 h and acidified back to values close to pH<sub>0</sub> three times (after 3.0, 4.0, and 5.0 h). In total, 24 reaction experiments were carried out in the two campaigns.

With regard to the execution of the reactions, a certain mass of the technical triazine solution (1.07, 2.13, 10.65, or 21.31 g) was diluted in distilled water, conditioned to the desired pH<sub>0</sub>, and brought to 25 mL with further addition of distilled water using a class A volumetric flask. A certain mass of Na<sub>2</sub>S·~3H<sub>2</sub>O (ca. 0.64 g), whose degree of hydration was preliminarily measured, was dissolved in distilled water, mixed with a certain amount of IS (ca. 0.21 g), pH-adjusted to the desired value, and brought to 25 mL with further addition of distilled water using a class A volumetric flask. The initial pH values of the two solutions were 9, 10, or 11. Two 10 mL aliquots of the solutions of HS<sup>-</sup> + IS and HET were withdrawn by means of glass volumetric pipettes (class A, 10 ± 0.02 mL), mixed in a Raman glass vial, closed with a threaded lid, and placed inside a dark camera for in situ monitoring of the scavenging reactions. The time elapsed from the start of the mixing of the reagent solutions (reaction time zero) to the start of the spectral acquisition was in the range of 18–25 s.

After 3 h of monitoring time, the pH of the reacting system was measured. The pH was found to increase in all cases. Then, the system was reacidified following the above-mentioned procedure. For all cases, the time elapsed from the end of a stage of the reaction (i.e., prior to a reacidification) to the start of new spectral acquisition (i.e., after the reacidification) was in the range of 2–5 min.

**2.3. Raman Spectroscopy and Data Analysis.** The quantitation of aqueous solutions containing HS<sup>-</sup> was carried out by Raman spectroscopy (Rxn1-785, Kaiser Optical Systems) using a 785 nm laser as the source of excitation light with a noncontact probe. The solutions were put into a glass vial suitable for Raman spectroscopy analyses (capacity 20 mL) placed inside a dark camera to avoid the entrance of external light into the system. The spectra were taken by the probe located around 1 cm from the vial. For each acquisition, three consequent spectra were recorded using 5 s excitation time and averaged to increase the signal-to-noise ratio.

To measure the concentration of HS<sup>-</sup>, a partial least squares regression (PLSR)<sup>19</sup> model was calibrated. The calibration was based on Raman spectra acquired for solutions containing 100 mM internal standard (IS) and HS<sup>-</sup> concentration varying in the range of 10–100 mM (10 concentration levels in total with equal step size). The pH of the solutions was set to 9.0 ± 0.2. Each standard solution was prepared independently and in triplicate giving 30 samples in total.

To make the regression model robust, the spectra were preprocessed and truncated before the calibration. The best results were achieved using a two-step preprocessing procedure: baseline correction using the alternating least squares method<sup>20</sup> with a lambda of 10<sup>5</sup> and a penalty of 0.025 and normalization of the corrected spectra to the sum of

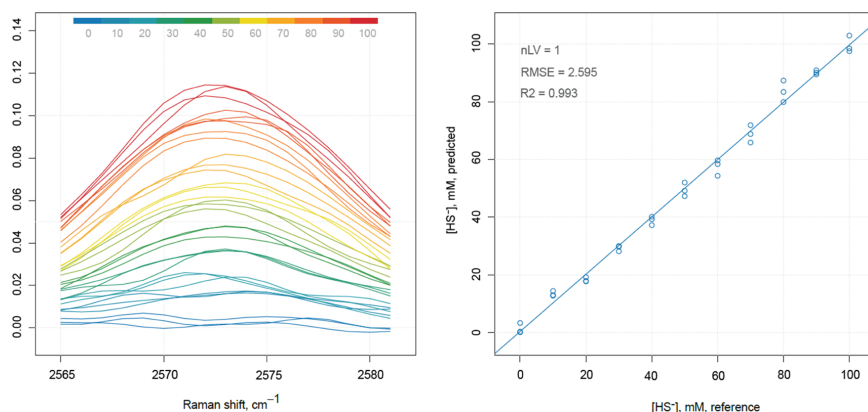


**Figure 2.** Calibration of the PLS regression model. The left plot shows the preprocessed and truncated Raman spectra used for the calibration of the model (the lines are color grouped according to the concentration of HS<sup>-</sup>) with the ordinate axis representing the peak intensity. The color legend shows the concentrations of HS<sup>-</sup> expressed in mM. The right plot shows predicted versus measured values and the main performance statistics for the final PLSR model (cross-validated results).

intensities between wavenumbers 2255 and 2265 cm<sup>-1</sup>, corresponding to the area around the IS peak. After that, the spectra were truncated around the characteristic Raman shift for HS<sup>-</sup> identified at 2575 cm<sup>-1</sup> (2565–2581 cm<sup>-1</sup>). The preprocessed and truncated spectra used for calibration of the PLSR model are shown in the left part of Figure 2. The color gradient is utilized to illustrate the concentration of HS<sup>-</sup> in the solution, for which the spectra were acquired. Because neither the characteristic peak of HS<sup>-</sup> nor the IS peak overlaps with the Raman peaks of the other reaction products, this procedure makes it possible to use the regression model also for the solutions, where other chemical components are present.

The selection of the best preprocessing conditions was carried out based on the cross-validation results using PLSR models with one component. The prediction performance of the final model is characterized by a coefficient of determination (R<sup>2</sup>) equal to 0.993 and root-mean-squared error (RMSE) equal to 2.595 mM. The right part of Figure 2 demonstrates the corresponding predicted versus measured values for HS<sup>-</sup> for cross-validated predictions.

The final model was also validated on a test set, i.e., another set of bisulfide solutions prepared using pH 9, 10, and 11. The test results showed that the prediction performance of the model calibrated using samples with pH 9 works equally well for the samples with pH 10 and 11, so the same regression model can be used for a wide range of pH values.

The developed PLSR model was then employed for online prediction of HS<sup>-</sup> during the scavenging reactions. The in situ analysis of the reaction mixtures was performed with autosampling acquiring the average of the three spectra for 5 s in intervals of 30 s. In total, 720 spectra were collected in each reaction experiment.

The data analysis and all visualizations were performed in R (v. 4.0.2)<sup>21</sup> using the package mdatools.<sup>22</sup> The package hyperSpec<sup>23</sup> was utilized to import spectral data from spectral files created by the spectrometer.

In addition, characteristic Raman bands were identified for HET, MEA, and DTZ by analyzing the Raman spectra of analytical standards. Aqueous solutions of the analytical

standards of HET (100 mM) and DTZ (20 mM) were prepared using distilled water, while analytical grade MEA was used without previous dilution. Spectra of the solutions were acquired with the same equipment and procedure described above. The spectra were slightly denoised using a Savitzky–Golay filter, normalized to a unit length, and truncated to the range from 300 to 2500 cm<sup>-1</sup>. Transformations and plots were performed in R using the package mdatools.<sup>22</sup>

### 3. RESULTS AND DISCUSSION

**3.1. Effect of HET Concentration and pH on the Scavenging Reactions.** The initial concentrations of HET, MEA, HS<sup>-</sup>, and IS, as well as the initial pH of the 12 operating conditions, are available in the Supporting Information (Table S1). Besides the scavenging reactions in the presence of HET, two additional experiments were carried out to verify the stability of the Raman peaks of MEA, HS<sup>-</sup>, and IS in the absence of HET. Both experiments revealed the stable intensity of the Raman peaks, as shown in the Supporting Information (Figures S1 and S2). All reaction samples were homogeneous and transparent in all runs and at any reaction time without any sign of solid precipitation.

Figures 3–5 show the effect of the initial concentration of HET and pH<sub>0</sub> on the conversion of HS<sup>-</sup>. The vertical dashed lines correspond to the acidification of the reacting system back to the initial pH carried out after 3 h. The dotted lines correspond to the additional reacidifications, which were carried out in the runs with an initial concentration of HET of 50 mM only (see Section 2.2). The plot also reports the values of pH after 3 h (just before the first acidification) and the pH values after 6 h. The figures refer to one of the two duplicates, for ease of visualization. The duplicates show the same features and match very well with ARD values in the first 3 h (prior to acidification) in the range of 3.1–10.4% for the 12 operating conditions, being 5.3% on average. After the first 3 h of reaction, qualitatively reproducible trends were observed for all executions. The complete set of figures, together with ARD values for each duplicate execution, is reported in Figures S3–S5 and Table S2 of the Supporting Information.



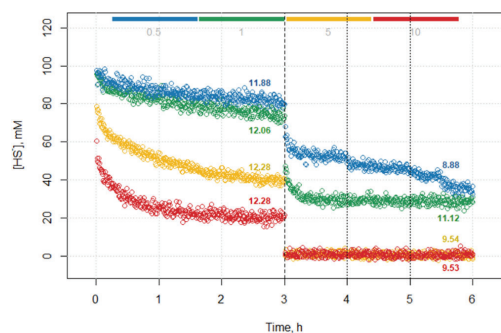


**Figure 3.** Effect of the initial concentration of HET on the conversion of HS<sup>-</sup> for pH<sub>0</sub> = 9. The colors are associated with different values of the initial concentration ratio HET/HS<sup>-</sup>: blue 0.5; green 1; yellow 5; and red 10. The numbers on the plot report the measured pH values after 3 h (before the first acidification) and 6 h. Vertical dashed line: reacidification after 3 h (all samples). Dotted lines: additional reacidifications (only for the initial concentration ratio HET/HS<sup>-</sup> of 0.5).

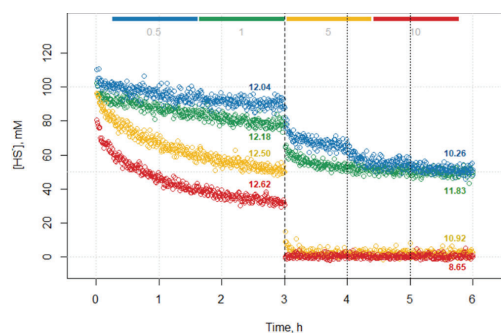


**Figure 4.** Effect of the initial concentration of HET on the conversion of HS<sup>-</sup> for pH<sub>0</sub> = 10. The colors are associated with different values of the initial concentration ratio HET/HS<sup>-</sup>: blue 0.5; green 1; yellow 5; and red 10. The numbers on the plot report the measured pH values after 3 h (before the first acidification) and 6 h. Vertical dashed line: reacidification after 3 h (all samples). Dotted lines: additional reacidifications (only for the initial concentration ratio HET/HS<sup>-</sup> of 0.5).

As can be seen from Figures 3–5, the decrease in the reaction rate is very pronounced as the time increases, with the concentration of HS<sup>-</sup> appearing not to reduce to zero. Concurrently, the pH of the reacting system largely increases during the reaction, reaching values above 11.8 for all runs. The increase of pH is in line with the reaction mechanism involving the protonation of HET and TDZ, as reported in Section 1. In fact, the consumption of HET and TDZ cations due to the scavenging reactions induces new HET and TDZ molecules to be protonated according to Le Chatelier's principle, thus consuming H<sub>3</sub>O<sup>+</sup> and raising the pH of the solution. In turn, higher pH values reduce the fraction of HET and TDZ existing in the protonated form, as typical pK<sub>a</sub> values of amines are in the range of 7–11,<sup>24</sup> thus reducing the availability of HET and TDZ cations and inhibiting the scavenging reactions themselves. The effect is particularly

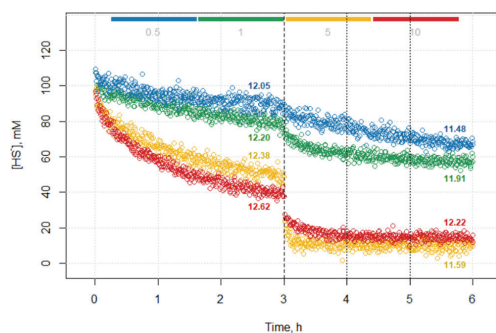


**Figure 5.** Effect of the initial concentration of HET on the conversion of HS<sup>-</sup> for pH<sub>0</sub> = 11. The colors are associated with different values of the initial concentration ratio HET/HS<sup>-</sup>: blue 0.5; green 1; yellow 5; and red 10. The numbers on the plot report the measured pH values after 3 h (before the first acidification) and 6 h. Vertical dashed line: reacidification after 3 h (all samples). Dotted lines: additional reacidifications (only for the initial concentration ratio HET/HS<sup>-</sup> of 0.5).

visible at the lowest initial pH (Figure 3) for the largest excess of HET (initial concentration ratio of 10), where approximately 60% of the initial HS<sup>-</sup> is converted in the first 7 min of reaction, while only additional 20% is converted by the end of 3 h. At this point, the concentration of HS<sup>-</sup> stabilizes at values around 20 mM even in the presence of a large excess of HET still available. As can be seen, the pH of the system reached values close to 12.3, at which the fraction of HET and TDZ existing in the protonated form must be extremely small when considering the abovementioned pK<sub>a</sub> values. Additionally, in this case, the acidification carried out at 3 h caused the swift and complete depletion of the unreacted HS<sup>-</sup> in only approximately 2 min, clearly showing that the previous reaction stop was caused by high pH and not by the reduction in the concentration of HET and HS<sup>-</sup>. The same pattern is observed for an initial concentration ratio of 5. The fact that HS<sup>-</sup> can be completely depleted shows that the scavenging process is irreversible at room temperature, provided that the pH is maintained at values below approximately 12. At lower HET/HS<sup>-</sup> initial concentration ratios, such an abrupt change in the rate of reaction is not observed because the reaction is slower and, therefore, the pH increase is also slower.

Figures 3–5 also show the effect of the excess of HET on the rate of reaction for given initial pH values. The rate of conversion of HS<sup>-</sup> is observed to increase substantially with the initial concentration of HET. Bakke and Buhaug<sup>6</sup> proposed a first-order reaction with respect to HET, with the information on the rate equation derived under the assumption of constant pH attained with a 0.5 M Na<sub>2</sub>HPO<sub>4</sub> buffer. We also carried out the reaction in the presence of the same buffer and measured the pH of the reacting system online (see Figure S6 in the Supporting Information); however, we observed a substantial variation of pH even in the presence of such a buffer. Therefore, the kinetic determinations of Bakke and Buhaug<sup>6</sup> are considered only qualitative. Overall, it can yet be stated that the positive correlation between the concentration of HET and the rate of reaction is not in disagreement with the findings of Bakke and Buhaug.<sup>6</sup>

Table 1 shows numerical examples of the fractional conversion of  $\text{HS}^-$  at specified times. For instance, after 1 h

**Table 1. Values of Fractional Conversion of  $\text{HS}^-$  ( $X$ ) before (1 and 3 h) and after Acid Injection (6 h) with Corresponding Standard Deviation (SD) Values**

[HET] <sub>0</sub> /[HS <sup>-</sup> ] <sub>0</sub>	pH <sub>0</sub>	X %		
		1 h	3 h	6 h
0.5	9	11.6 ± 5.4	21.8 ± 2.5	63.2 ± 0.2
0.5	10	6.0 ± 3.1	12.7 ± 1.1	50.9 ± 1.0
0.5	11	5.8 ± 1.4	12.5 ± 3.3	38.9 ± 8.5
1	9	17.3 ± 1.3	28.3 ± 3.0	72.4 ± 1.3
1	10	11.4 ± 1.5	20.9 ± 0.6	48.7 ± 1.9
1	11	7.8 ± 4.5	17.2 ± 2.0	42.3 ± 0.5
5	9	47.5 ± 4.7	59.7 ± 0.4	99.0 ± 1.4
5	10	31.9 ± 0.7	49.9 ± 0.0	99.8 ± 0.3
5	11	30.7 ± 9.7	45.9 ± 7.8	79.5 ± 11.5
10	9	71.8 ± 2.8	79.9 ± 2.1	99.0 ± 0.4
10	10	53.1 ± 2.0	68.7 ± 1.1	99.6 ± 0.5
10	11	41.4 ± 2.4	63.7 ± 2.1	86.1 ± 2.5

of reaction for pH<sub>0</sub> = 9, the fractional conversion of  $\text{HS}^-$  increases from 12 to 72% as the initial concentration of HET is increased from 50 to 1000 mM. The same trend is observed at higher initial pH values, i.e., 10 and 11, even though the maximum fractional conversions obtained for the cases with 1000 mM HET reach 53 and 41%, respectively, due to the

inhibition of high pH values. For fixed values of the initial concentration ratio HET/ $\text{HS}^-$  and reaction time, the reduction of the fractional conversion with the increase of the initial pH is clearly visible in Table 1.

**3.2. Identification and Monitoring of Key Species in the Scavenging Reactions.** The acquired spectra of analytical standards of HET, DTZ, and MEA were analyzed to identify characteristic Raman peaks to monitor qualitatively the progress of the scavenging reactions, besides the quantitative analysis of the rate of disappearance of  $\text{HS}^-$  discussed in Section 3.1. The acquired spectra are shown in Figure S7 in the Supporting Information. As a result of the analysis, the peaks used as indicators of HET, DTZ, and MEA are, respectively, 923, 675, and 840  $\text{cm}^{-1}$ , which are consistent with the information available in the literature.<sup>15,16,18</sup>

Figure 6 shows the evolution of the spectra over time in one of the reaction runs for pH<sub>0</sub> = 9 and an HET/ $\text{HS}^-$  initial concentration ratio of 0.5 in the period between 3 and 6 h of reaction. The selected peaks for HET, DTZ, and MEA are clearly observable in the reaction spectra. Even though the selected peak for DTZ is partially overlapping with a broad peak from HET (approximately 700  $\text{cm}^{-1}$ ), the latter is observed to be constant during the scavenging reaction. This makes it possible to associate, on a qualitative level, the variations of the peak at 675  $\text{cm}^{-1}$  with the variations of the concentration of DTZ. Noticeably, there is a clear decrease in the peaks of  $\text{HS}^-$  and HET and a concurrent increase in the peaks of MEA and DTZ. The development of the peak at 634

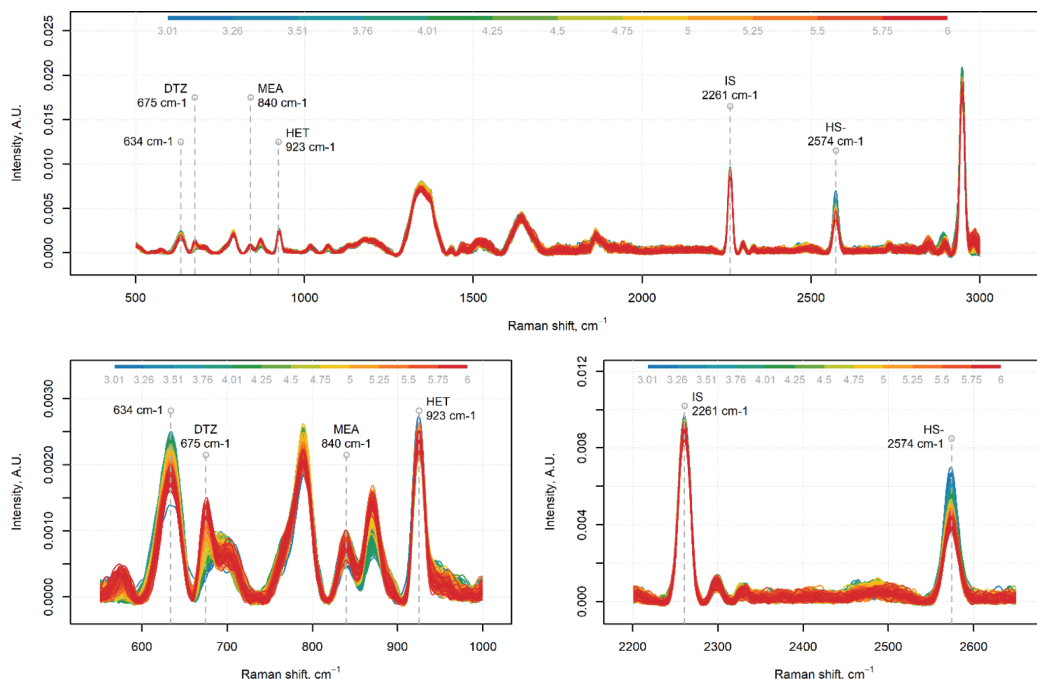


**Figure 6.** Raman spectra of the aqueous phase reaction between  $\text{HS}^-$  and HET at pH<sub>0</sub> = 9 and an initial concentration ratio of 0.5, from  $t = 3$  to 6 h (after acidification), colored by reacting time. The color legend shows the reaction times in hours. Selected peaks for HET, DTZ, and MEA, as well as peaks for  $\text{HS}^-$  and internal standard (IS), are indicated with gray dashed lines.

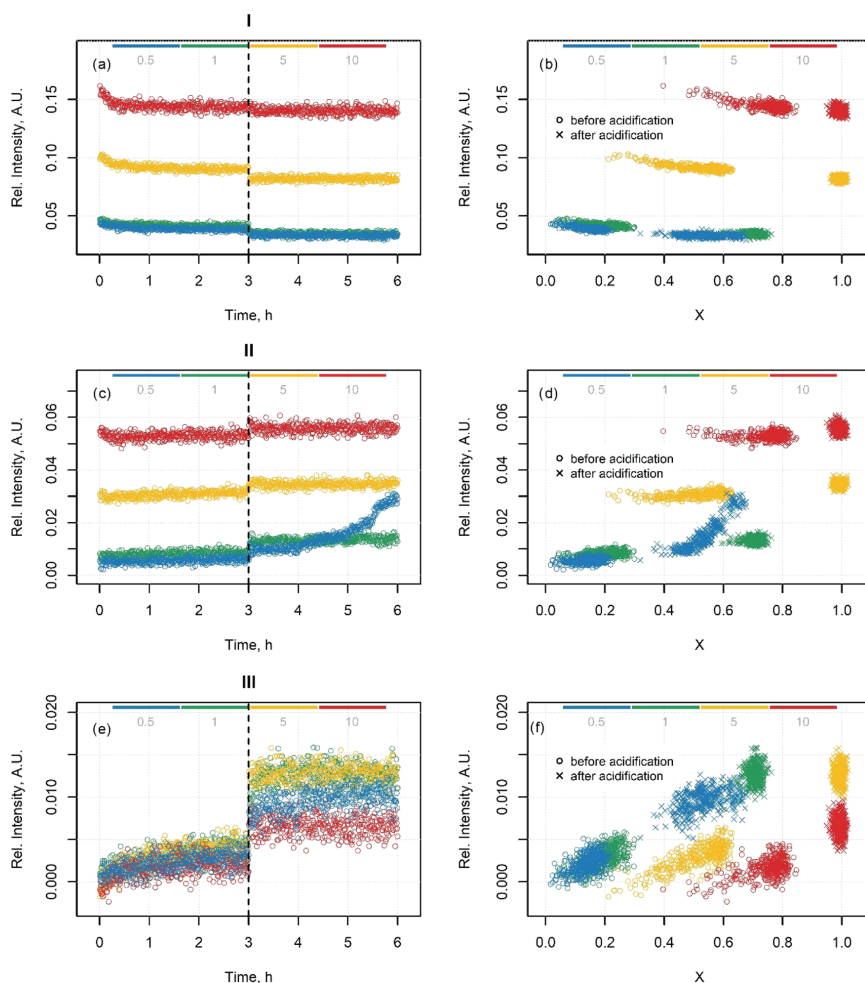


**Figure 7.** Relative intensity of peaks for executions at  $\text{pH}_0 = 9$  as a function of time (a, c, e) and as a function of  $\text{HS}^-$  fractional conversion (b, d, f) for HET (I), DTZ (II), and MEA (III).

$\text{cm}^{-1}$  is also noted, which shows a maximum point followed by a decrease with the advancement of the scavenging reaction, suggesting to be related to an intermediate product of the series of reactions. This peak may be representative of TDZ, in line with the Raman band associated with TDZ by Perez Pineiro et al.<sup>15</sup> Moreover, Figure 7 shows the relative intensity (with respect to the height of the IS peak) of the selected peaks as a function of time and the fractional conversion of  $\text{HS}^-$  ( $X$ ) corresponding to reactions at  $\text{pH}_0 = 9$  and four levels of HET/ $\text{HS}^-$  initial concentration ratios. In all of the cases, the acidification of the system at  $t = 3$  h causes a sudden change in the intensity of the peaks of HET, DTZ, and MEA, which clearly indicates how the pH reduction increases the rate of the scavenging reactions. In the cases of HET/ $\text{HS}^-$  initial concentration ratios of 5 and 10, i.e., large excess of HET, the sudden change is associated with swift and complete

depletion of  $\text{HS}^-$  ( $X = 1$ ), and it is therefore followed by stable signals. For an HET/ $\text{HS}^-$  initial concentration ratio of 1, the sudden change is associated with a swift increase in the fractional conversion of  $\text{HS}^-$ , from approximately 0.3 to 0.6, which is followed by the slow additional consumption of HET and the formation of DTZ. For an HET/ $\text{HS}^-$  initial concentration ratio of 0.5, the acidification leads to a swift increase in the fractional conversion of  $\text{HS}^-$ , from approximately 0.2 to 0.4. Interestingly, in this case, the trend of the intensity of the DTZ peak exhibits an upward concavity until approximately 5.5 h, meaning that the rate of formation of DTZ increases over time, which is observed only at these conditions. This can be explained by the second scavenging reaction progressing to a larger extent, compared to cases where a large excess of HET is present, where the scavenging of  $\text{HS}^-$  is mainly attained by the first scavenging reaction.

Regarding MEA ( $840 \text{ cm}^{-1}$ ), a linear increase of its peak intensity with respect to the fractional conversion of  $\text{HS}^-$  is observed. This is in line with the expected formation of MEA from both the first and second scavenging reactions, with a 1:1 stoichiometric ratio with respect to  $\text{HS}^-$  in both reactions. All of the cases related to the trends of the selected peaks at different initial pH values are available in Figures S8–S22 in the Supporting Information.

#### 4. CONCLUSIONS

We are the first to provide quantitative measurements of  $\text{HS}^-$ , the prevailing form of  $\text{H}_2\text{S}$  in basic aqueous solutions of scavengers, during the aqueous phase scavenging reactions with MEA-triazine. This result was accomplished by in situ acquisition of Raman spectra and the application of a PLS regression model. The results confirm that the rate of the scavenging process with MEA-triazine is strongly dependent on pH and that high pH values inhibit the reactions. This is in line with the currently accepted reaction mechanism, which is based on the protonation of HET and DTZ followed by the reaction with  $\text{HS}^-$ . A remarkable dependence of the rate of disappearance of  $\text{HS}^-$  on the concentration of HET is also observed with the  $\text{HS}^-$  conversion being faster at higher concentrations of HET. In addition, it is observed that the buildup of DTZ is strongly dependent on the initial HET/ $\text{HS}^-$  ratio: low amounts of DTZ are formed in the presence of high excess of HET, whereas a substantial buildup of DTZ can be observed with the stoichiometric ratio HET/ $\text{HS}^-$  (i.e., 0.5) in the feed and long reaction times. The experimental measurements and the qualitative observations of this work are expected to pave the way for the development of kinetic models of the aqueous phase reactions between  $\text{HS}^-$  and HET, which are still lacking in the literature.

#### ■ ASSOCIATED CONTENT

##### Supporting Information

The Supporting Information is available free of charge at <https://pubs.acs.org/doi/10.1021/acs.iecr.1c03833>.

Initial concentrations and initial pH values for the two experimental campaigns and the stability tests of  $\text{HS}^-$ , MEA, and IS in water; plots showing the effect of the initial concentration of HET on the conversion of  $\text{HS}^-$  for duplicate executions at  $\text{pH}_0 = 9, 10, \text{ and } 11$ ; average relative deviation (ARD) of all of the executions before the first acidification; online pH measurements for one reaction experiment using a pH buffer solution; Raman spectra of analytical standards of HET, DTZ, and MEA; and plots of the intensity of the peaks at 923, 634, 675, and  $840 \text{ cm}^{-1}$  for all of the executions at  $\text{pH}_0 = 9, 10, \text{ and } 11$  (PDF)

#### ■ AUTHOR INFORMATION

##### Corresponding Author

Marco Maschietti – Department of Chemistry and Bioscience, Aalborg University Esbjerg, 6700 Esbjerg, Denmark;  
● [orcid.org/0000-0002-3120-7560](https://orcid.org/0000-0002-3120-7560); Email: [marco@bio.aau.dk](mailto:marco@bio.aau.dk)

##### Authors

Iveth Romero – Department of Chemistry and Bioscience, Aalborg University Esbjerg, 6700 Esbjerg, Denmark

Sergey Kucheryavskiy – Department of Chemistry and Bioscience, Aalborg University Esbjerg, 6700 Esbjerg, Denmark

Complete contact information is available at:  
<https://pubs.acs.org/10.1021/acs.iecr.1c03833>

#### Notes

The authors declare no competing financial interest.

#### ■ ACKNOWLEDGMENTS

This work was financially supported by the Energiteknologiske Udviklings-og Demonstrationsprogram (EUDP, Energy Technology Development and Demonstration Program), Denmark (SCAVOP project, project number 64018-0819). The authors are grateful to Anders Andreassen (Ramboll) for the inspiring discussions on the topic in general and for his comments on the manuscript, to Rudi P. Nielsen (Aalborg University) for the inspiring discussions on technical aspects of the experimental executions, and to Susanne Tolstrup for proof-reading the manuscript.

#### ■ REFERENCES

- (1) Wylde, J. J.; Taylor, G. N.; Sorbie, K. S.; Samaniego, W. N. Formation, Chemical Characterization and Oxidative Dissolution of Amorphous Polymeric Dithiazine (Apdtz) During the Use of the  $\text{H}_2\text{S}$  Scavenger Monoethanolamine-Triazine. *Energy Fuels* **2020**, *34*, 9923–9931.
- (2) Kelland, M. Hydrogen Sulfide Scavengers. In *Production Chemicals for the Oil and Gas Industry*; CRC Press: Boca Raton, 2014; pp 353–368.
- (3) Taylor, G.; Smith-Gonzalez, M.; Wylde, J.; Oliveira, A.  $\text{H}_2\text{S}$  Scavenger Development During the Oil and Gas Industry Search for an MEA Triazine Replacement in Hydrogen Sulfide Mitigation and Enhanced Monitoring Techniques Employed During Their Evaluation, Proceedings of the SPE International Conference on Oilfield Chemistry, Galveston, Texas, 2019; SPE-193536-MS.
- (4) Taylor, G. N.; Matherly, R. Gas Chromatography Mass Spectrometric Analysis of Chemically Derivatized Hexahydrotriazine-Based Hydrogen Sulfide Scavengers: 1. *Ind. Eng. Chem. Res.* **2010**, *49*, 5977–5980.
- (5) Bakke, J. M.; Buhaug, J.; Riha, J. Hydrolysis of 1,3,5-Tris(2-Hydroxyethyl)Hexahydro-S-Triazine and Its Reaction with  $\text{H}_2\text{S}$ . *Ind. Eng. Chem. Res.* **2001**, *40*, 6051–6054.
- (6) Bakke, J. M.; Buhaug, J. B. Hydrogen Sulfide Scavenging by 1,3,5-Triazinanes. Comparison of the Rates of Reaction. *Ind. Eng. Chem. Res.* **2004**, *43*, 1962–1965.
- (7) Taylor, G. N.; Matherly, R. Gas Chromatographic-Mass Spectrometric Analysis of Chemically Derivatized Hexahydrotriazine-Based Hydrogen Sulfide Scavengers: Part II. *Ind. Eng. Chem. Res.* **2010**, *49*, 6267–6269.
- (8) Taylor, G. N.; Matherly, R. Structural Elucidation of the Solid Byproduct from the Use of 1,3,5-Tris(Hydroxyalkyl)Hexahydro-S-Triazine Based Hydrogen Sulfide Scavengers. *Ind. Eng. Chem. Res.* **2011**, *50*, 735–740.
- (9) Madsen, H. T.; Sogaard, E. G. Use of ESI-MS to Determine Reaction Pathway for Hydrogen Sulphide Scavenging With 1,3,5-Tris(2-Hydroxyethyl)-Hexahydro-S-Triazine. *Eur. J. Mass Spectrom.* **2012**, *18*, 377–383.
- (10) Taylor, G. N.; Prince, P.; Matherly, R.; Ponnappati, R.; Tompkins, R.; Vaithilingam, P. Identification of the Molecular Species Responsible for the Initiation of Amorphous Dithiazine Formation in Laboratory Studies of 1,3,5-Tris(Hydroxyethyl)-Hexahydro-S-Triazine as a Hydrogen Sulfide Scavenger. *Ind. Eng. Chem. Res.* **2012**, *51*, 11613–11617.

(11) Madsen, H. T.; Søgaard, E. G. Fouling Formation During Hydrogen Sulfide Scavenging with 1,3,5-Tri-(Hydroxyethyl)-Hexahydro-S-Triazine. *Pet. Sci. Technol.* **2014**, *32*, 2230–2238.

(12) Fiorot, R. G.; Carneiro, J. W. D. M. The Mechanism for H<sub>2</sub>S Scavenging by 1,3,5-Hexahydrotriazines Explored by DFT. *Tetrahedron* **2020**, *76*, No. 131112.

(13) Montesantos, N.; Fini, M. N.; Muff, J.; Maschietti, M. Proof of Concept of Hydrothermal Oxidation for Treatment of Triazine-Based Spent and Unspent H<sub>2</sub>S Scavengers from Offshore Oil and Gas Production. *Chem. Eng. J.* **2022**, *427*, No. 131020.

(14) Lioliou, M. G.; Jenssen, C. B.; Øvsthus, K.; Brurås, A. M.; Aasen, Ø. L. Design Principles for H<sub>2</sub>S Scavenger Injection Systems. Presented at the Oilfield Chemistry Symposium, Geilo, Norway, March 2018.

(15) Perez Pineiro, R.; Peeples, C. A.; Hendry, J.; Hoshowski, J.; Hanna, G.; Jenkins, A. Raman and DFT Study of the H<sub>2</sub>S Scavenger Reaction of HET-TRZ Under Simulated Contactor Tower Conditions. *Ind. Eng. Chem. Res.* **2021**, *60*, 5394–5402.

(16) Perez Pineiro, R.; Cruz-Perez, D.; Hoshowski, J.; Zhang, H.; Hendry, J. *H<sub>2</sub>S Scavenger Tower Operational Efficiency Achieved Through Onsite Compositional Analysis*. Volume 1, Paper No. 11553, Proceedings of the Corrosion Conference and Expo 2018; NACE International: Houston, TX, 2018; p 5336.

(17) Johansen, L. N.; Kloster, L.; Andreassen, A.; Kucheryavskiy, S.; Nielsen, R. P.; Maschietti, M. Raman Spectroscopy for Monitoring Aqueous Phase Hydrogen Sulfide Scavenging Reactions with Triazine: A Feasibility Study. *Chem. Eng. Trans.* **2019**, *74*, 541–546.

(18) OndaVia, Inc. Chemical Identification with Raman Spectroscopy: Part 2. <https://www.ondavia.com/node/99> (accessed December 2020).

(19) Wold, S.; Sjöström, M.; Eriksson, L. PLS-Regression: A Basic Tool of Chemometrics. *Chemom. Intell. Lab. Syst.* **2001**, *58*, 109–130.

(20) Eilers, P. H. C. A Perfect Smoother. *Anal. Chem.* **2003**, *75*, 3631–3636.

(21) R Development Core Team and the R Foundation. The R project for Statistical Computing. <https://www.R-project.org> (accessed May 2021).

(22) Kucheryavskiy, S. mdatools - R Package for Chemometrics. *Chemom. Intell. Lab. Syst.* **2020**, *198*, No. 103937.

(23) Beleites, C.; Sergo, V. *hyperSpec: A Package to Handle Hyperspectral Data Sets in R*. R package version 0.100.0. <https://github.com/cbeleites/hyperSpec> (accessed May 2021).

(24) Rayer, A. V.; Sumon, K. Z.; Jaffari, L.; Henni, A. Dissociation Constants (pK<sub>a</sub>) of Tertiary and Cyclic Amines: Structural and Temperature Dependences. *J. Chem. Eng. Data* **2014**, *59*, 3805–3813.

# Experimental study of the aqueous phase reaction of hydrogen sulfide with MEA-triazine using in situ Raman spectroscopy

Iveth Romero, Sergey Kucheryavskiy, Marco Maschietti

Department of Chemistry and Bioscience, Aalborg University Esbjerg, Niels Bohrs Vej 8, 6700, Esbjerg, Denmark

Supporting Information

Table S1. Experimental conditions of the reaction experiments and stability tests at room temperature.

Subscript zero represents the values in the reactor at the initial reaction time  $t = 0$ . Each experimental condition for the reaction experiments was carried out in duplicate.

$[\text{HS}^-]_0$ , mM	$[\text{HET}]_0$ , mM	$[\text{MEA}]_0$ , mM	$[\text{IS}]_0$ , mM	$\text{pH}_0$
100	50	40	100	9
100	100	79	100	9
100	500	396	100	9
100	1000	792	100	9
100	50	40	100	10
100	100	79	100	10
100	500	396	100	10

---

100	1000	792	100	10
100	50	40	100	11
100	100	79	100	11
100	500	396	100	11
100	1000	792	100	11
200	0	0	200	9
100	0	792	100	9

---

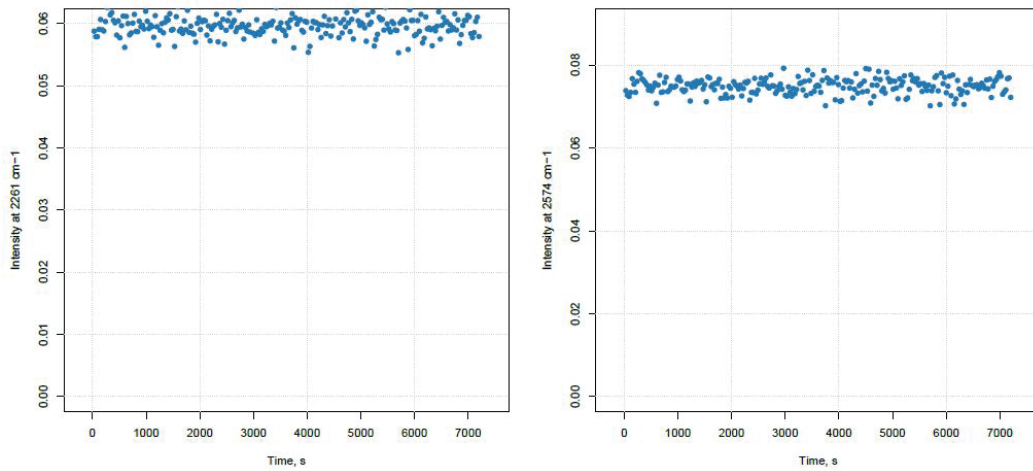


Figure S1. Intensity of the peak for HS<sup>-</sup> (2574 cm<sup>-1</sup>) and IS (2261 cm<sup>-1</sup>) in aqueous solution of HS<sup>-</sup> (200 mM) and IS (200 mM) at pH 9 monitored over 2 hours at room temperature.



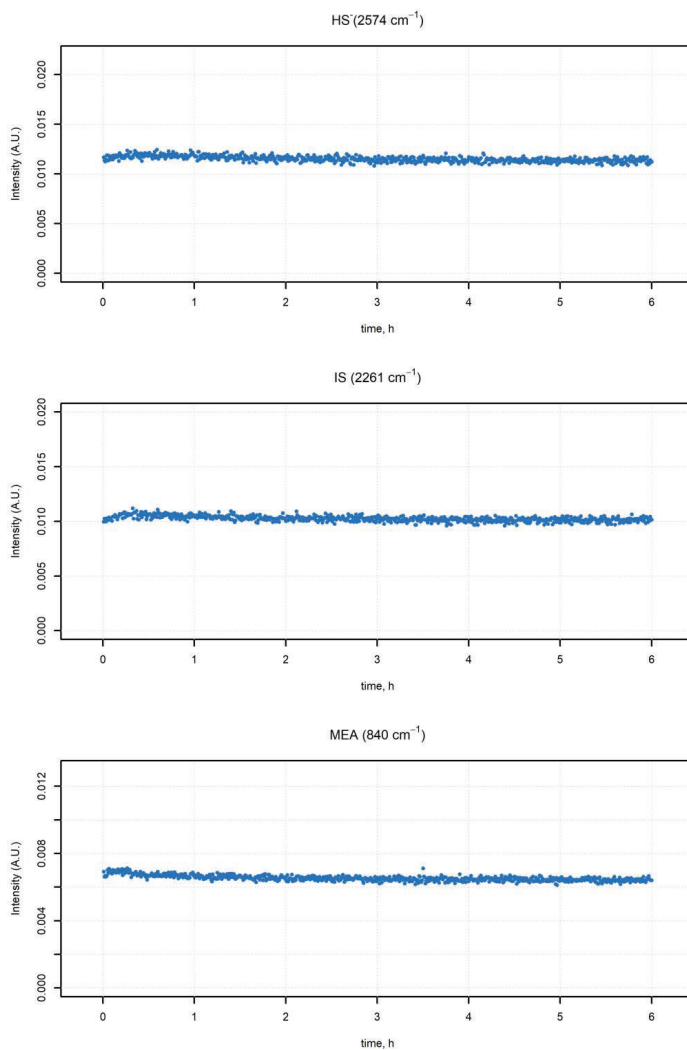


Figure S2. Intensity of peaks of HS<sup>-</sup> (2574 cm<sup>-1</sup>), IS (2261 cm<sup>-1</sup>), and MEA (840 cm<sup>-1</sup>) in aqueous solutions of HS<sup>-</sup> (100 mM), IS (100 mM), and MEA (792 mM) at pH 9 monitored over 6 hours at room temperature.

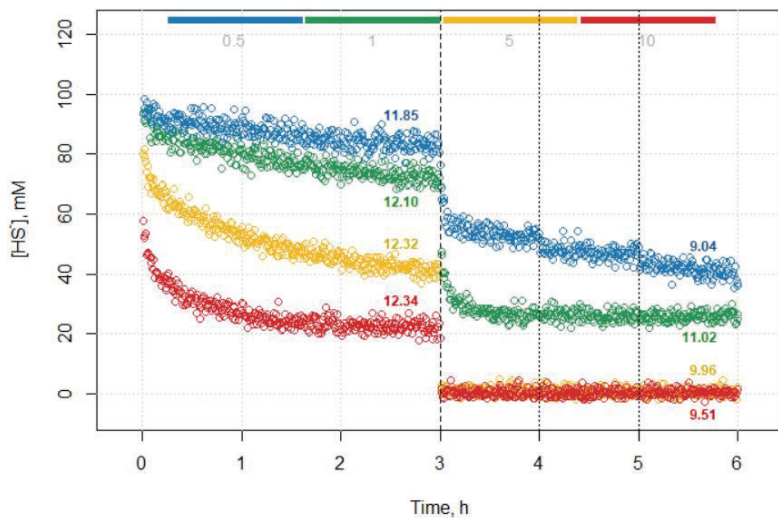


Figure S3. Effect of the initial concentration of HET on the conversion of  $\text{HS}^-$  for  $\text{pH}_0 = 9$  (execution b). The colors are associated with different values of the initial concentration ratio  $\text{HET}/\text{HS}^-$ : blue 0.5; green 1; yellow 5; red 10. The numbers on the plot also report the measured pH values after 3 h (before the first acidification) and after 6 h. Vertical dashed line: re-acidification after 3 hours (all samples). Dotted lines: additional re-acidifications (only for the initial concentration ratio  $\text{HET}/\text{HS}^-$  of 0.5).

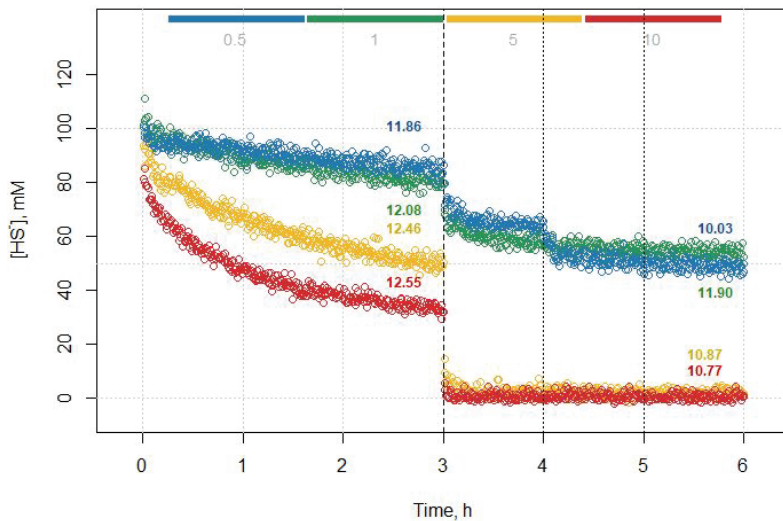


Figure S4. Effect of the initial concentration of HET on the conversion of  $\text{HS}^-$  for  $\text{pH}_0 = 10$  (execution b). The colors are associated with different values of the initial concentration ratio  $\text{HET}/\text{HS}^-$ : blue 0.5; green 1; yellow 5; red 10. The numbers on the plot also report the measured pH values after 3 h (before the first acidification) and after 6 h. Vertical dashed line: re-acidification after 3 hours (all samples). Dotted lines: additional re-acidifications (only for the initial concentration ratio  $\text{HET}/\text{HS}^-$  of 0.5).

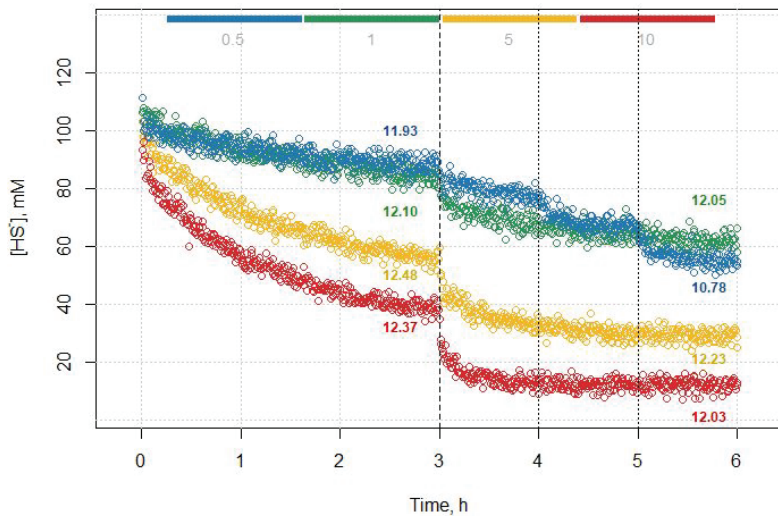


Figure S5. Effect of the initial concentration of HET on the conversion of  $\text{HS}^-$  for  $\text{pH}_0 = 11$  (execution b). The colors are associated with different values of the initial concentration ratio  $\text{HET}/\text{HS}^-$ : blue 0.5; green 1; yellow 5; red 10. The numbers on the plot also report the measured pH values after 3 h (before the first acidification) and after 6 h. Vertical dashed line: re-acidification after 3 hours (all samples). Dotted lines: additional re-acidifications (only for the initial concentration ratio  $\text{HET}/\text{HS}^-$  of 0.5).

Table S2. Average relative deviation (ARD) for all executions before acidification (first 3 hours).

<b>[HET]/[HS<sup>-</sup>] ratio</b>	<b>pH<sub>0</sub></b>	<b>ARD, %</b>
0.5	9	3.1
0.5	10	5.1
0.5	11	3.5
1	9	3.8
1	10	3.5
1	11	5.3
5	9	5.0
5	10	3.9
5	11	10.4
10	9	9.9
10	10	5.3
10	11	4.9

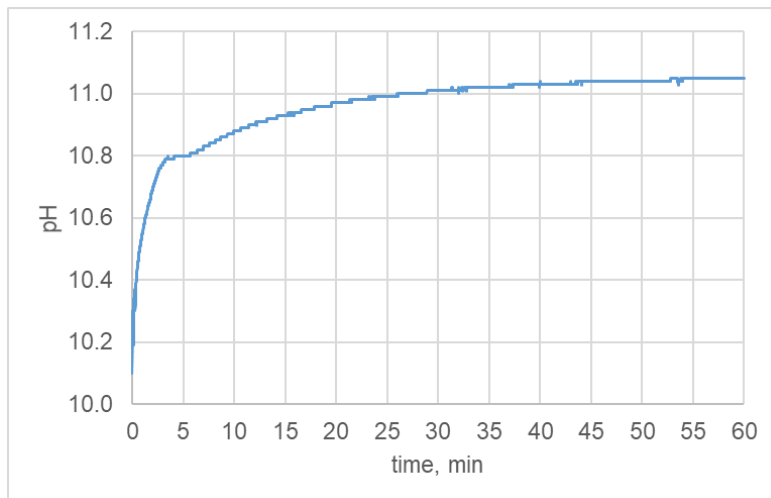


Figure S6. On-line pH measurements for 1 hour of reaction using a 0.5 M solution of  $\text{Na}_2\text{HPO}_4$  as pH buffer. Reaction at room temperature,  $\text{pH}_0 = 10$ , initial concentrations of HET and  $\text{HS}^-$  equal to 100 mM each.

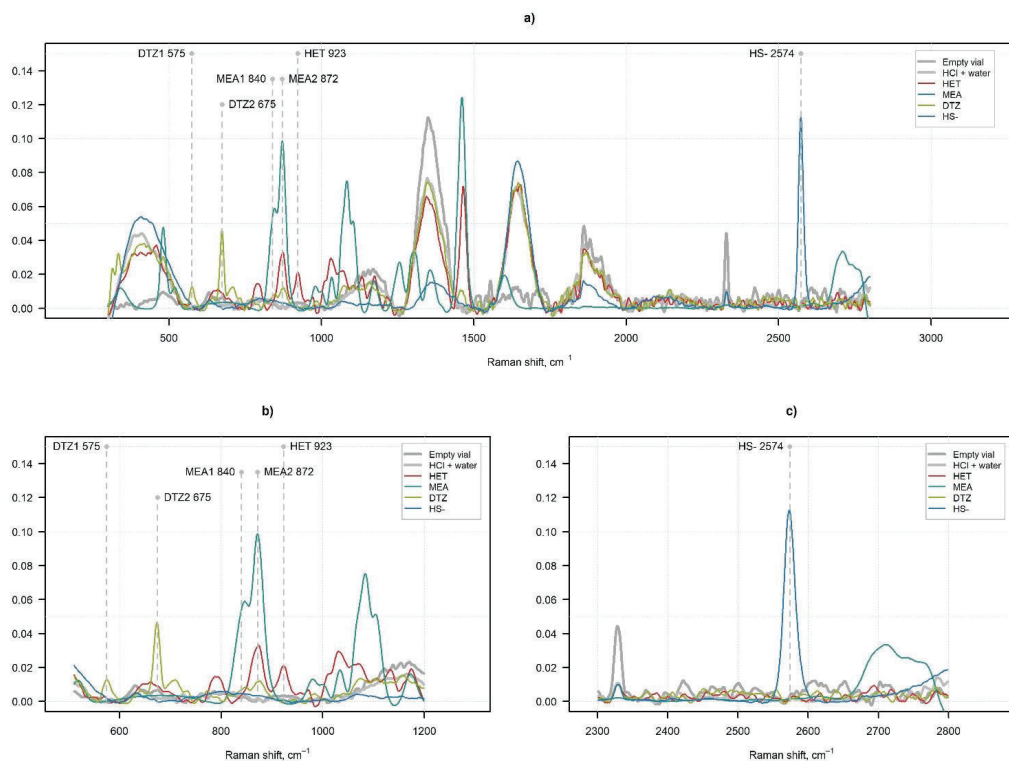


Figure S7. Spectra of analytical standards of HET, DTZ and MEA, as well as acetoneitrile (IS) and bisulfide ( $\text{HS}^-$ ), used for identification of their corresponding Raman bands. a) Spectra obtained by juxtaposition of the Raman acquisition on different analytical standard of individual species. Spectra of glass vial, water and solution for pH adjustment (HCl) are also indicated. b) Zoom in region 500 – 1200  $\text{cm}^{-1}$ . c) Zoom in region 2300 – 2800  $\text{cm}^{-1}$  for better visualization of  $\text{HS}^-$  peak.

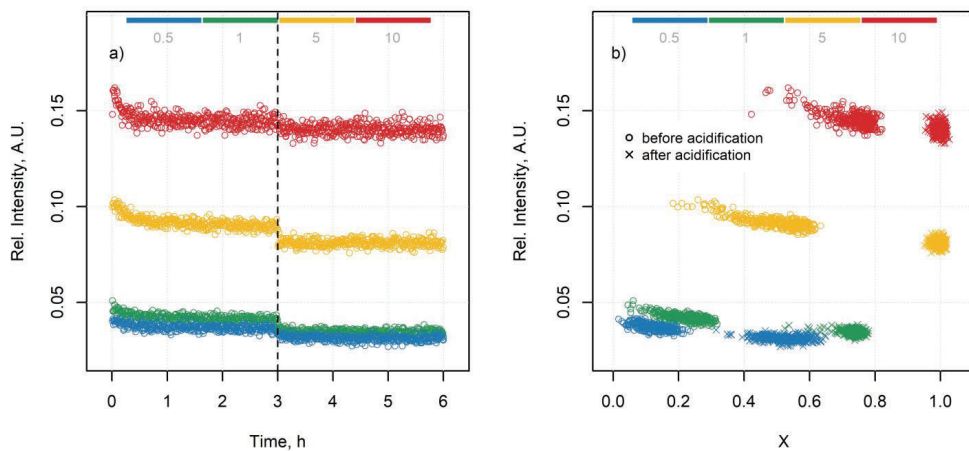


Figure S8. Intensity of the peak at Raman shift  $923\text{ cm}^{-1}$  (characteristic peak for HET) for executions at  $\text{pH}_0 = 9$  (execution b): a) trend as a function of time; b) trend as a function of the fractional conversion of  $\text{HS}^-$  ( $X$ ). The color legends indicate the HET/ $\text{HS}^-$  initial concentration ratio.

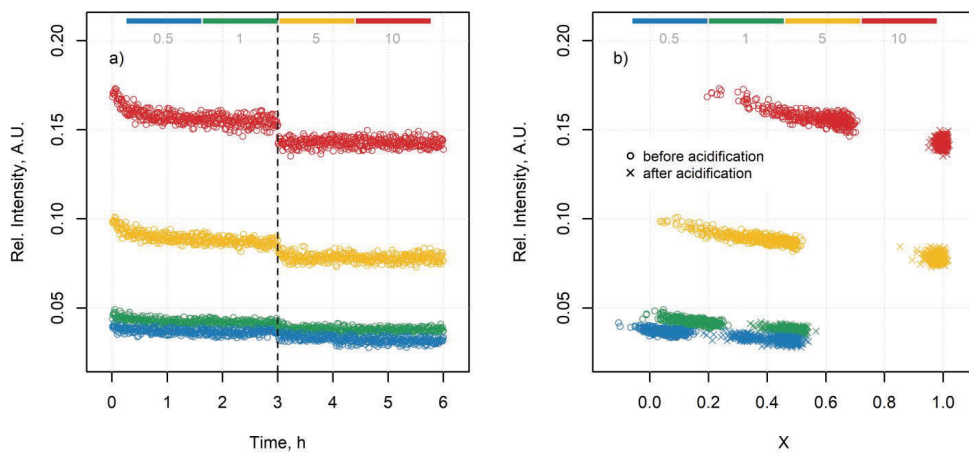




Figure S9. Intensity of the peak at Raman shift  $923\text{ cm}^{-1}$  (characteristic peak for HET) for executions at  $\text{pH}_0 = 10$  (execution a): a) trend as a function of time; b) trend as a function of the fractional conversion of  $\text{HS}^-$  ( $X$ ). The color legends indicate the HET/ $\text{HS}^-$  initial concentration ratio.

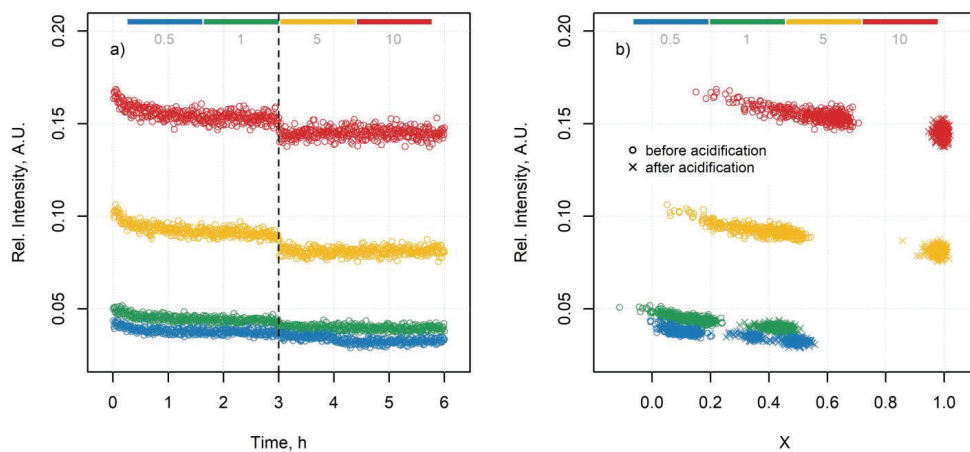


Figure S10. Intensity of the peak at Raman shift  $923\text{ cm}^{-1}$  (characteristic peak for HET) for executions at  $\text{pH}_0 = 10$  (execution b): a) trend as a function of time; b) trend as a function of the fractional conversion of  $\text{HS}^-$  ( $X$ ). The color legends indicate the HET/ $\text{HS}^-$  initial concentration ratio.

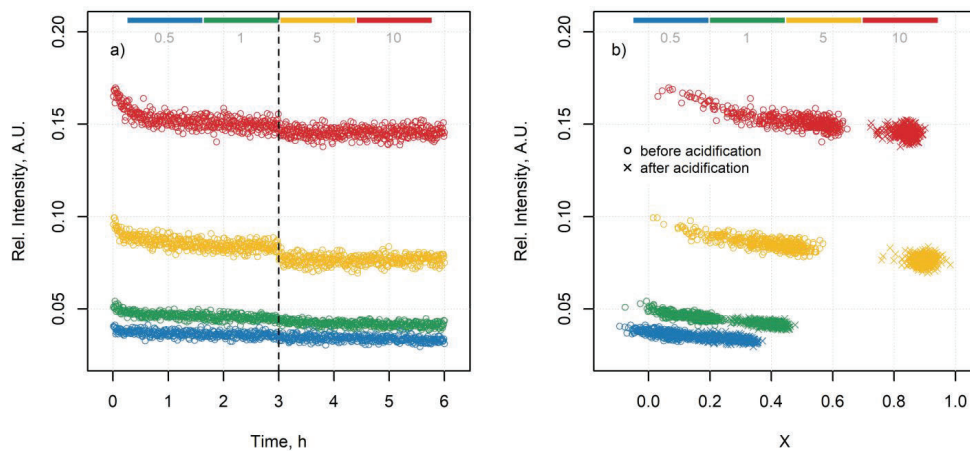


Figure S11. Intensity of the peak at Raman shift  $923\text{ cm}^{-1}$  (characteristic peak for HET) for executions at  $\text{pH}_0 = 11$  (execution a): a) trend as a function of time; b) trend as a function of the fractional conversion of  $\text{HS}^-$  ( $X$ ). The color legends indicate the HET/ $\text{HS}^-$  initial concentration ratio.

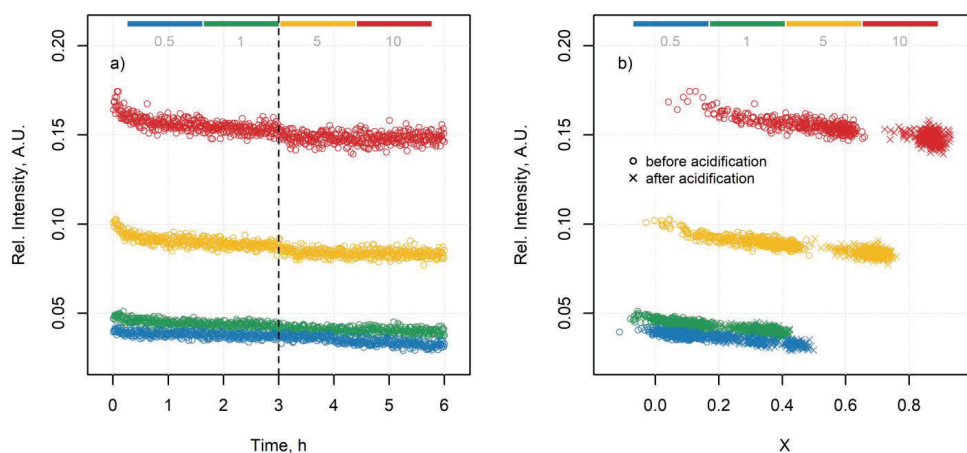


Figure S12. Intensity of the peak at Raman shift  $923\text{ cm}^{-1}$  (characteristic peak for HET) for executions at  $\text{pH}_0 = 11$  (execution b): a) trend as a function of time; b) trend as a function of the fractional conversion of  $\text{HS}^-$  ( $X$ ). The color legends indicate the HET/ $\text{HS}^-$  initial concentration ratio.

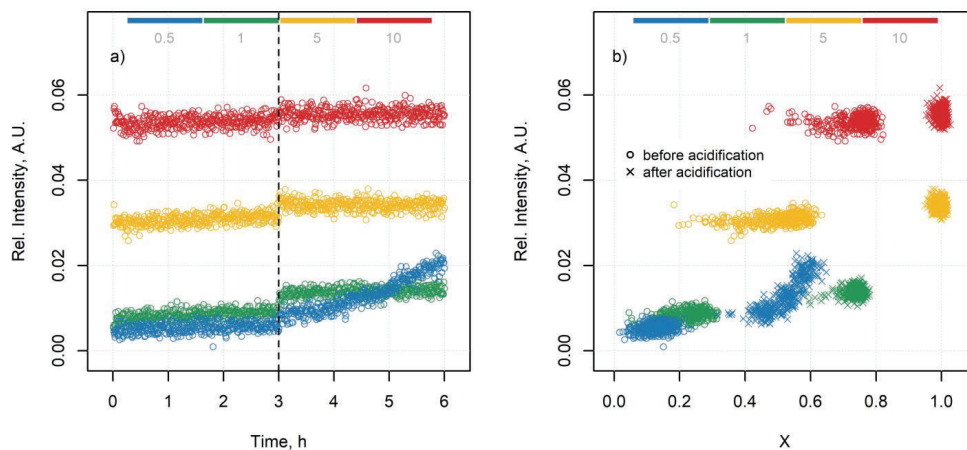


Figure S13. Intensity of the peak at Raman shift  $675\text{ cm}^{-1}$  (characteristic peak for DTZ) for executions at  $\text{pH}_0 = 9$  (execution b): a) trend as a function of time; b) trend as a function of the fractional conversion of  $\text{HS}^-$  (X). The color legends indicate the HET/ $\text{HS}^-$  initial concentration ratio.

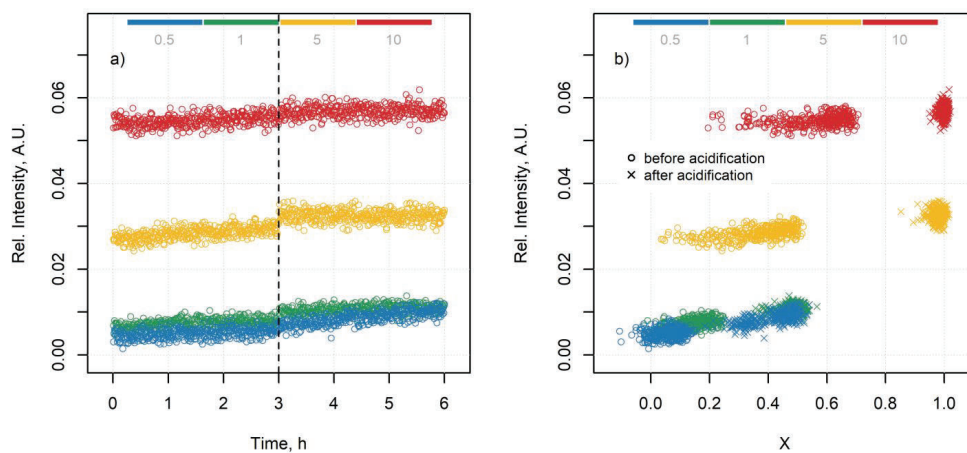


Figure S14. Intensity of the peak at Raman shift  $675\text{ cm}^{-1}$  (characteristic peak for DTZ) for executions at  $\text{pH}_0 = 10$  (execution a): a) trend as a function of time; b) trend as a function of the fractional conversion of  $\text{HS}^-$  (X). The color legends indicate the HET/ $\text{HS}^-$  initial concentration ratio.

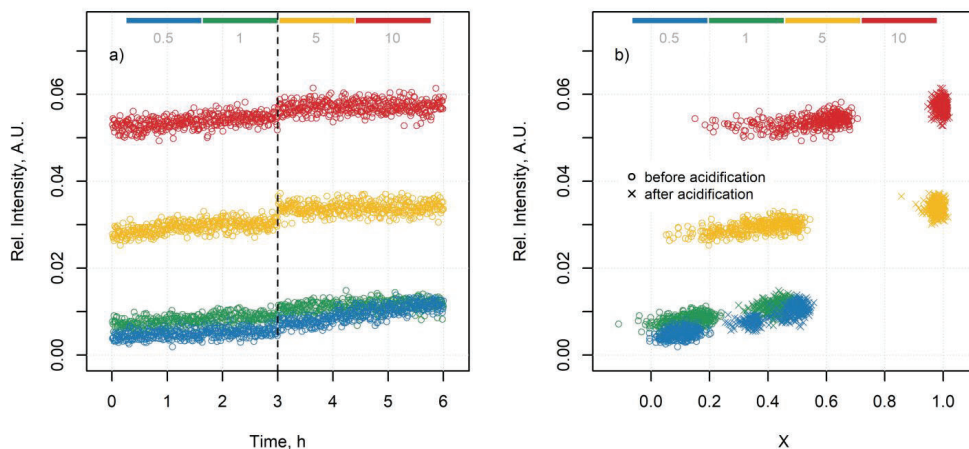


Figure S15. Intensity of the peak at Raman shift  $675\text{ cm}^{-1}$  (characteristic peak for DTZ) for executions at  $\text{pH}_0 = 10$  (execution b): a) trend as a function of time; b) trend as a function of the fractional conversion of  $\text{HS}^-$  ( $X$ ). The color legends indicate the  $\text{HET}/\text{HS}^-$  initial concentration ratio.

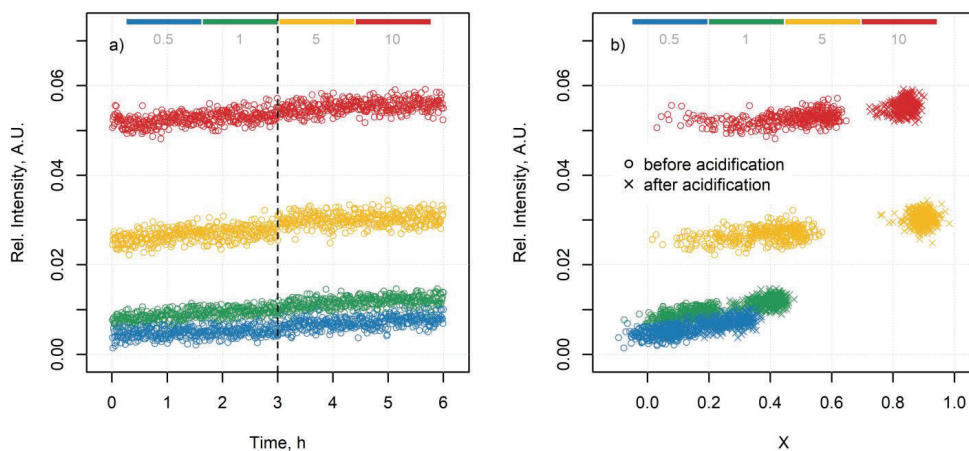


Figure S16. Intensity of the peak at Raman shift  $675\text{ cm}^{-1}$  (characteristic peak for DTZ) for executions at  $\text{pH}_0 = 11$  (execution a): a) trend as a function of time; b) trend as a function of the fractional conversion of  $\text{HS}^-$  ( $X$ ). The color legends indicate the  $\text{HET}/\text{HS}^-$  initial concentration ratio.

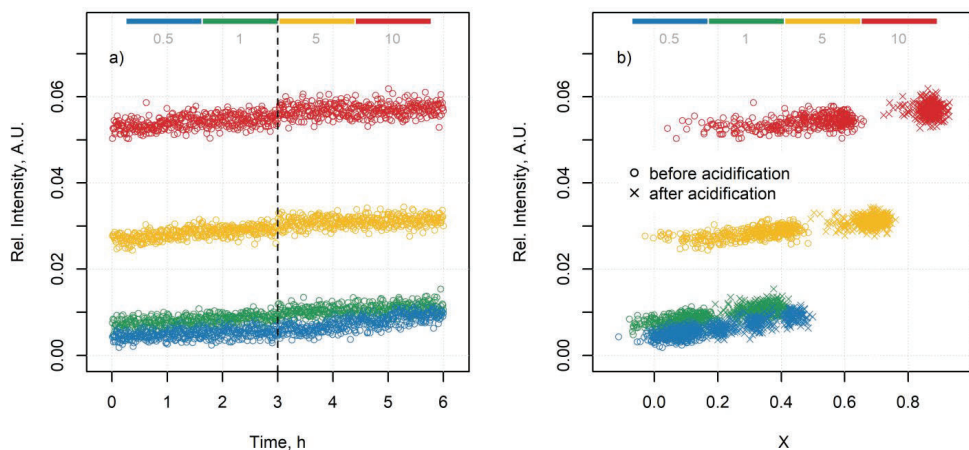


Figure S17. Intensity of the peak at Raman shift  $675\text{ cm}^{-1}$  (characteristic peak for DTZ) for executions at  $\text{pH}_0 = 11$  (execution b): a) trend as a function of time; b) trend as a function of the fractional conversion of  $\text{HS}^-$  ( $X$ ). The color legends indicate the  $\text{HET}/\text{HS}^-$  initial concentration ratio.

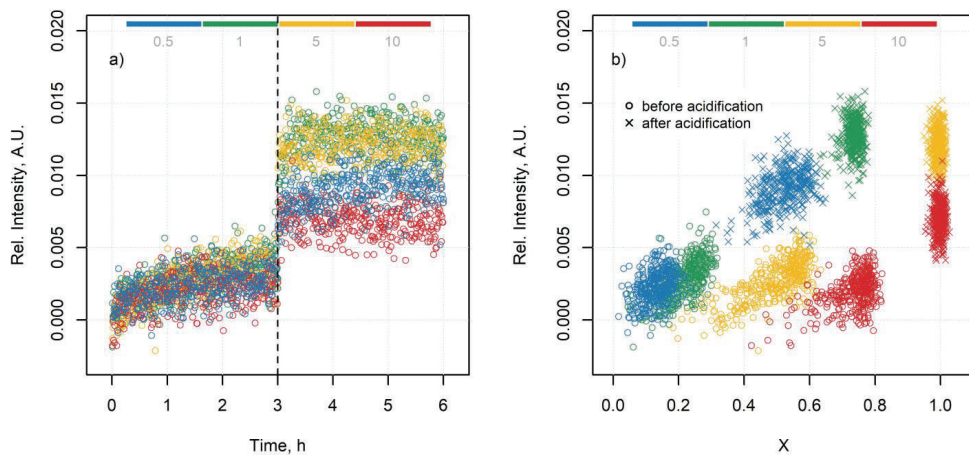


Figure S18. Intensity of the peak at Raman shift  $840\text{ cm}^{-1}$  (characteristic peak for MEA) for executions at  $\text{pH}_0 = 9$  (execution b): a) trend as a function of time; b) trend as a function of the fractional conversion of  $\text{HS}^-$  ( $X$ ). The color legends indicate the  $\text{HET}/\text{HS}^-$  initial concentration ratio.

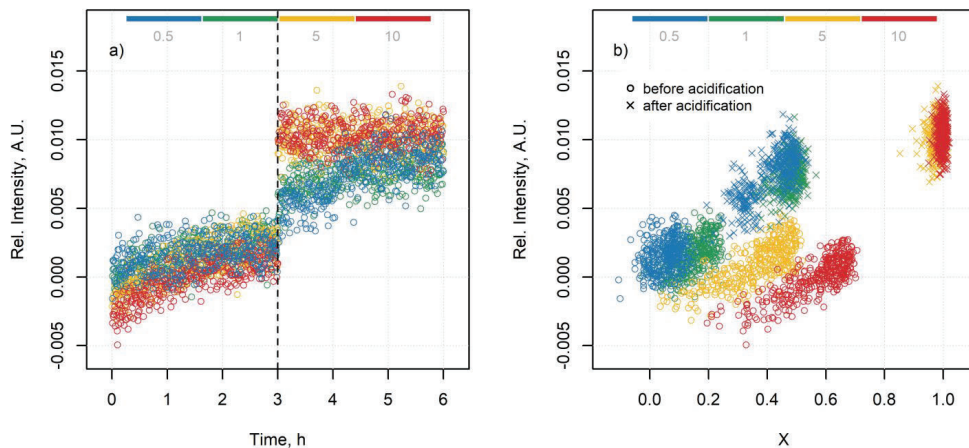


Figure S19. Intensity of the peak at Raman shift  $840\text{ cm}^{-1}$  (characteristic peak for MEA) for executions at  $\text{pH}_0 = 10$  (execution a): a) trend as a function of time; b) trend as a function of the fractional conversion of  $\text{HS}^-$  ( $X$ ). The color legends indicate the  $\text{HET}/\text{HS}^-$  initial concentration ratio.

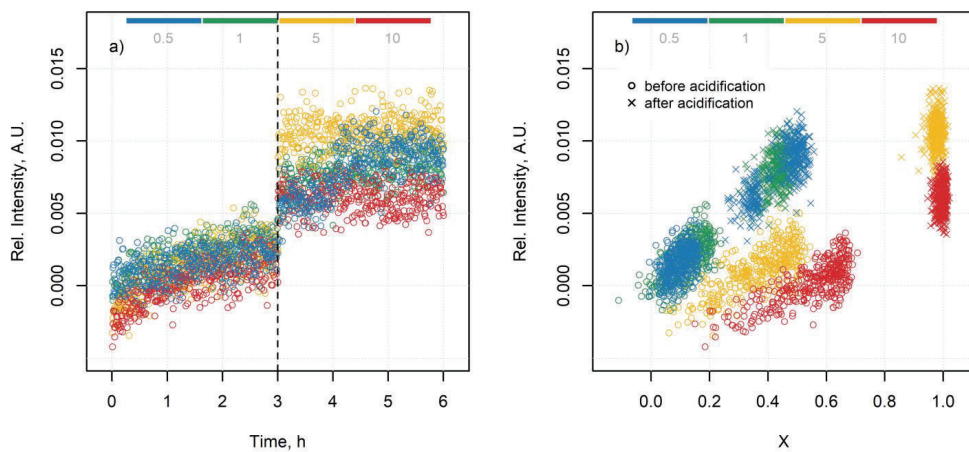


Figure S20. Intensity of the peak at Raman shift  $840\text{ cm}^{-1}$  (characteristic peak for MEA) for executions at  $\text{pH}_0 = 10$  (execution b): a) trend as a function of time; b) trend as a function of the fractional conversion of  $\text{HS}^-$  ( $X$ ). The color legends indicate the  $\text{HET}/\text{HS}^-$  initial concentration ratio.

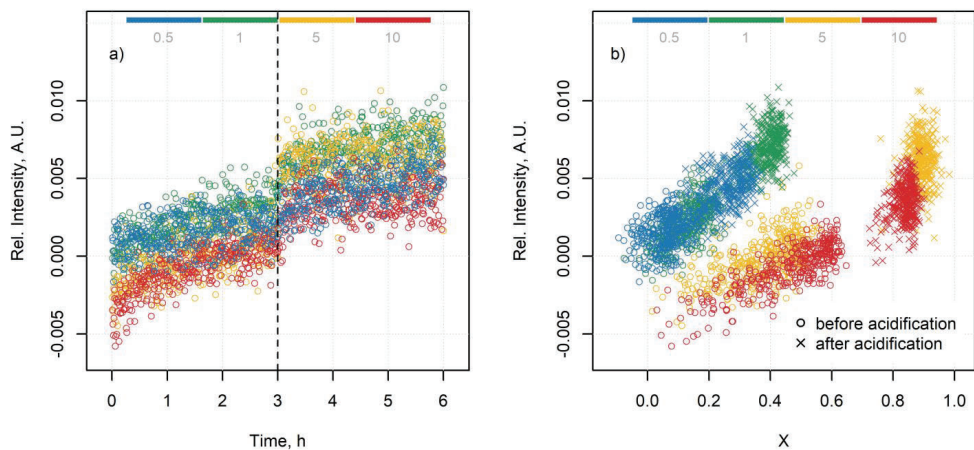


Figure S21. Intensity of the peak at Raman shift  $840\text{ cm}^{-1}$  (characteristic peak for MEA) for executions at  $\text{pH}_0 = 11$  (execution a): a) trend as a function of time; b) trend as a function of the fractional conversion of  $\text{HS}^-$  ( $X$ ). The color legends indicate the  $\text{HET}/\text{HS}^-$  initial concentration ratio.

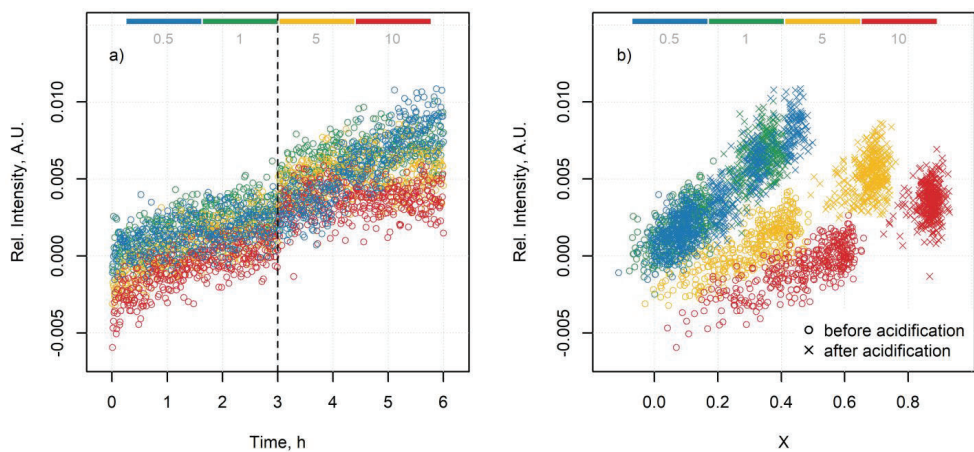


Figure S22. Intensity of the peak at Raman shift  $840\text{ cm}^{-1}$  (characteristic peak for MEA) for executions at  $\text{pH}_0 = 11$  (execution b): a) trend as a function of time; b) trend as a function of the fractional conversion of  $\text{HS}^-$  ( $X$ ). The color legends indicate the  $\text{HET}/\text{HS}^-$  initial concentration ratio.





## PAPER B

Temperature- and pH-dependent kinetics of the aqueous-phase hydrogen sulfide scavenging reactions with MEA-triazine

Iveth Romero, Fernando Montero, Sergey Kucheryavskiy, Reinhard Wimmer, Anders Andreasen, Marco Maschietti

The manuscript has been published in the journal

*Industrial & Engineering Chemistry Research*, Volume 62, Pages 8269-8280, 2023



# Temperature- and pH-Dependent Kinetics of the Aqueous Phase Hydrogen Sulfide Scavenging Reactions with MEA-Triazine

Iveth Romero, Fernando Montero, Sergey Kucheryavskiy, Reinhard Wimmer, Anders Andreasen, and Marco Maschietti\*



Cite This: *Ind. Eng. Chem. Res.* 2023, 62, 8269–8280



Read Online

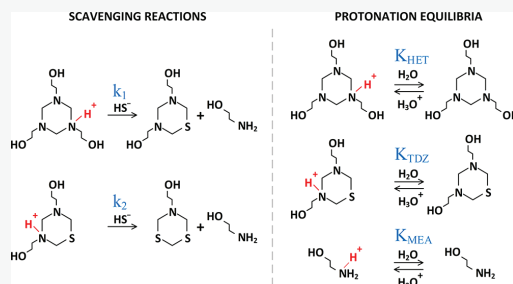
ACCESS |

Metrics & More

Article Recommendations

Supporting Information

**ABSTRACT:** A novel kinetic model for the aqueous phase hydrogen sulfide scavenging reactions using MEA-triazine (HET) is proposed. The assumptions of the model are based on experimental observations obtained by NMR spectroscopy, supporting the existence of 3,5-bis(2-hydroxyethyl)hexahydro-1,3,5-thiadiazine (TDZ) as a quantitative reaction intermediate and showing the protonation behavior of HET and the lack of protonation of 5-(2-hydroxyethyl)hexahydro-1,3,5-dithiazine (DTZ). Experimental kinetic data were obtained with a new in situ Raman spectroscopy setup, which enabled monitoring the time-variation of bisulfide concentrations in a batch stirred reacting system at temperatures of up to 75 °C for HET/HS<sup>-</sup> initial concentration ratios from 0.5 to 5. The optimal model parameters were regressed from the experimental data using a brute force optimization method. The rate constants of the first and second scavenging reactions were estimated to be 0.435 and 0.004 L mol<sup>-1</sup> s<sup>-1</sup> at 25 °C, and the activation energies were 68 and 57 kJ mol<sup>-1</sup>, respectively.



## 1. INTRODUCTION

The injection of aqueous solutions of MEA-triazine (i.e., 1,3,5-tris(2-hydroxyethyl)-hexahydro-*s*-triazine, henceforth also indicated as HET) has been the preferred method for removing hydrogen sulfide (H<sub>2</sub>S) from gas production for over 30 years in locations where alkanolamine contact and regeneration are not available.<sup>1–3</sup> The reasons for the success of MEA-triazine can be attributed to its capability of converting H<sub>2</sub>S into sulfides via fast and irreversible formation of C–S–C bonds and its relatively low cost.<sup>2,4</sup> The chemical conversion of H<sub>2</sub>S into sulfides makes MEA-triazine selective toward H<sub>2</sub>S removal, in contrast to, e.g., caustic or monoethanolamine (MEA) solutions, which merely absorb sour species such as H<sub>2</sub>S and CO<sub>2</sub> in an essentially non-selective and reversible manner.

Despite the widespread use of MEA-triazine, the kinetics governing the H<sub>2</sub>S scavenging reactions with HET (the scavenger) in the aqueous phase are still poorly understood. This is considered one of the main reasons for the large excess of scavenger utilized in offshore practice, which leads to high costs for the operators and unnecessary discharge into the sea of unreacted HET in the spent H<sub>2</sub>S scavenger wastewaters.<sup>5,6</sup> A better understanding of the kinetics of the scavenging reactions will allow a better design of the process with a smaller consumption of MEA-triazine for a given H<sub>2</sub>S abatement

specification, hence reducing both operating costs and environmental impact.

The seminal work of Bakke et al.<sup>7</sup> established a fundamental understanding of the aqueous phase reaction between HET and H<sub>2</sub>S. The removal of H<sub>2</sub>S can be represented via a multiple reaction scheme consisting of two reactions in series with respect to HET and in parallel with respect to H<sub>2</sub>S, as presented in Figure 1. As the reactions occur at basic pH values, the bisulfide ion (HS<sup>-</sup>) is the actual form of H<sub>2</sub>S in solution. The observed dependence of the reaction rate on the pH suggested the protonation of the ring nitrogen atom as necessary for the reaction to occur.<sup>4,7</sup> The main products of the reaction were identified as 3,5-bis(2-hydroxyethyl)-hexahydro-1,3,5-thiadiazine (thiadiazine, TDZ), 5-(2-hydroxyethyl)hexahydro-1,3,5-dithiazine (dithiazine, DTZ), and monoethanolamine (MEA).<sup>7</sup> Furthermore, Bakke et al.<sup>7</sup> observed that the reaction of TDZ with HS<sup>-</sup> is slower than that of HET, while DTZ showed no reaction with HS<sup>-</sup> at pH from 10 down to 2.

Received: March 1, 2023

Revised: May 2, 2023

Accepted: May 5, 2023

Published: May 16, 2023



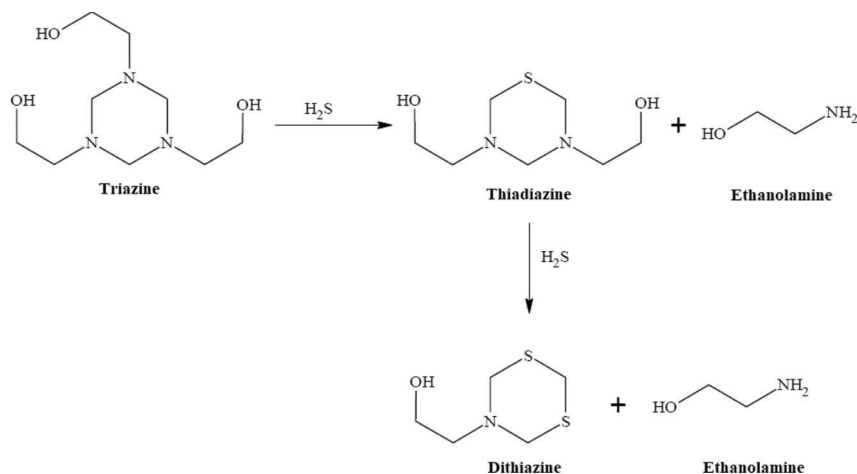


**Figure 1.** Scheme of the reactions between MEA-triazine (HET) and  $\text{H}_2\text{S}$ .

An important aspect debated in the literature is the existence of TDZ as a long-lived intermediate product of the series reactions. In the work of Bakke et al.,<sup>7</sup> TDZ was detected via  $^1\text{H}$  NMR and  $^{13}\text{C}$  NMR spectroscopy and was established as a product of the aqueous phase reaction of HET and  $\text{HS}^-$  when starting with an equimolar amount of reactants under room temperature operation. Madsen and Sogaard<sup>8</sup> also reported the identification of TDZ, in this case through electrospray ionization mass spectrometry (ESI-MS), as the main product of the gas–liquid reaction at room temperature between  $\text{H}_2\text{S}$  and HET in a 2:1 initial concentration ratio, while DTZ was the only identified product, when a 4:1 initial concentration ratio was applied. These results suggest that TDZ is present at room temperature in partially spent samples, while disappearing in highly spent samples. On the other hand, Taylor and Matherly<sup>9</sup> and Wylde et al.<sup>2</sup> reported the absence of TDZ even in partially spent scavenger samples from a laboratory gas tower, attributing this absence to the higher reactivity of TDZ, compared to HET, with  $\text{H}_2\text{S}$ , which is in contrast with the abovementioned observations reported in the work of Bakke et al.<sup>7</sup> Wylde et al.<sup>2</sup> also noted that “several aspects of this reaction are at present uncertain and are open to speculation”. Among other things, they noted that satisfactory explanations for the absence of a further scavenging reaction of DTZ with  $\text{HS}^-$  are lacking and hypothesized the  $\text{p}K_{\text{a}}$  of DTZ to be insufficiently basic. In a recent work, Perez Pineiro et al.<sup>10</sup> claimed the identification of TDZ using Raman spectroscopy in spent scavenger samples resulting from the gas–liquid reaction at room temperature of aqueous solutions of HET with  $\text{H}_2\text{S}$  gas.

Rate equations for the aqueous phase reactions between  $\text{HS}^-$  and HET have not been reported in the literature, except for the experimental work of Bakke and Buhaug,<sup>11</sup> which was, however, delimited to a large excess of  $\text{HS}^-$  and to the first scavenging reaction only. More specifically, a rate equation of pseudo first order with respect to the concentration of HET was proposed for the first scavenging reaction with the rate constant incorporating the protonation equilibrium constant of HET. It is noted that since HET is typically used in excess in oil and gas production and since the  $\text{H}_2\text{S}$  that transfers from

the gas to the aqueous phase reacts fast with HET, the conditions typically found in applications are characterized by excess of HET rather than excess of  $\text{HS}^-$ . Therefore, rate equations at conditions of interest for the applications are lacking in the literature.

In this work, we propose a novel kinetic model for the aqueous phase scavenging reactions, which accounts for the rate of the reactions of the protonated forms of HET and TDZ with  $\text{HS}^-$  (i.e., both the scavenging reactions) as well as for the protonation equilibria of HET, TDZ, and MEA. The model is validated on a new set of experimental data obtained using *in situ* Raman spectroscopy, which extends the experimental body of knowledge of our previous works<sup>12,13</sup> including kinetic data at three temperatures (25, 50, and 75 °C) and for different HET to  $\text{HS}^-$  ratios. The model assumes that TDZ is a long-lived and detectable reaction intermediate and that DTZ cannot protonate. To prove the correctness of the assumptions, a thorough NMR analysis was carried out, leading to the identification of TDZ as a long-lived and detectable intermediate compound of the scavenging reactions and showing the lack of protonation of DTZ due to low  $\text{p}K_{\text{a}}$ .

## 2. MATERIALS AND METHODS

**2.1. Materials.** Aqueous solutions of HET (CAS 4719-04-4; technical purity) and disodium sulfide about trihydrate ( $\text{Na}_2\text{S}\cdot 3\text{H}_2\text{O}$ ; CAS 27610-45-3) were used as the  $\text{H}_2\text{S}$  scavenger and solute of bisulfide aqueous solutions, respectively, for studying the scavenging reactions via Raman spectroscopy and for synthesizing TDZ. The technical solution of HET was quantitated by quantitative NMR applying the PULCON method<sup>14</sup> implemented in TopSpin 3.6.2 using an external solution of 2 mM sucrose in water (10%  $\text{D}_2\text{O}$ ) as a standard. The solute concentrations resulted in  $2371 \pm 85$  mM HET,  $805 \pm 30$  mM ethanolamine, and  $37.0 \pm 1.3$  mM formaldehyde (error estimates as evaluated by TopSpin). More details of the quantitation can be found in the Supporting Information (Section S1). The mass fraction of water in the hydrated disodium sulfide was measured via Karl Fischer titration and resulted to be  $0.391 \pm 0.002$ . Phenylacetic acid (PAA; CAS 103-82-2, product ID P16621-100G, purity >99 wt

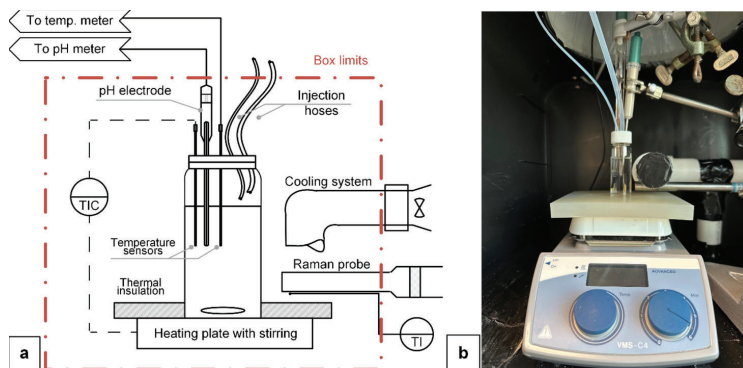


**Figure 2.** (a) Scheme of the experimental setup for in situ monitoring of scavenging reactions by means of Raman spectroscopy. (b) Photograph of the experimental setup.

% from Sigma-Aldrich was used as an internal standard (IS) in the scavenging reaction experiments using in situ Raman spectroscopy. PAA is a Raman active compound with a stable response within the pH range of the herein-analyzed scavenging reactions, which makes it suitable for quantitation purposes. Solutions of 6 M hydrochloric acid (HCl) and 6 M sodium hydroxide (NaOH) were used to prepare and adjust the pH of the reacting solutions.

High-purity DTZ (CAS 88891-55-8; product ID D493850, purity >98 wt %) from Toronto Research Chemicals and the abovementioned HET technical solution were used to study the protonation behavior of these species via proton nuclear magnetic resonance spectroscopy ( $^1\text{H}$  NMR). High-purity HET from Santa Cruz Biotechnology (CAS 4719-04-4; product ID sc-474806; purity  $\geq 95$  wt %) and the bisulfide aqueous solutions were used as reagents of scavenging reaction experiments aimed at confirming the identification of TDZ via NMR. Deuterium oxide from Eurisotop (CAS 7789-20-0, product ID D216, purity 99.85%) was used as the solvent of the TDZ-identification scavenging reactions, and deuterium oxide with 0.75 wt % 3-(trimethylsilyl)-propionic-2,2,3,3- $d_4$  acid sodium salt ( $\text{D}_2\text{O}$  with TSP- $d_4$ ; CAS 7789-20-0; product ID 293040-25G, purity 99.9 atom % D) from Sigma-Aldrich was used as the reference for chemical shift identification in NMR studies. Water (CAS 7732-18-5, product ID 83645.320, LC-MS grade, VWR International) supplemented with 0.05% diethylamine (CAS 109-89-7, product ID A11716, 99%, Alfa Aesar) and acetonitrile (CAS 75-05-8, product ID 83640.320, LC-MS grade, VWR International) supplemented with 0.05% diethylamine were used for LC-MS analyses related to the identification of TDZ via NMR.

## 2.2. TDZ Synthesis, Purification, and Identification.

1.5 g (11.36 mmol)  $\text{Na}_2\text{S} \cdot 3\text{H}_2\text{O}$  ( $M = 132.09$  g/mol) was added to 5 mL of a 2.371 M solution of HET (11.86 mmol HET) in water. 10 drops of 37% HCl in water were added, and the solution was stirred for 30 min at room temperature. After 30 min, another 10 drops of 37% HCl in water were added, and the solution was stirred for 30 more minutes. All solid  $\text{Na}_2\text{S}$  had vanished by that time.

TDZ was purified by preparative high-performance liquid chromatography (HPLC). Details on the HPLC procedure and equipment used for purification are reported in Section S2.1 of the Supporting Information. Fractions of purified TDZ were collected, freeze-dried, and redissolved in  $\text{D}_2\text{O}$  containing

0.7 mM TSP- $d_4$ . The pH\* (uncorrected meter reading) of the final solution was adjusted to 10.0 by addition of small aliquots of NaOD in  $\text{D}_2\text{O}$ .  $^1\text{H}$  NMR,  $^{13}\text{C}$  NMR, heteronuclear single quantum coherence spectroscopy ( $[^1\text{H}, ^{13}\text{C}]$ -HSQC), and heteronuclear multiple bond correlation ( $[^1\text{H}, ^{13}\text{C}]$ -HMBC, optimized for  $J_{\text{H,C}} = 8$  Hz) spectra were recorded on a BRUKER AVIII-600 MHz NMR spectrometer equipped with a 5 mm cryogenic inverse CPP-TCI probe at 298.1 K. High-resolution MS data were obtained on a BRUKER compact electrospray ionization-quadrupole time-of-flight (ESI-qTOF) mass spectrometer.  $^1\text{H}$  NMR was recorded with an interscan delay of 30 s, not employing water suppression in order to get a reliable integration of the broad peak closest to the water resonance.  $^{13}\text{C}$  NMR was recorded in an inverse-gated way without the usual build-up of a steady-state NOE (nuclear Overhauser effect) during the relaxation delay to obtain integrable  $^{13}\text{C}$  NMR spectra. The interscan delay was set to 60 s to ensure full relaxation of all  $^{13}\text{C}$ -spins prior to excitation between every scan.  $^1\text{H}$  and  $^{13}\text{C}$  longitudinal ( $T_1$ ) relaxation times were determined using the inversion-recovery pulse sequence. For  $^1\text{H}$ , eight relaxation delays were used (1, 16, 64, 256, 784, 2048, 6144, and 16384 ms), and the interscan delay was set to 16384 ms. For  $^{13}\text{C}$ , eight relaxation delays were used (0.25, 0.5, 1, 2, 4, 8, 16, and 32 s), the interscan delay was set to 32 s and the spectra were recorded in an inverse-gated way without the build-up of a steady-state NOE during the interscan delays.

In another experiment, an aqueous-phase reaction of high-purity HET and  $\text{HS}^-$  in equimolar concentrations (50 mM each) at an initial pH of 8 was run at room temperature as the basis of identification of TDZ via  $^1\text{H}$  NMR (with water suppression by pre-saturation through a 5 s continuous wave irradiation on the water resonance with a  $\gamma\text{B}_1/\pi = 50$  Hz) and  $[^1\text{H}, ^{13}\text{C}]$ -HSQC recorded at 298.1 K. Experimental details on the reaction for the identification of TDZ are reported in Section S2.2 of the Supporting Information.

## 2.3. Analysis of the Protonation Equilibrium of HET and DTZ Using $^1\text{H}$ NMR.

Single-component stock solutions of technical-purity HET (24 mM) and DTZ (86 mM) were prepared in Milli-Q water and 5% (v/v)  $\text{D}_2\text{O}$  with TSP- $d_4$ . From the HET stock solution, aliquots of 600  $\mu\text{L}$  were transferred to 11 micro centrifuge tubes and placed in a dry block thermostat to keep the temperature of each sample at 25  $^\circ\text{C}$ . At this temperature, the pH of each sample was adjusted to

one value in the range of 7 to 12 with a step size of ca. 0.5 between each sample. After pH adjustment, each sample was transferred to an NMR tube for the acquisition of spectra at 25 °C. A similar procedure was followed for the DTZ stock solution, adjusting the pH of 13 aliquots to one value of pH in a broader range that included pH values of 3 and 5. The HET samples were then heated to 50 and 75 °C, and the corresponding pH values were noted. <sup>1</sup>H NMR spectra were recorded on the NMR spectrometer at 298.1, 323.1, and 348.1 K for HET and 298.1 K for DTZ.

**2.4. Real-Time Monitoring of Reactions Using Raman Spectroscopy.** The reaction experiments between HET and HS<sup>-</sup> were performed in a custom-made Raman box shown in Figure 2. The setup allows monitoring the aqueous-phase scavenging reactions by means of in situ Raman spectroscopy. The box acts as a dark room, preventing external light from entering the Raman probe. The setup consists of a 45 mL glass vial (batch reactor), equipped with a magnetic stir bar, placed over a magnetic stirrer with a PID temperature controller, which can be operated up to 80 °C. The surface of the heating plate is thermally insulated to avoid overheating of the Raman probe, located sideward to the glass vial, at approximately a 1 cm distance (Figure 2a). The temperature of the Raman probe can be kept below 30 °C during reaction experiments by means of a continuous flux of air directed over it. The lid of the glass vial is provided with nozzles for the insertion of a pH microelectrode, platinum resistance thermometers (Pt 1000) for monitoring and controlling the temperature of the reacting mixture, one hose for the injection of acid into the vial for pH adjustment, and another hose for the injection of HET to start the reaction.

The reaction experiments were run with an initial concentration of HS<sup>-</sup> of 100 mM, initial pH of 9.0 ± 0.2, and a concentration of IS (PAA) of 200 mM. The experimental campaign was based on a 3<sup>2</sup> full factorial design: initial concentration of HET (46, 91, and 456 mM) and temperature (25, 50, and 75 °C) preparing two independent solutions for each combination, totaling 18 reaction runs. All runs were carried out in a randomized order. Additional runs were executed for the combinations 456 mM HET/25 °C and 456 mM HET/50 °C for further confirmation of the observed trends. Each reaction was monitored for 3.5 h. Details about the preparation of solutions can be retrieved from Section S3 of the Supporting Information.

An aliquot of 20 mL of the bisulfide solution was placed in the batch reactor. Then, the reactor was placed inside the Raman box with all sensors and accessories in place. Once the desired operating temperature was reached inside the batch reactor, the Raman box was closed, and the Raman acquisition started. After 15 s of spectral acquisition, 10 mL of the HET solution was fed to the vial through the dedicated injection hose, and the reaction progressed for 3.5 h. The pH of the aqueous reacting phase was observed to increase in all runs, which causes the rate of the scavenging reactions to drop.<sup>12</sup> The reacting solution was re-acidified by the injection of 200 μL of HCl 6 M after 3 h of monitoring time to reactivate the scavenging reactions.

**2.5. Raman Spectroscopy Data Analysis.** The reactions were monitored using a Raman spectrometer (Rxn1, Kaiser Optical Systems) equipped with a 785 nm laser as the source of excitation light and a non-contact probe connected to the spectrometer by a fiber in the auto sampling mode. The reaction data were acquired with 30 s intervals by averaging

three consecutive spectra taken with a 5 s excitation time, collecting 420 spectra for each experimental condition.

The spectra were used for the quantitative estimation of the HS<sup>-</sup> concentration by applying a partial least squares regression (PLSR) model.<sup>15</sup> The model was preliminarily calibrated under the same conditions (temperature, stirring rate, probe-vial distance) as for the reaction experiments and validated using Raman spectra acquired for standard solutions containing 200 mM of IS and HS<sup>-</sup> concentrations varying in the range of 0 to 100 mM (10 concentration levels in total with an equal step size) for each temperature level at pH 9.0 ± 0.2. Each standard solution was prepared independently and in triplicate, giving 30 samples for each temperature level.

The preprocessing of the spectra for the calibration of the regression model, as well as the selection of the best preprocessing conditions, was done as described elsewhere.<sup>12</sup> In a previous work, it was proved that the prediction performance of the model is unaltered for pH values in the range of 9 to 11.<sup>12</sup> The prediction performance of the final model obtained using one-level-out cross-validation for each temperature is summarized in Table 1. The data analysis and visualization were performed in R (v. 4.0.5)<sup>16</sup> with packages *mdatools*<sup>17</sup> and *hyperSpec*.<sup>18</sup>

**Table 1. Prediction Performance of the PLSR Models for the Quantitation of HS<sup>-</sup> at Each Temperature Level Including the Coefficient of Determination (R<sup>2</sup>) and the Root Mean Squared Error for Cross-Validation (RMSECV)**

temperature, °C	R <sup>2</sup>	RMSECV, mM
25	0.995	2.269
50	0.996	2.014
75	0.995	2.300

### 3. NMR RESULTS AND KINETIC MODEL DEVELOPMENT

**3.1. Identification of TDZ.** A representative chromatogram of the reaction mixture from the synthesis of TDZ is shown in Figure S3. Fractions from preparative HPLC were lyophilized and analyzed by NMR. One fraction, eluting after 8 min, contained a colorless, oily residue that showed <sup>1</sup>H and <sup>13</sup>C NMR spectra (Figure 3) very similar to the spectra expected for TDZ. Like with HET, the ring hydrogen atoms are severely broadened, probably due to a ring inversion at an intermediate timescale with respect to the NMR chemical shift difference. Also, the ethanolamine-CH<sub>2</sub> group closest to the nitrogen atom is affected by exchange broadening. This is further corroborated by the fact that heating the solution to 45 °C leads to a narrower set of lines (Figure S4). Longitudinal (T<sub>1</sub>) relaxation times were determined in order to ascertain that the relaxation delay chosen for quantitative <sup>1</sup>H and <sup>13</sup>C spectra, respectively, was sufficient to ensure full relaxation between subsequent scans (>7 T<sub>1</sub>). The inversion recovery spectra are shown in Figure S5 (<sup>1</sup>H) and S6 (<sup>13</sup>C), and T<sub>1</sub> relaxation times of TDZ are given in Table S1 of the Supporting Information.

A [<sup>1</sup>H,<sup>13</sup>C]-HSQC spectrum (Figure 3C) reveals the correct number of signals at the expected chemical shifts. The [<sup>1</sup>H,<sup>13</sup>C]-HMBC spectrum and the correlations observed are shown in Figure S7. They corroborate the structure and assignment of the molecule. The <sup>1</sup>H NMR spectrum of TDZ is also clearly different from that of HET, DTZ, and ethanol-

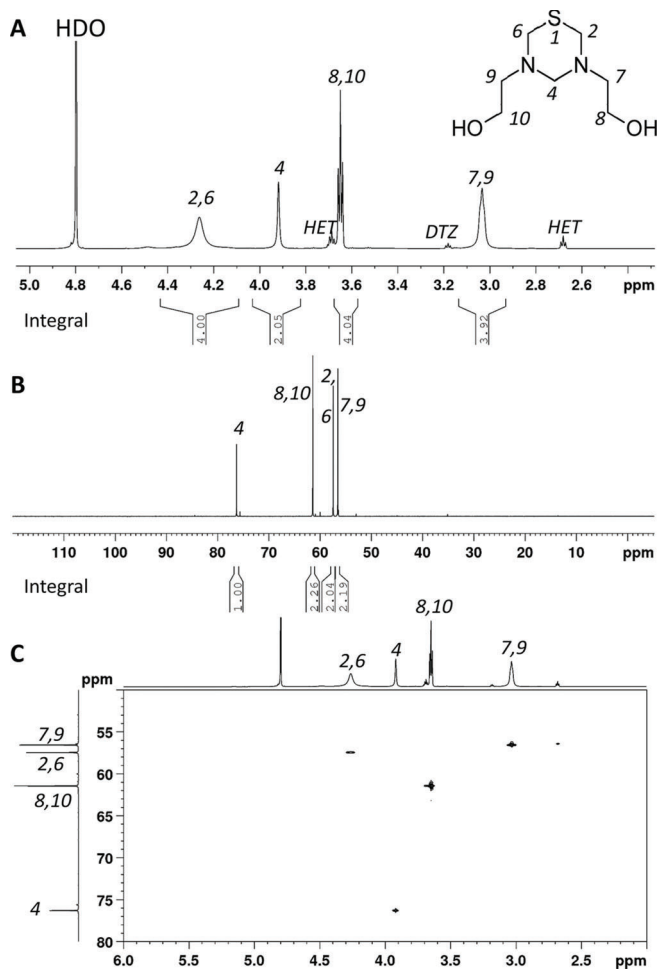


**Figure 3.** NMR of TDZ in D<sub>2</sub>O, pH\* = 10.0, at 298.1 K, with the assignment of resonances to atoms. Both HET and DTZ were present as impurities, and their signals were labeled accordingly. The residual water signal is labeled HDO. (A) <sup>1</sup>H NMR spectrum (600 MHz); (B) quantitative <sup>13</sup>C NMR spectrum (150.9 MHz); (C) [<sup>1</sup>H,<sup>13</sup>C]-HSQC spectrum.

amine (Figure 4). The total yield of TDZ was 92.7 mg (0.48 mmol, 4.2% of the theoretical yield). The purity of TDZ thus obtained was 90% (mol/mol), with 6% DTZ and 4% HET. Different batches of purification gave the same result within a few percent, and repurification of TDZ did not yield a purer product, although DTZ and HET can be chromatographically separated very well from TDZ (Figure S3). This suggests that TDZ may slowly convert into HET and DTZ until reaching an equilibrium.

ESI-qTOF MS (Figure 5) yielded a [M + H]<sup>+</sup> of 193.1000 and a [M + Na]<sup>+</sup> of 215.0827 consistent with a molecular formula of C<sub>7</sub>H<sub>16</sub>N<sub>2</sub>O<sub>2</sub>S (theoretical [M + H]<sup>+</sup> of 193.1005 ( $\Delta m/m = 2.6$  ppm) and [M + Na]<sup>+</sup> of 215.0825 ( $\Delta m/m = 0.9$  ppm)).

The mass difference between the A + 2 peak ( $m/z = 217.0789$ ) and the A + 1 peak ( $m/z = 216.0848$ ) is <1, further corroborating the presence of a sulfur atom in the molecule.

The intensity distribution of the isotope pattern (A + 1: 9.1%, A + 2: 4.5%) fits the theoretical isotope distribution (A + 1: 9.4%, A + 2: 5.3%). The intensity of the A + 2 peak compared to the A + 1 peak further points at the presence of sulfur, with natural sulfur containing 4.5% <sup>34</sup>S.

The [<sup>1</sup>H,<sup>13</sup>C]-HSQC signals of the pure molecule are also present in the reaction mixture prepared for the identification of TDZ, as stated in Section 2.2, confirming that the compound is a long-lived reaction intermediate of the series reaction pathway. Table 2 summarizes the NMR characterization of TDZ in D<sub>2</sub>O.

**3.2. Protonation Equilibrium of HET and DTZ.** During the pH titration of HET, followed by <sup>1</sup>H NMR (Figures S8–S10), it became evident that three coupled equilibria exist: (i) the protonation/deprotonation equilibrium of HET; (ii) a pH-dependent hydrolysis of HET to MEA; and (iii) the protonation/deprotonation equilibrium of MEA. The proto-

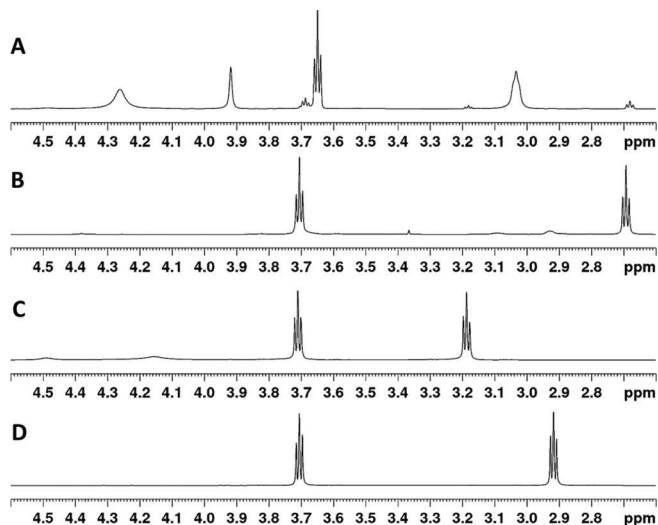


**Figure 4.**  $^1\text{H}$  NMR spectra (600 MHz) of (A) TDZ, (B) HET, (C) DTZ, and (D) ethanolamine. TDZ is obtained from our synthesis and contains impurities of HET and DTZ, while the other samples are obtained commercially. All spectra were recorded at pH 10,  $T = 298.1\text{ K}$ , and they were all referenced to internal  $\text{TSP-}d_4$ .

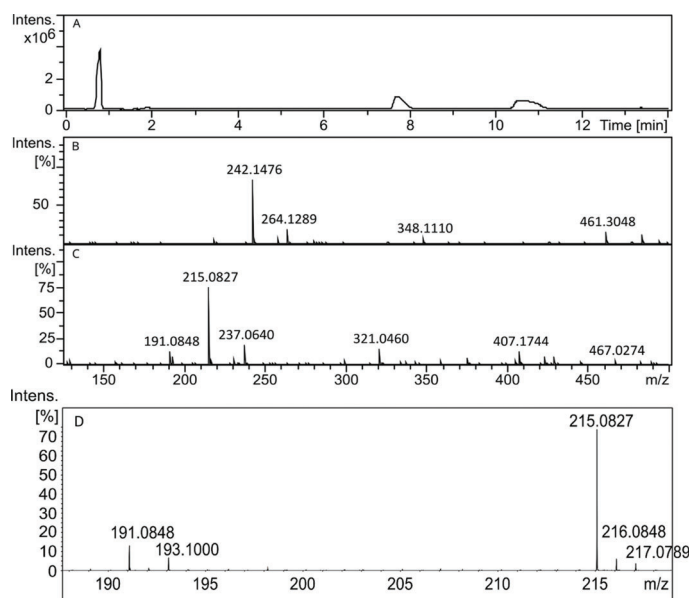


**Figure 5.** (A) LC-MS chromatogram of purified TDZ, containing ca. 3% of HET. The peak at 0.8 min retention time is sodium formate, an IS injected into the MS at the start of the chromatography to calibrate the  $m/z$  axis. The mass spectrum at  $\text{RT} = 7.7\text{ min}$  is shown in panel (B), and it corresponds to HET. The mass spectrum at  $\text{RT} = 10.8\text{ min}$  is shown in panel (C), and it corresponds to TDZ. The ionization efficiency of HET is considerably larger than that of TDZ. Panel (D) shows a zoom of the spectrum of TDZ showing the isotopical pattern.

nation/deprotonation equilibrium of HET was revealed by the positioning of the chemical shift of the  $\text{NH}_2\text{-CH}_2\text{-}$  group of HET, which was invariant at a pH above 9.5, while it varied at lower pH values. Concurrently, the small amount of MEA, initially present in HET as an impurity, was observed to

increase when going toward lower pH values. At the lowest pH, HET was barely detectable since all HET had hydrolyzed to MEA. For all these reasons, it was impossible to derive an exact  $\text{pK}_a$  value for HET.



**Table 2.** NMR Characterization of TDZ in D<sub>2</sub>O and Assigned Protons in TDZ Molecule

atom <sup>a</sup>	$\delta_C$ [ppm], type	$\delta_H$ [ppm] (J in Hz)	HMBC <sup>b</sup>
4	76.24, CH <sub>2</sub>	3.92 (s, broad)	2/6, 7/9
2/6	57.45, CH <sub>2</sub>	4.26 (s, broad)	
7/9	56.53, CH <sub>2</sub>	3.03 (t, 5.9 Hz, broad)	2/6, 4, 8/10
8/10	61.41, CH <sub>2</sub>	3.64 (t, 5.9 Hz)	7/9

<sup>a</sup>Atom numbering is shown in Figure 3. <sup>b</sup>HMBC correlations optimized for 8 Hz are given from the hydrogen atoms to the indicated carbon atoms. They are also illustrated in Figure S4.

On the other hand, the <sup>1</sup>H NMR spectra of DTZ samples (Figure S11) showed a stable chemical shift of the two triplets assigned to DTZ in a pH range of 12.0 to 5.0. At pH 3.0, there was a change of the chemical shift. Therefore, it can be concluded that no protonation of DTZ occurs at typical pH values of the scavenging reactions in oil and gas practice, as well as in the pH range of the present work (i.e., pH > 9).

**3.3. Kinetic Model.** A kinetic model of the aqueous phase reactions of H<sub>2</sub>S scavenging with HET was developed in this work, aiming at the pH range of interest in the industrial applications of the process, i.e., approximately 9 to 11. The model was developed taking as the starting point the multiple reaction scheme reported in the literature (see Figure 1) and the NMR observations of this work. More specifically, the proposed model is based on the following hypotheses: (i) HS<sup>-</sup> is the only species pertaining to the ionization equilibrium of H<sub>2</sub>S that is present in the system at the pH of interest, in line with the pK<sub>s</sub> value of H<sub>2</sub>S, which is around 7 at room temperature;<sup>19,20</sup> (ii) the protonated forms of HET and TDZ are the ones reacting with HS<sup>-</sup>, based on the works of Bakke et al.,<sup>7</sup> Fiorot and Carneiro,<sup>21</sup> and the observation of the strong decrease in the rate of the scavenging reactions with increasing pH;<sup>12</sup> (iii) the protonation of HET and TDZ is always at equilibrium (infinitely fast reactions); (iv) MEA, which is present in the reacting mixture as an impurity of the technical triazine as well as a reaction product, also undergoes protonation in the pH range of interest,<sup>22</sup> and this reaction is also always at equilibrium (infinitely fast reaction), like for HET and TDZ; (v) no protonation occurs for DTZ, as the NMR observations (Section 3.2) proved this species to be stable in the pH range of interest; (vi) the first and second scavenging reactions with protonated HET and protonated TDZ, respectively, are irreversible;<sup>2,23</sup> (vii) the first and second scavenging reactions are first-order reactions with respect to their corresponding two reactants; and (viii) the hydrolysis of HET is negligible at the high pH values of interest.<sup>7</sup> Overall, a five-reaction scheme is proposed

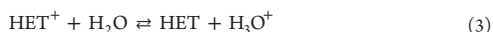
First scavenging reaction



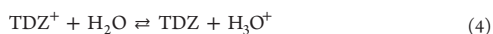
Second scavenging reaction



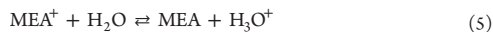
Protonation equilibrium of HET



Protonation equilibrium of TDZ



Protonation equilibrium of MEA



The rate of consumption of HS<sup>-</sup> is thus given by

$$(-r_{\text{HS}^-}) = k_1[\text{HET}^+][\text{HS}^-] + k_2[\text{TDZ}^+][\text{HS}^-] \quad (6)$$

where  $k_1$  and  $k_2$  are the rate constants of the two scavenging reactions. In this work, terms in square brackets indicate molarity. The concentration-based equilibrium constants for the reactions 3–5 are given by

$$K_{\text{HET}} = \frac{[\text{HET}][\text{H}_3\text{O}^+]}{[\text{HET}^+]} \quad (7)$$

$$K_{\text{TDZ}} = \frac{[\text{TDZ}][\text{H}_3\text{O}^+]}{[\text{TDZ}^+]} \quad (8)$$

$$K_{\text{MEA}} = \frac{[\text{MEA}][\text{H}_3\text{O}^+]}{[\text{MEA}^+]} \quad (9)$$

Furthermore, the balance of neutral and protonated species can be imposed

$$[\text{HET}^*] = [\text{HET}^+] + [\text{HET}] \quad (10)$$

$$[\text{TDZ}^*] = [\text{TDZ}^+] + [\text{TDZ}] \quad (11)$$

$$[\text{MEA}^*] = [\text{MEA}^+] + [\text{MEA}] \quad (12)$$

where the terms denoted with the superscript \* indicate the total concentration, which must be the sum of the concentration of the protonated and the neutral species.

Introducing the extent of the reactions as  $x_k = \frac{\Delta N_{i_k}}{\nu_{i_k}}$ , where  $k$  indicates the generic reaction ( $k = 1, \dots, 5$ ),  $\Delta N_{i_k}$  is the variation of the number of moles of the species  $i$  due to the advancement of the reaction  $k$ , and  $\nu_{i_k}$  is the stoichiometric coefficient of species  $i$  in the reaction  $k$  taken positive for products and negative for reactants, and assuming ideal mixing in the glass vial due to the intense stirring and constant density of the reacting mixture, two independent molar balances can be written

$$\frac{dx_1}{dt} = k_1([\text{HET}^+]_0 - x_1 - x_3)([\text{HS}^-]_0 - x_1 - x_2) \quad (13)$$

$$\frac{dx_2}{dt} = k_2([\text{TDZ}^+]_0 - x_2 - x_4)([\text{HS}^-]_0 - x_1 - x_2) \quad (14)$$

The subscript 0 refers to the concentrations at a conventional initial time, where the extent of the reactions is null. In addition, expressing the protonation equilibrium conditions as a function of the extent of reactions, one gets

$$K_{\text{HET}} = \frac{([\text{HET}]_0 + x_3)([\text{H}_3\text{O}^+]_0 + x_3 + x_4 + x_5)}{([\text{HET}^+]_0 - x_1 - x_3)} \quad (15)$$

$$K_{\text{TDZ}} = \frac{([\text{TDZ}]_0 + x_1 + x_4)([\text{H}_3\text{O}^+]_0 + x_3 + x_4 + x_5)}{([\text{TDZ}^+]_0 - x_2 - x_4)} \quad (16)$$

$$K_{\text{MEA}} = \frac{([\text{MEA}]_0 + x_1 + x_2 + x_5)([\text{H}_3\text{O}^+]_0 + x_3 + x_4 + x_5)}{([\text{MEA}^+]_0 - x_5)} \quad (17)$$

The kinetic model is thus represented by eqs 13–17, which form a system of differential and algebraic equations (DAE). Details of the derivation are provided in the Supporting Information (Section S6).

The rate constants of the two scavenging reactions ( $k_1$ ,  $k_2$ ) as well as the protonation equilibrium constants for HET and TDZ ( $K_{\text{HET}}$ ,  $K_{\text{TDZ}}$ ) and the initial pH of the reacting system were treated as regression parameters. The reaction rate constants were only constrained to be positive and to increase with temperature. The  $\text{p}K_a$  values of the protonation equilibrium of HET and TDZ were constrained in the range of 5.0 to 9.5, as values below 5 would be unreasonable for amines,<sup>22</sup> and the NMR shift of HET did not show any noticeable protonation above pH 9.5. On the other hand, the protonation equilibrium constants of MEA ( $K_{\text{MEA}}$ ) at different temperatures were retrieved from the literature<sup>27</sup> and therefore used as known fixed parameters in the model, with the values being  $10^{-9.45}$ ,  $10^{-8.72}$ ,  $10^{-8.22}$  at 25, 50, and 75 °C, respectively.

The experimental pH of the reacting system was observed to increase very rapidly after the injection of HET. This made it virtually impossible to obtain a reliable pH measurement at the initial time of the reaction ( $t = 0$ ), which was set at the mid-time of the first Raman spectral acquisition after the injection of HET and occurred within 7.5 and 22.5 s after the injection of HET. For this reason, the decision was made to take the pH of the reacting mixture at time  $t = 0$  as an additional regression parameter ( $\text{pH}_0$ ), which was constrained in the range of 9.0 to 10.6. The concentration of  $\text{HS}^-$  at time  $t = 0$  ( $[\text{HS}^-]_0$ ) was calculated from the first Raman spectral acquisition, whereas the total concentration of HET and MEA at time  $t = 0$  was estimated assuming that the second scavenging reaction did not occur in the first 30 s of mixing; therefore, according to the stoichiometric relations

$$[\text{HET}^*]_0 = [\text{HET}^*]_n + [\text{HS}^-]_0 - [\text{HS}^-]_n \quad (18)$$

$$[\text{MEA}^*]_0 = [\text{MEA}^*]_n + [\text{HS}^-]_n - [\text{HS}^-]_0 \quad (19)$$

where the subscript  $n$  indicates the nominal concentration, that is the one calculated from the solution preparation. This also implies that the concentration of DTZ at time  $t = 0$  was set to zero.

The optimal values of the regression parameters were found by a two-stage brute force optimization. The optimization grid for each stage is defined in Table S2 in the Supporting Information. For each combination of the regression parameters ( $k_1$ ,  $k_2$ ,  $\text{p}K_{\text{HET}}$ , and  $\text{p}K_{\text{TDZ}}$ ) from the optimization grid, the optimal  $\text{pH}_0$  values were estimated by minimizing the mean squared error (MSE) between experimental and calculated values for each experimental execution done at a certain nominal HET concentration and the same temperature. This process was executed separately for the data before and after acidification. The combination of the parameters yielding the minimum MSE for the first stage of the procedure (larger grid) was selected, and then, the optimization was repeated in the second stage on a finer grid centered around the abovementioned optimal combination of the parameters. This task was done using Julia programming language (1.7.2)<sup>24</sup> with packages *DifferentialEquations.jl*<sup>25</sup> and *Sundials.jl*.<sup>26</sup>

#### 4. RESULTS AND DISCUSSION

Figures 6–8 show the experimental and calculated concentrations of  $\text{HS}^-$  over time, which were obtained using the

optimal values of the regression parameters reported in Table 3.

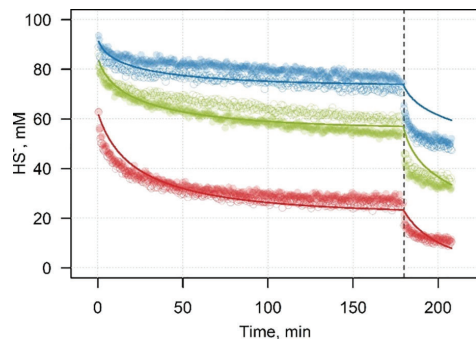


**Figure 6.** Experimental (colored dots) and calculated (continuous lines) concentrations of  $\text{HS}^-$  at 25 °C. Blue for 46 mM HET, green for 91 mM HET, and red for 456 mM HET. The dashed vertical line represents the time of system reacidification (180 min). Duplicate experiments for each initial concentration of HET are reported (filled and empty markers).

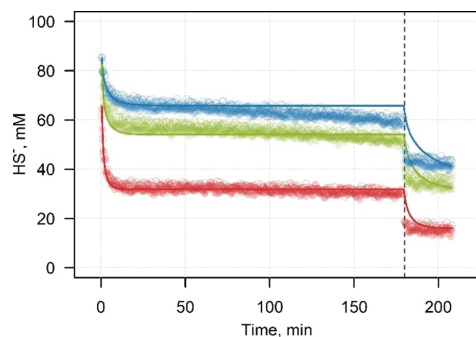


**Figure 7.** Experimental (colored dots) and calculated (continuous lines) concentrations of  $\text{HS}^-$  at 50 °C. Blue for 46 mM HET, green for 91 mM HET, and red for 456 mM HET. The dashed vertical line represents the time of system reacidification (180 min). Duplicate experiments for each initial concentration of HET are reported (filled and empty markers).

The plots show the duplicate experiments for each initial concentration of HET, evidencing the good reproducibility of the data set with an average ARD (average relative deviation) of 5.2% for all executions before acidification and 11.8% after acidification. The pH of the reacting mixture was observed to increase from 9.0 (prior to HET injection) to values of around 10.0–11.0 within a few minutes, up to values of around 12.0–12.5 within 3 h of reaction.

As can be seen from Figures 6–8, the rate of removal of  $\text{HS}^-$  decreases remarkably over time, even in the presence of large residual concentrations of unreacted HET and  $\text{HS}^-$ . This trend, which was already observed at room temperature<sup>12</sup> is confirmed in this work and also observed at 50 and 75 °C. For example, considering the red curve (initial HET concentration of 456 mM) of Figure 8 (75 °C), the removal of  $\text{HS}^-$  is very fast in the first minutes of reactions, while it is basically stopping even in the presence of around 27 mM of residual

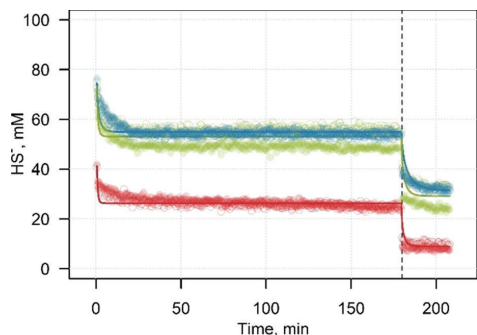


**Figure 8.** Experimental (colored dots) and calculated (continuous lines) concentrations of  $\text{HS}^-$  at 75 °C. Blue for 46 mM HET, green for 91 mM HET, and red for 456 mM HET. The dashed vertical line represents the time of system reacidification (180 min). Duplicate experiments for each initial concentration of HET are reported (filled and empty markers).

**Table 3. Optimal Parameters Found by Experimental Data Regression with the Kinetic Model for the  $\text{H}_2\text{S}$  Scavenging Reactions in the Aqueous Phase**

temperature, °C	$k_{11}$ , $\text{L mol}^{-1} \text{s}^{-1}$	$k_{21}$ , $\text{L mol}^{-1} \text{s}^{-1}$	$\text{p}K_{\text{HET}}$	$\text{p}K_{\text{TDZ}}$	initial pH
25	0.435	0.004	7.58	9.04	9.3–10.1
50	3.260	0.018	7.50	9.10	9.0–10.1
75	22.200	0.110	7.05	9.05	9.0–9.8

$\text{HS}^-$  and a large amount of unreacted HET. The experimental data of Figures 6–8 at short reaction times also show that the rate of consumption of  $\text{HS}^-$  increases with temperature.

The abovementioned remarkable decrease of the rate of disappearance of  $\text{HS}^-$  over time can be explained by the scavenging reactions slowing down, as the pH of the reacting mixture increases, which causes a reduced availability of  $\text{HET}^+$  and  $\text{TDZ}^+$  according to the equilibrium relationships of eqs 7 and 8. As can be seen, this behavior is well captured by the kinetic model proposed in this work. It can be added that this behavior could not be described without considering  $\text{HET}^+$  and  $\text{TDZ}^+$  as the reacting species, together with their protonation equilibria. From a quantitative standpoint, as can be seen in Table 4, the model provides an adequate representation of the experimental data pertaining to the first 3 h of reaction (i.e., before the acidification) with ARDs in the range of 2 to 7%. The accuracy of the predictions is lower after

**Table 4. ARD between Experimental and Calculated Values before Acidification (BA) and after Acidification (AA)**

temperature, °C	HET, mM	ARD BA, %	ARD AA, %
25	46	2.12	22.39
	91	2.61	11.75
	456	7.48	18.30
50	46	3.86	10.08
	91	3.65	8.24
	456	2.86	13.13
75	46	1.94	3.82
	91	2.05	3.33
	456	4.19	9.09

the acidification (ARD values 3 to 22%), but this is attributed to the higher experimental uncertainty associated with the acidification after the first 3 h of reaction, also supported by the larger values of the experimental ARD of the duplicates after acidification reported in previous lines. Nonetheless, even after the acidification, the model captures well the trends of the rate of the reaction, with a sharp increase of the rate immediately after the acidification, followed by the reaction remarkably slowing down, or basically stopping after some time due to the re-increase of pH.

The optimal values of the regression parameters (see Table 3) show that the rate constant for the first scavenging reaction is 2 orders of magnitude higher than that for the second scavenging reaction. Even though data of the rate constants for the two scavenging reactions were not reported in the literature prior to this work, the higher value of the rate constant for the first scavenging reaction is qualitatively in line with the considerations reported in previous works.<sup>7,8</sup> In addition, the optimal values of  $\text{p}K_{\text{a}}$  of HET denote a decreasing trend with increasing temperature, in line with the observed trend of amines.<sup>22</sup>

The trend of the rate constants with temperature follows well the Arrhenius relationship with the activation energies for the first and second scavenging reactions estimated to be 68 and 57 kJ/mol, respectively. These values imply that both scavenging reactions present a significant dependence on temperature. Details on the estimation of the activation energies are available in the Supporting Information (Figures S12, S13).

Regarding the protonation equilibrium constants, the optimal  $\text{p}K_{\text{a}}$  values for HET were found in the range of 7.0 to 7.6, while they were around 9 for TDZ. These values are in line with  $\text{p}K_{\text{a}}$  values for amines, which are typically in the range of 7 to 11.<sup>22</sup> In particular, the values for HET are qualitatively in line with the first signs of protonation detected at pH values below 9.5 by means of NMR (see Section 3.2). The higher  $\text{p}K_{\text{a}}$  value for TDZ suggests that this species is more prone to protonation than HET.<sup>2</sup>

The only kinetic data available in the literature for this reacting system pertain to the first scavenging reaction and were reported by Bakke and Buhaug,<sup>11</sup> who estimated  $k_1/K_{\text{HET}}$  to  $9.1 \times 10^7 \text{ L}^2 \text{ mol}^{-2} \text{ s}^{-1}$ . The data of our work indicate this parameter to be  $1.65 \times 10^7 \text{ L}^2 \text{ mol}^{-2} \text{ s}^{-1}$ , which is in the same order of magnitude.

The kinetic model, validated on the experimental data of the rate of disappearance of  $\text{HS}^-$ , was used to estimate the trends of the total concentration of the main reaction components: HET, TDZ, DTZ, and MEA. The data at 50 °C are shown in Figure 9 and used for the discussion. Analogous trends are found at 25 and 75 °C, with the corresponding figures reported in the Supporting Information (Figures S14, S15).

The model predicts the predominance of the first scavenging reaction before acidification, as evidenced by the increasing concentration of TDZ and the concomitant decrease of the HET concentration in all reaction executions with small DTZ formation. In particular, considering the calculated values before acidification for the reaction at 46 mM HET, the concentration of DTZ after 3 h reaches only 3.1 mM, while the maximum theoretical concentration of DTZ is 46 mM, denoting that the second scavenging reaction has advanced only to a small extent. After acidification, however, the model predicts a maximum value for the concentration of TDZ with a

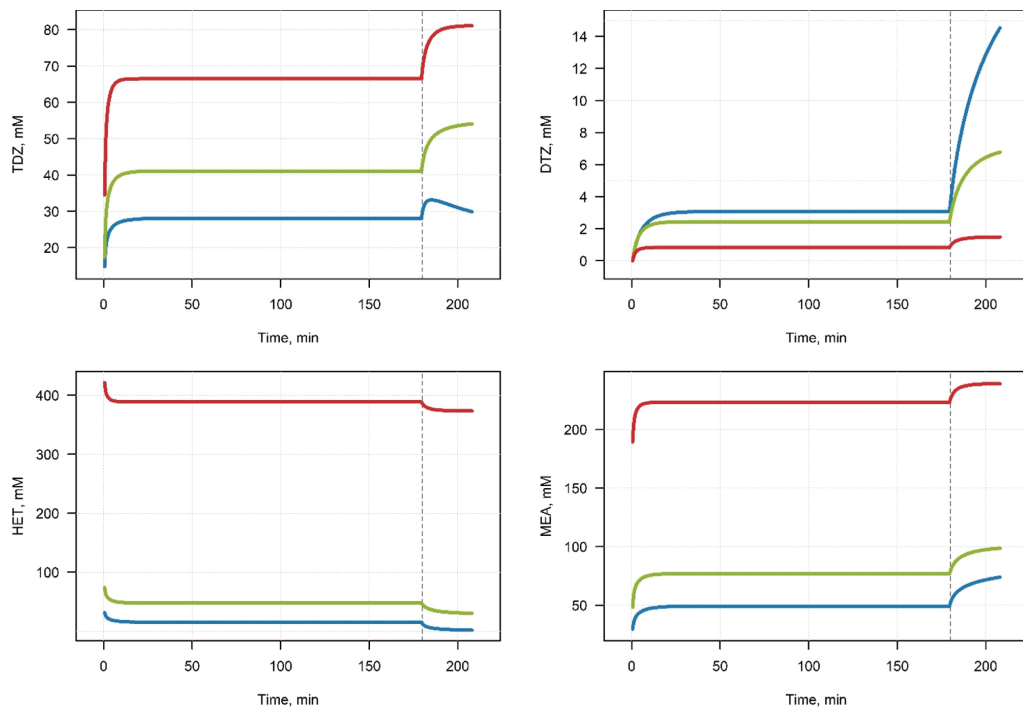


**Figure 9.** Calculated concentration of the main reaction components: HET, TDZ, DTZ, and MEA for the reactions run at 50 °C. Blue for 46 mM HET, green for 91 mM HET, and red for 456 mM HET. The dashed vertical line represents the time of system reacidification (180 min).

final concentration of 29.9 mM. Simultaneously, the calculated concentration of DTZ increases sharply up to 14.5 mM, while the concentration of HET decreases down to 1.6 mM. Therefore, at the conditions under investigation, the overall consumption of  $\text{HS}^-$  is mainly due to the first scavenging reaction, even though at long reaction times the second scavenging reaction becomes predominant.

## 5. CONCLUSIONS

The experimental observations of this work show that TDZ is stable enough to be obtained as a product of the aqueous phase reaction of  $\text{HET}^+$  and  $\text{HS}^-$ , starting from equimolar reactants and carrying out the reaction up to 50 °C for 2 h. TDZ was separated from the reaction mixture, purified up to 90% (molar basis) by HPLC, and identified via NMR spectroscopy at a temperature up to 45 °C. At high pH (indicatively above 10) and room temperature, TDZ was observed to be stable for several days.

The experimental evidence supports that a model based on protonation/deprotonation equilibria of HET, TDZ, and MEA and two second-order bisulfide scavenging reactions (first order with respect to the protonated species and first order with respect to bisulfide) can adequately represent the reaction kinetics of the aqueous-phase scavenging reactions with HET. The model explains on a quantitative level, at temperatures up to 75 °C, the strong effect of the pH on the rate of scavenging of  $\text{HS}^-$ , which determines the availability of protonated HET and TDZ. The lack of further reaction of DTZ with  $\text{HS}^-$  can

be explained by the lack of protonation of DTZ due to low  $\text{p}K_a$ , as observed via NMR.

The values found for the set of optimal regression parameters suggest that the rate constant of the first scavenging reaction is 2 orders of magnitude higher than the constant for the second reaction, which supports the premise of accumulation of TDZ in the reacting system in the presence of excess of triazine at the conditions investigated in the laboratory in this work. The activation energies of the first and second scavenging reactions were estimated to be 68 and 57 kJ/mol, respectively, evidencing a significant dependency on temperature.

The kinetic model developed in this work provides the kinetics of the aqueous phase reactions involving bisulfide and MEA-triazine at pH values above 9. Coupling this kinetic model with mass transfer models, representing the transfer of  $\text{H}_2\text{S}$  from the gas phase into the basic aqueous phase containing MEA-triazine, will allow the realization of physicochemical models representing the  $\text{H}_2\text{S}$  scavenging of gas streams via injection of aqueous solutions of MEA-triazine, such as the processes currently applied in several offshore oil and gas installations.

## ■ ASSOCIATED CONTENT

### Supporting Information

The Supporting Information is available free of charge at <https://pubs.acs.org/doi/10.1021/acs.iecr.3c00668>.

Compositional determination of technical HET via NMR spectroscopy; TDZ purification and identification;

methodology for execution of scavenging reactions experiments for kinetic data; NMR results for the identification of TDZ (LC–MS total ion chromatogram of purification of TDZ;  $^1\text{H}$  NMR spectra of TDZ at different temperatures;  $^1\text{H}$ - and  $^{13}\text{C}$ -inversion recovery spectra of TDZ to determine  $T_1$  relaxation times;  $T_1$  relaxation times for TDZ; and [ $^1\text{H}$ ,  $^{13}\text{C}$ ]-HMBC spectra of TDZ); NMR results of protonation equilibrium analyses ( $^1\text{H}$  NMR spectra of solutions of HET at different pH values at 25, 50, and 75 °C and  $^1\text{H}$  NMR spectra of solutions of DTZ at different pH values at 25 °C); and kinetic model for the  $\text{H}_2\text{S}$  scavenging reactions in the aqueous phase (derivation of the model; optimization grid for regression parameters of the kinetic model; Arrhenius plots for the first and second scavenging reactions; calculated concentration of the main reaction components: and HET, TDZ, DTZ, and MEA for the reactions run at 25 and 75 °C) (PDF)

## ■ AUTHOR INFORMATION

### Corresponding Author

Marco Maschietti – Department of Chemistry and Bioscience, Section of Chemical Science and Engineering, Aalborg University Esbjerg, 6700 Esbjerg, Denmark; [orcid.org/0000-0002-3120-7560](https://orcid.org/0000-0002-3120-7560); Email: [marco@bio.aau.dk](mailto:marco@bio.aau.dk)

### Authors

Iveth Romero – Department of Chemistry and Bioscience, Section of Chemical Science and Engineering, Aalborg University Esbjerg, 6700 Esbjerg, Denmark; Ramboll Energy, Energy Transition, Process Department, 6700 Esbjerg, Denmark

Fernando Montero – Department of Chemistry and Bioscience, Section of Chemical Science and Engineering, Aalborg University Esbjerg, 6700 Esbjerg, Denmark; Ramboll Energy, Energy Transition, Process Department, 6700 Esbjerg, Denmark; [orcid.org/0000-0002-6191-3482](https://orcid.org/0000-0002-6191-3482)

Sergey Kucheryavskiy – Department of Chemistry and Bioscience, Section of Chemical Science and Engineering, Aalborg University Esbjerg, 6700 Esbjerg, Denmark; [orcid.org/0000-0002-3145-7244](https://orcid.org/0000-0002-3145-7244)

Reinhard Wimmer – Department of Chemistry and Bioscience, Section of Bioscience and Engineering, Aalborg University, 9220 Aalborg Ø, Denmark; [orcid.org/0000-0001-6942-5056](https://orcid.org/0000-0001-6942-5056)

Anders Andreasen – Ramboll Energy, Energy Transition, Process Department, 6700 Esbjerg, Denmark; [orcid.org/0000-0003-0475-323X](https://orcid.org/0000-0003-0475-323X)

Complete contact information is available at:  
<https://pubs.acs.org/10.1021/acs.iecr.3c00668>

### Notes

The authors declare no competing financial interest.

## ■ ACKNOWLEDGMENTS

This work was financially supported by the Energiteknologiske Udviklings-og Demonstrationsprogram (EUDP) [Energy Technology Development and Demonstration Program], Denmark [SCAVOP project, project number 64018-0819]. The NMR laboratory at Aalborg University is supported by the Obel Family, SparNord, and Carlsberg Foundations. The

authors are grateful to Susanne Tolstrup for proof-reading the manuscript.

## ■ REFERENCES

- (1) Taylor, G. N.; Wilde, J. J.; Müller, T.; Murison, J.; Schneider, F. Fresh insight into the  $\text{H}_2\text{S}$  scavenging mechanism of MEA-triazine vs. MMA-triazine. Paper Presented at the SPE International Conference on Oilfield Chemistry: Montgomery, Texas, USA, April 2017. Paper number: SPE-184529-MS.
- (2) Wylde, J. J.; Taylor, G. N.; Sorbie, K. S.; Samaniego, W. N. Formation, chemical characterization and oxidative dissolution of amorphous polymeric dithiazine (apDTZ) during the use of the  $\text{H}_2\text{S}$  scavenger monoethanolamine-triazine. *Energy Fuels* **2020**, *34*, 9923–9931.
- (3) Lioliou, M. G.; Jenssen, C. B.; Øvsthus, K.; Brurås, A. M.; Aasen, Ø. L. Design Principles for  $\text{H}_2\text{S}$  Scavenger Injection Systems. Paper presented at the Oilfield Chemistry Symposium: Geilo, Norway, March 2018.
- (4) Owens, T.; Clark, P. Triazine Chemistry: Removing  $\text{H}_2\text{S}$  and Mercaptans. *ASRL Quat. Bull.* **2010**, *47*, 1–21.
- (5) Montesantos, N.; Fini, M. N.; Muff, J.; Maschietti, M. Proof of Concept of Hydrothermal Oxidation for Treatment of Triazine-Based Spent and Unspent  $\text{H}_2\text{S}$  Scavengers from Offshore Oil and Gas Production. *Chem. Eng. J.* **2022**, *427*, 131020.
- (6) Montesantos, N.; Skjolding, L.; Baun, A.; Muff, J.; Maschietti, M. Reducing the environmental impact of offshore  $\text{H}_2\text{S}$  scavenging wastewater via hydrothermal oxidation. *Water Res.* **2023**, *230*, 119507.
- (7) Bakke, J. M.; Buhaug, J.; Riha, J. Hydrolysis of 1,3,5-Tris(2-Hydroxyethyl)Hexahydro-S-Triazine and Its Reaction with  $\text{H}_2\text{S}$ . *Ind. Eng. Chem. Res.* **2001**, *40*, 6051–6054.
- (8) Madsen, H. T.; Sogaard, E. G. Use of ESI-MS to Determine Reaction Pathway for Hydrogen Sulphide Scavenging With 1,3,5-Tri(2-Hydroxyethyl)-Hexahydro-S-Triazine. *Eur. J. Mass Spectrom.* **2012**, *18*, 377–383.
- (9) Taylor, G. N.; Matherly, R. Gas Chromatographic-Mass Spectrometric Analysis of Chemically Derivatized Hexahydrotriazine-Based Hydrogen Sulfide Scavengers: Part II. *Ind. Eng. Chem. Res.* **2010**, *49*, 6267–6269.
- (10) Perez Pineiro, R.; Peeples, C. A.; Hendry, J.; Hoshowski, J.; Hanna, G.; Jenkins, A. Raman and DFT Study of the  $\text{H}_2\text{S}$  Scavenger Reaction of HET-TRZ Under Simulated Contactor Tower Conditions. *Ind. Eng. Chem. Res.* **2021**, *60*, 5394–5402.
- (11) Bakke, J. M.; Buhaug, J. B. Hydrogen Sulfide Scavenging by 1,3,5-Triazinanes. Comparison of the Rates of Reaction. *Ind. Eng. Chem. Res.* **2004**, *43*, 1962–1965.
- (12) Romero, I.; Kucheryavskiy, S.; Maschietti, M. Experimental study of the aqueous phase reaction of hydrogen sulfide with MEA-triazine using in situ Raman spectroscopy. *Ind. Eng. Chem. Res.* **2021**, *60*, 15549–15557.
- (13) Johansen, L. N.; Kloster, L.; Andreasen, A.; Kucheryavskiy, S.; Nielsen, R. P.; Maschietti, M. Raman Spectroscopy for Monitoring Aqueous Phase Hydrogen Sulfide Scavenging Reactions with Triazine: A Feasibility Study. *Chem. Eng. Trans.* **2019**, *74*, 541–546.
- (14) Dreier, L.; Wider, G. Concentration measurements by PULCON using X-filtered or 2D NMR spectra. *Magn. Reson. Chem.* **2006**, *44*, S206–S212.
- (15) Wold, S.; Sjöström, M.; Eriksson, L. PLS-regression: a basic tool of chemometrics. *Chemom. Intell. Lab. Syst.* **2001**, *58*, 109–130.
- (16) R Core Team A Language and Environment for Statistical Computing; R Foundation for Statistical Computing: Vienna, Austria, 2020. <https://www.R-project.org>.
- (17) Kucheryavskiy, S. mdatools—R package for chemometrics. *Chemom. Intell. Lab. Syst.* **2020**, *198*, 103937.
- (18) Beleites, C.; Sergio, V. *hyperSpec: A Package to Handle Hyperspectral Data Sets in R*, 2020. <https://github.com/r-hyperspec/hyperSpec>.
- (19) Ellis, A.; Golding, R. 25. Spectrophotometric determination of the acid dissociation constants of hydrogen sulphide. *J. Chem. Soc.* **1959**, 127–130.

(20) Loy, H.; Himmelblau, D. The first ionization constant of hydrogen sulfide in water. *J. Phys. Chem.* **1961**, *65*, 264–267.

(21) Fiorot, R. G.; Carneiro, J. W. M. The Mechanism for H<sub>2</sub>S Scavenging by 1,3,5-Hexahydrotriazines Explored by DFT. *Tetrahedron* **2020**, *76*, 131112.

(22) Rayer, A.; Sumon, K.; Jaffari, L.; Henni, A. Dissociation constants (pK<sub>a</sub>) of tertiary and cyclic amines: structural and temperature dependences. *J. Chem. Eng. Data* **2014**, *59*, 3805–3813.

(23) Perez Pineiro, R.; Cruz-Perez, D.; Hoshowski, J.; Zhang, H.; Hendry, J. H<sub>2</sub>S Scavenger Tower Operational Efficiency Achieved through Onsite Compositional Analysis. *Paper presented at the CORROSION 2018*: Phoenix, Arizona, USA, April 2018. Paper Number: NACE-2018-11553.

(24) Bezanson, J.; Edelman, A.; Karpinski, S.; Shah, V. B. Julia: A Fresh Approach to Numerical Computing. *Soc. Ind. Appl. Math., Rev.* **2017**, *59*, 65–98.

(25) Rackauckas, C.; Nie, Q. DifferentialEquations.jl—A performant and feature-rich ecosystem for solving differential equations in Julia. *J. Open Res. Software* **2017**, *5*, 15.

(26) Hindmarsh, A.; Brown, P.; Grant, K.; Lee, S.; Serban, R.; Shumaker, D.; Woodward, C. SUNDIALS: Suite of nonlinear and differential/algebraic equation solvers. *ACM Trans. Math Software* **2005**, *31*, 363–396.

## Recommended by ACS

### Theoretical Investigation of Key Properties of the Pyrolysis of Methyl, Ethyl, and Dimethyl Dioxolane Isomers

Malte Döntgen, K. Alexander Heufer, *et al.*

OCTOBER 31, 2022  
THE JOURNAL OF PHYSICAL CHEMISTRY A

READ 

### High-Level Coupled-Cluster Study on Substituent Effects in H<sub>2</sub> Activation by Low-Valent Aluminy Anions

Nery Villegas-Escobar, Henry F. Schaefer III, *et al.*

JANUARY 23, 2023  
THE JOURNAL OF PHYSICAL CHEMISTRY A

READ 

### Improved Apparatus for Dynamic Column-Breakthrough Measurements Relevant to Direct Air Capture of CO<sub>2</sub>

W. Sean McGivern, Jeffrey A. Manion, *et al.*

MAY 17, 2023  
INDUSTRIAL & ENGINEERING CHEMISTRY RESEARCH

READ 

### Activation of Nitrogen-Doped Carbon Materials on the C–N Bond and C–O Bond: Modeling Study Toward Enhanced Pyrolysis Products

Ding Jiang, Bin Cao, *et al.*

MAY 26, 2022  
ACS SUSTAINABLE CHEMISTRY & ENGINEERING

READ 

Get More Suggestions >

## Supporting Information

# Temperature and pH Dependent Kinetics of the Aqueous Phase Hydrogen Sulfide Scavenging Reactions with MEA-triazine

*Iveth Romero<sup>a,c</sup>, Fernando Montero<sup>a,c</sup>, Sergey Kucheryavskiy<sup>a</sup>, Reinhard Wimmer<sup>b</sup>, Anders Andreasen<sup>c</sup>,  
Marco Maschietti<sup>a\*</sup>*

<sup>a</sup> Department of Chemistry and Bioscience, Section of Chemical Science and Engineering, Aalborg  
University Esbjerg, Niels Bohrs Vej 8, 6700, Esbjerg, Denmark.

<sup>b</sup> Department of Chemistry and Bioscience, Section of Bioscience and Engineering, Aalborg  
University, Frederik Bajers vej 7H, 9220 Aalborg Ø, Denmark

<sup>c</sup> Ramboll Energy, Energy Transition, Process Department, Bavnehøjvej 5, 6700 Esbjerg, Denmark.

\*Corresponding author (e-mail: [marco@bio.aau.dk](mailto:marco@bio.aau.dk), postal address: Ole Rømers Vej 5, 6700 Esbjerg,  
Denmark)

## S1. Compositional determination of technical HET via NMR spectroscopy

### S1.1. Method

NMR spectra were recorded on a BRUKER AVIII-600 MHz NMR spectrometer equipped with a 5 mm cryogenic inverse CPP-TCI probe.

20  $\mu\text{L}$  of technical MEA-triazine solution was diluted with 574  $\mu\text{L}$  of  $\text{D}_2\text{O}$  and 6  $\mu\text{L}$  of DSS (12.38 mM) in  $\text{D}_2\text{O}$  was added.  $^1\text{H}$ -NMR was recorded using water suppression by presaturation, using a recycling time of 25 s to allow for absolute quantitation. The spectrum is shown in Figure S1.

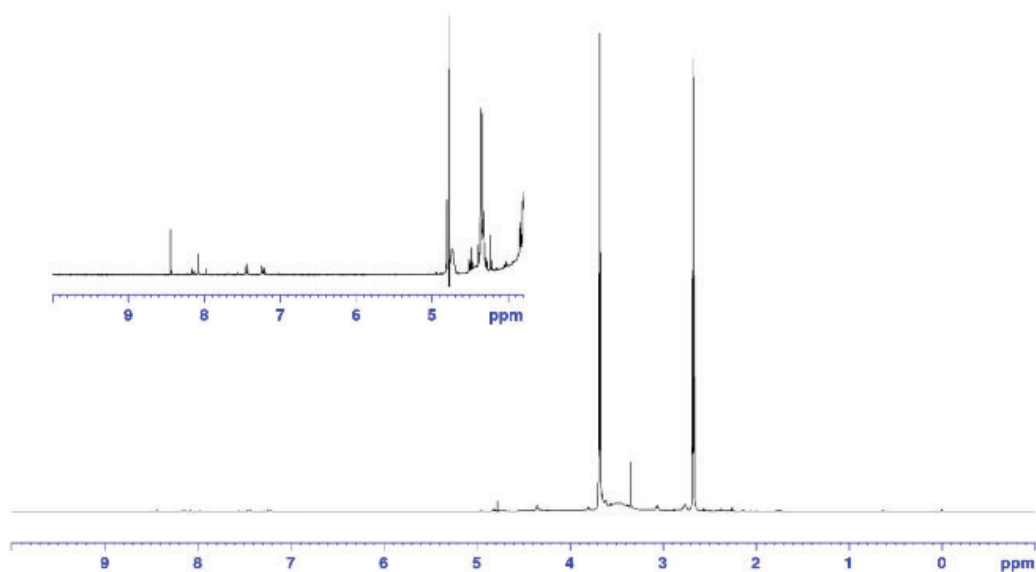


**Figure S1.**  $^1\text{H}$ -NMR of technical HET sample in  $\text{D}_2\text{O}$  at  $25\text{ }^\circ\text{C}$ .



Figure S1 shows two triplets at 2.67 ppm and 3.68 ppm. The triplet at 3.68 ppm is consistent with the CH<sub>2</sub> group bound to the OH in the side chain of HET (shown in magenta in Figure S2), while the triplet at 2.67 ppm is consistent with the CH<sub>2</sub> group bound to the nitrogen (shown in green in Figure S2). These triplets were therefore used for determination of the concentration of HET in the technical sample by quantitative NMR.

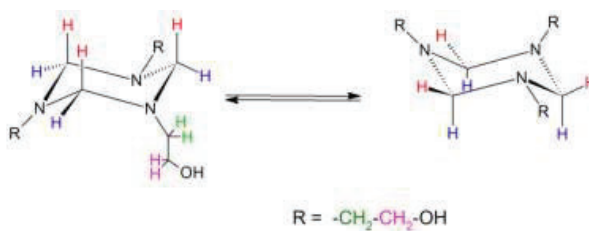


**Figure S2.** Structure and ring-flip equilibrium of HET illustrating the different hydrogen atoms.

## S2. TDZ purification and identification

**S2.1. Purification:** Aliquots of the abovementioned reacting mixture were taken for TDZ purification by preparative high performance liquid chromatography (HPLC) on a Waters Autopurifier system, consisting of a Waters 2767 autosampler/fraction collector, a Waters 2545 binary gradient pump, a Waters SFO system fluidics organizer, a Waters 515 make-up pump, a Waters 2998 Diode Array detector, and a Waters Acquity QDa ESI-MS detector. A Waters XBridge C8 column (19x250 mm, 5  $\mu\text{m}$ ) was used as stationary phase. Elution started with water (+0.05% diethylamine). At first, the content of acetonitrile (+0.05% diethylamine) was increased linearly to 10% over five minutes, whereafter the content of acetonitrile (+0.05% diethylamine) was increased linearly to 99% over the next 5 minutes. This eluent composition was held for another three minutes. The flowrate was 20 mL/min. The detector was set to positive ionization mode with a cone voltage of 45 V.

**S2.2. Identification:** A certain mass of high-purity HET (ca. 23 mg) was dissolved in 450  $\mu\text{L}$  of pure  $\text{D}_2\text{O}$  and 50  $\mu\text{L}$  of  $\text{D}_2\text{O}$  with TSP- $\text{d}_4$ , and pH adjusted to 8 at room temperature. After pH adjustment, the sample was taken to 1 mL with further addition of pure  $\text{D}_2\text{O}$ . The final pH of the HET solution was 8.44 at room temperature. The same procedure was followed for the preparation of the bisulfide solution, using  $\text{Na}_2\text{S}\cdot\sim 3\text{H}_2\text{O}$  (ca. 13 mg). The final pH of the bisulfide solution was 8.03 at room temperature. An aliquot of 500  $\mu\text{L}$  of the HET solution was transferred to a micro centrifuge tube, mixed with an aliquot of 500  $\mu\text{L}$  of the bisulfide solution, stirred and heated to 50  $^\circ\text{C}$  for 2 hours. After this time, the reacting mixture was left at room temperature overnight and NMR spectra recorded.

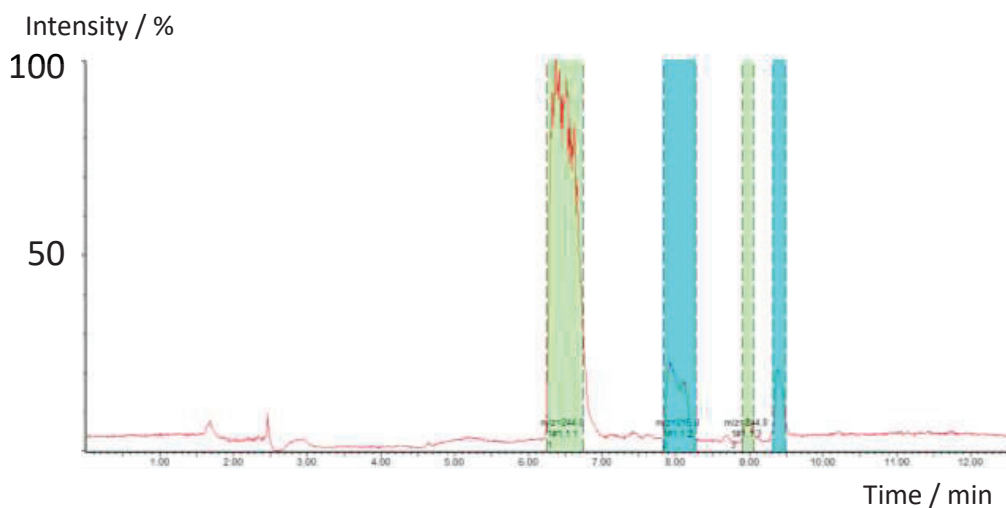
### **S3. Methodology for execution of scavenging reactions experiments for kinetics data**

HET aqueous solutions for the reactions were prepared by weighing appropriate amounts of technical triazine solution (1.60 g, 3.20 g, or 16.00 g) and diluting them with 20 mL distilled water. The solutions were conditioned to  $\text{pH } 9.0 \pm 0.2$  (measured at the reaction temperature) by adding HCl 6 M and brought to 25 mL with further addition of distilled water using a class A volumetric flask.

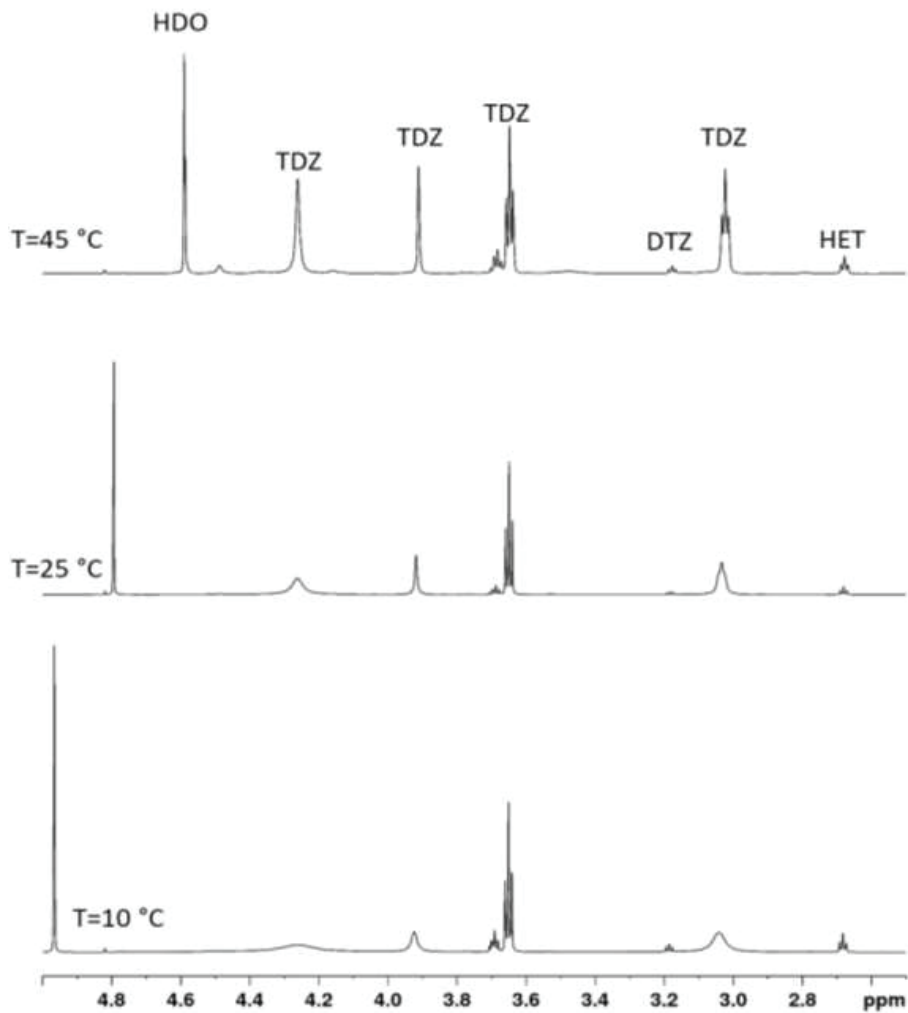
Bisulfide aqueous solutions for the reactions, containing the IS, were prepared by weighing the appropriate amount of PAA (1.03 g) and dissolving it in a NaOH aqueous solution of ca. 0.4 M before dilution of  $\text{Na}_2\text{S} \cdot 3\text{H}_2\text{O}$  (ca. 0.48 g). Upon dissolution of the salt, the solution was taken to  $\text{pH } 9.0 \pm 0.2$  (measured at the reaction temperature) by adding HCl 6 M and brought to 25 mL with further addition of distilled water using a class A volumetric flask.

Aliquots from both solutions were withdrawn by means of class A glass volumetric pipettes (20 mL  $\pm$  0.02 mL and 10 mL  $\pm$  0.02 mL).

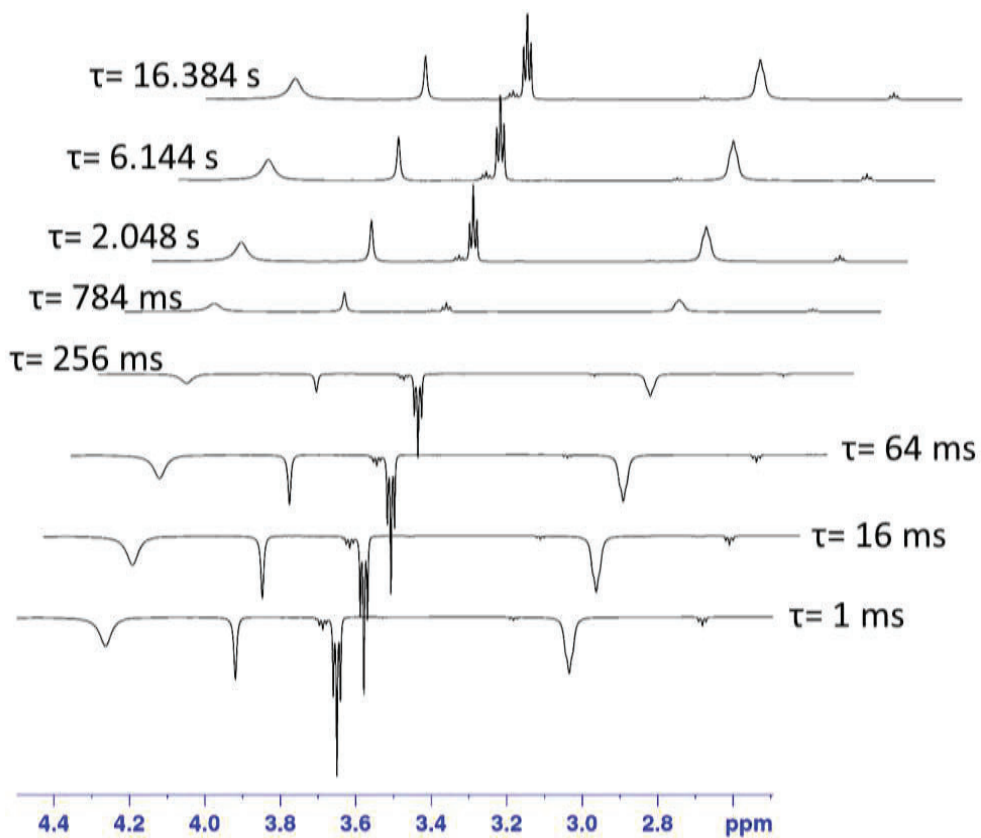
#### S4. NMR results for the identification of TDZ



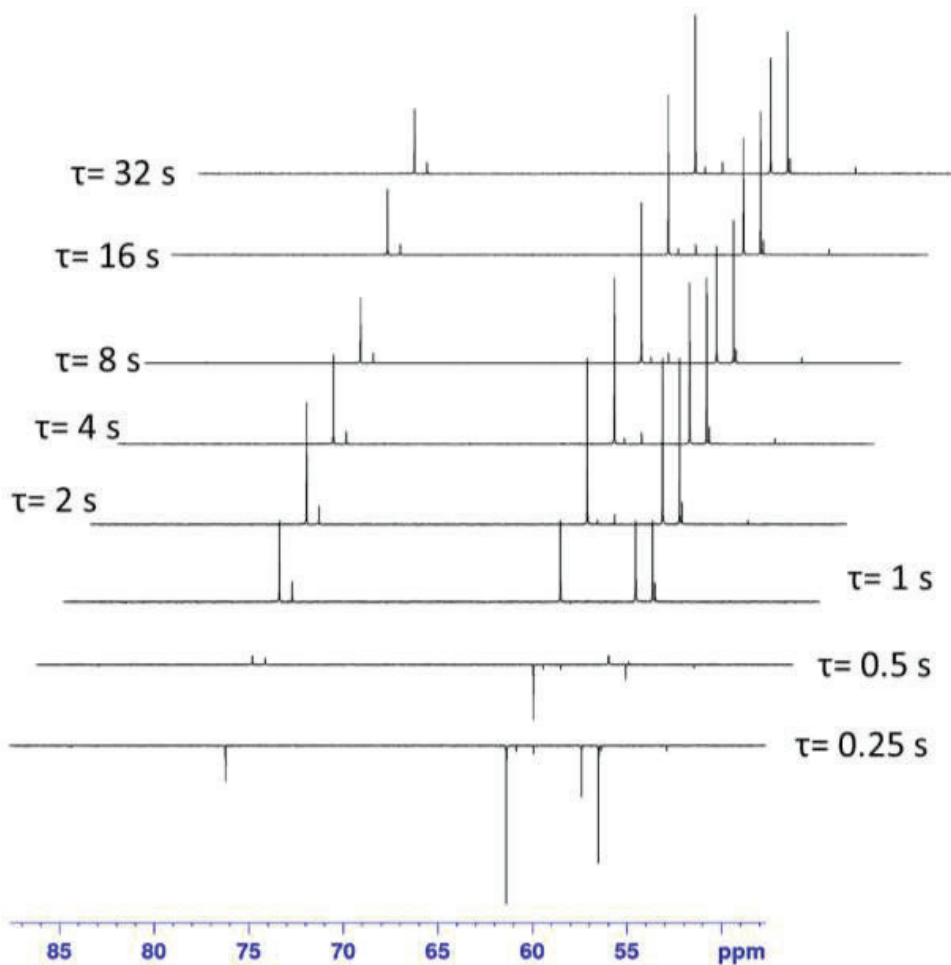
**Figure S3.** Representative LC-MS Total Ion Chromatogram of purification of TDZ from reaction mixture. The four collected fractions are shown with green/cyan in the chromatogram. Subsequent NMR analysis showed that the first fraction contained HET, the second fraction contained TDZ, the third fraction contained a mixture of unidentified compounds at low concentrations and the fourth fraction contained DTZ.



**Figure S4.** <sup>1</sup>H-NMR spectra (600 MHz) of TDZ at different temperatures. The resonances of TDZ clearly show a temperature-dependent line broadening which is indicative of chemical exchange at an intermediate timescale comparable to the chemical shift differences between the two forms. All spectra are referenced to internal TSP-d<sub>4</sub>.



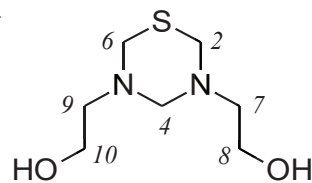
**Figure S5.**  $^1\text{H}$ -Inversion Recovery spectrum of TDZ to determine  $T_1$  relaxation times. The individual relaxation delays are given in the figure.



**Figure S6.**  $^{13}\text{C}$ -Inversion Recovery spectrum of TDZ to determine  $T_1$  relaxation times. The individual relaxation delays are given in the figure.

**Table S1.** T<sub>1</sub> relaxation times for TDZ

Atom	<sup>1</sup> H-T <sub>1</sub> [s]	<sup>13</sup> C-T <sub>1</sub> [s]
4	0.60	0.63
2/6	0.66	0.58
7/9	0.74	0.85
8/10	1.04	1.03





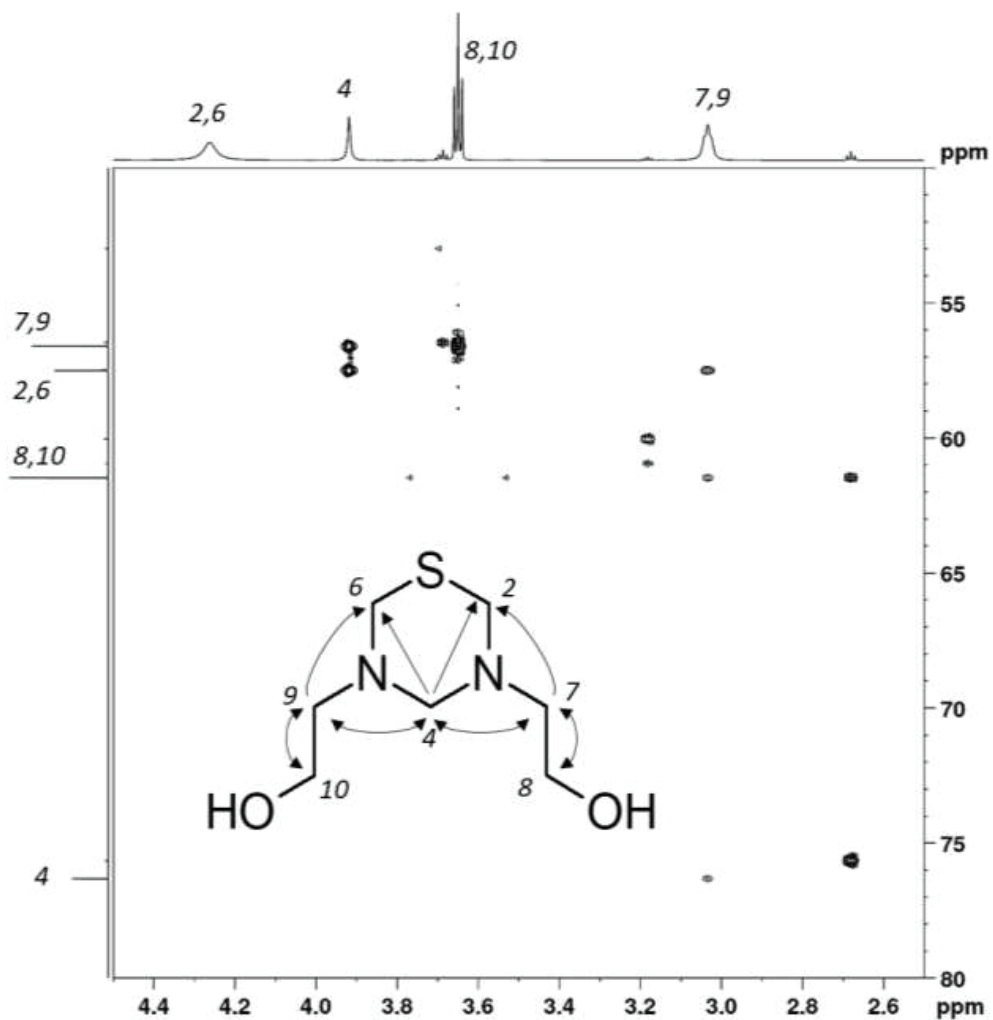


**Figure S7.** [ $^1\text{H}$ , $^{13}\text{C}$ ]-HMBC spectrum of TDZ, including an illustration of the observed correlations. Correlations are drawn as arrows from the hydrogen atom to the carbon atom in the correlation. A double arrow indicates that the correlation could be observed in both directions.

## S5. NMR results of protonation equilibrium analyses

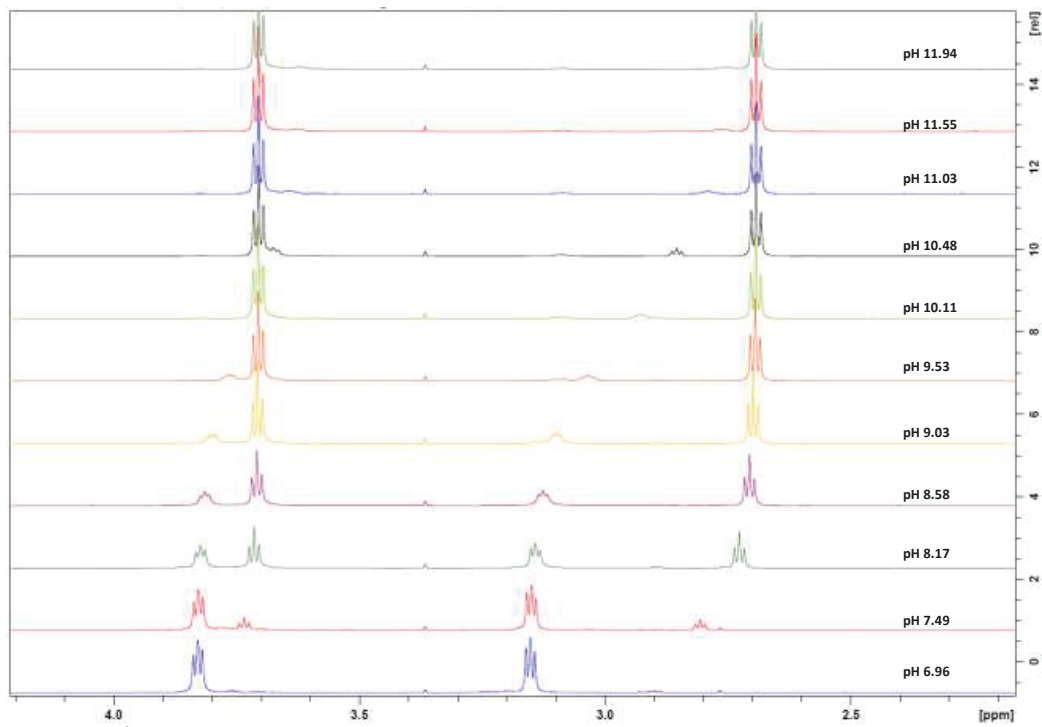
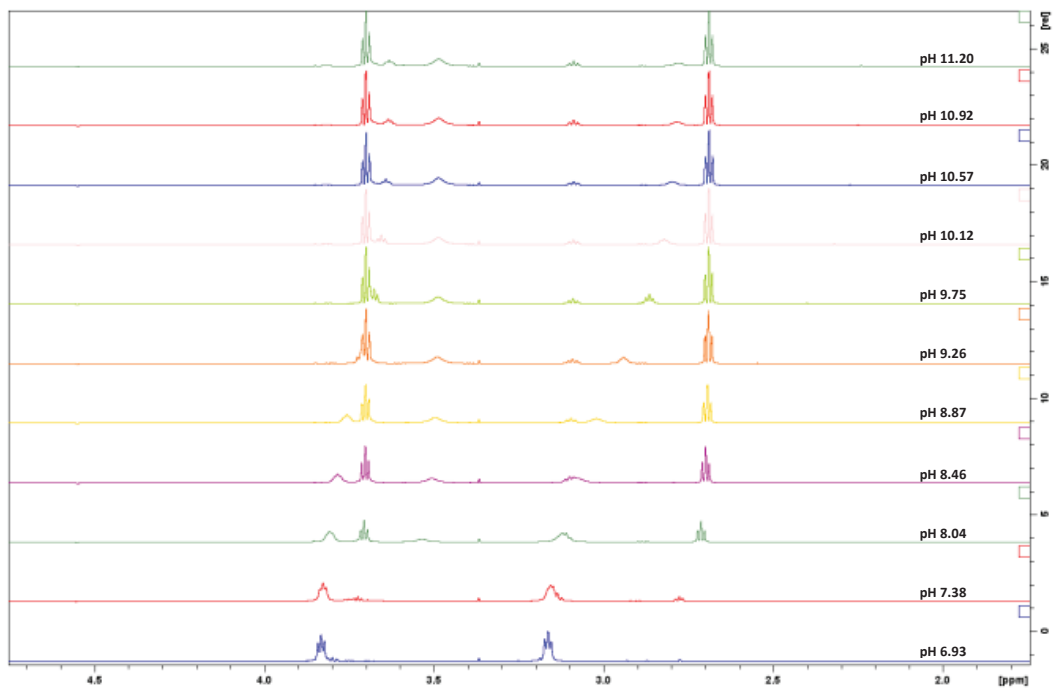
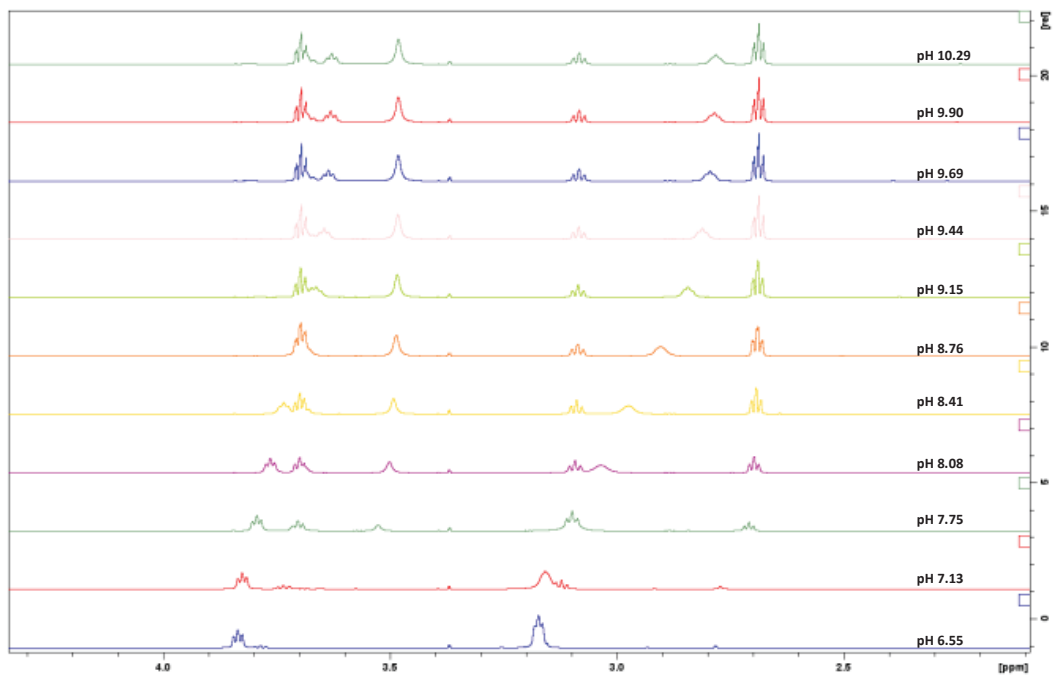


Figure S8. <sup>1</sup>H-NMR spectra of solutions of HET at different pH values at 25°C.



**Figure S9.** <sup>1</sup>H-NMR spectra of solutions of HET at different pH values at 50°C.



**Figure S10.** <sup>1</sup>H-NMR spectra of solutions of HET at different pH values at 75°C.

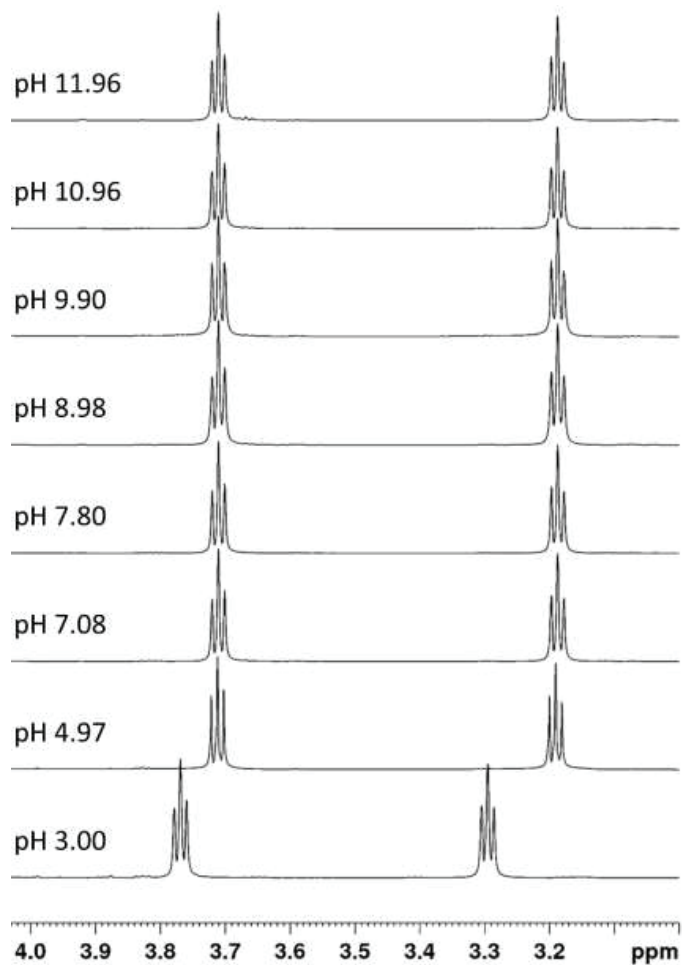


**Figure S11.** <sup>1</sup>H-NMR spectra of solutions of DTZ at different pH values at 25°C. The triplet at 3.8 ppm corresponds to the CH<sub>2</sub> group bound to the OH and the triplet at ca. 3.2 ppm corresponds to the CH<sub>2</sub> group bound to the nitrogen.

## S6. Kinetic model for the H<sub>2</sub>S scavenging reactions in aqueous phase

The molar balances for the species in the constant-density reacting mixture can be expressed in terms of the extent ( $x_i$ ) of the five reactions (Reactions S1 to S5):

$$[HS^-] = [HS^-]_0 - x_1 - x_2 \quad (S1)$$

$$[HET^+] = [HET^+]_0 - x_1 - x_3 \quad (S2)$$

$$[HET] = [HET]_0 + x_3 \quad (S3)$$

$$[TDZ^+] = [TDZ^+]_0 - x_2 - x_4 \quad (S4)$$

$$[TDZ] = [TDZ]_0 + x_1 + x_4 \quad (S5)$$

$$[DTZ] = x_2 \quad (S6)$$

$$[MEA^+] = [MEA^+]_0 - x_5 \quad (S7)$$

$$[MEA] = [MEA]_0 + x_1 + x_2 + x_5 \quad (S8)$$

$$[H_3O^+] = [H_3O^+]_0 + x_3 + x_4 + x_5 \quad (S9)$$

Considering the total rate of consumption of bisulfide expressed in Eq. (S1), the design equation of an ideal BSTR can be written with respect to the concentration of bisulfide as in Eq. (S10):

$$-\frac{d[HS^-]}{dt} = k_1[HET^+][HS^-] + k_2[TDZ^+][HS^-] \quad (S10)$$

The sum of Eq. (S2) and Eq. (S3) gives:

$$[HET^*] = [HET^*]_0 - x_1$$

which shows that the consumption of the total triazine ( $HET^*$ ) is given by the consumption of the protonated triazine from the first scavenging reaction only (Reaction 1), as the equilibrium of triazine (Reaction 3) does not affect the total amount of triazine. Therefore, the design equation of the ideal BSTR written in terms of total triazine gives:

$$-\frac{d([HET^+]+[HET])}{dt} = k_1[HET^+][HS^-] \quad (S11)$$

The substitution of the molar balances in terms of extent of reactions into the design equations Eq. (S10) and (S11) leads to Eqs. (S12) and (S13), which represent two differential equations in terms of the extent of reactions.

$$\frac{dx_1}{dt} = k_1([HET^+]_0 - x_1 - x_3)([HS^-]_0 - x_1 - x_2) \quad (S12)$$

$$\frac{dx_2}{dt} = k_2([TDZ^+]_0 - x_2 - x_4)([HS^-]_0 - x_1 - x_2) \quad (S13)$$

**Table S2.** Optimization grid for regression parameters of the kinetic model.

Optimization grid 1		Optimization grid 2
$10^{-1} \leq k_1 \leq 10^2$	<i>step</i> $10^{0.1}$	<i>step</i> 0.001
$10^{-2} \leq k_2 \leq 10^1$	<i>step</i> $10^{0.1}$	<i>step</i> 0.001
$5 \leq pK_{HET} \leq 9.5$	<i>step</i> 0.1	<i>step</i> 0.01
$5 \leq pK_{HET} \leq 9.5$	<i>step</i> 0.1	<i>step</i> 0.01

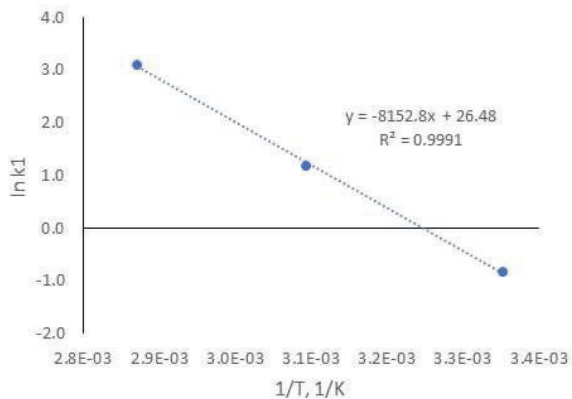


**Figure S12.** Arrhenius plot for the first scavenging reaction.

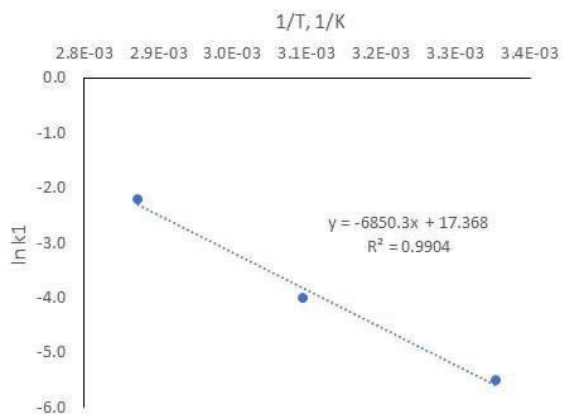


**Figure S13.** Arrhenius plot for the second scavenging reaction.



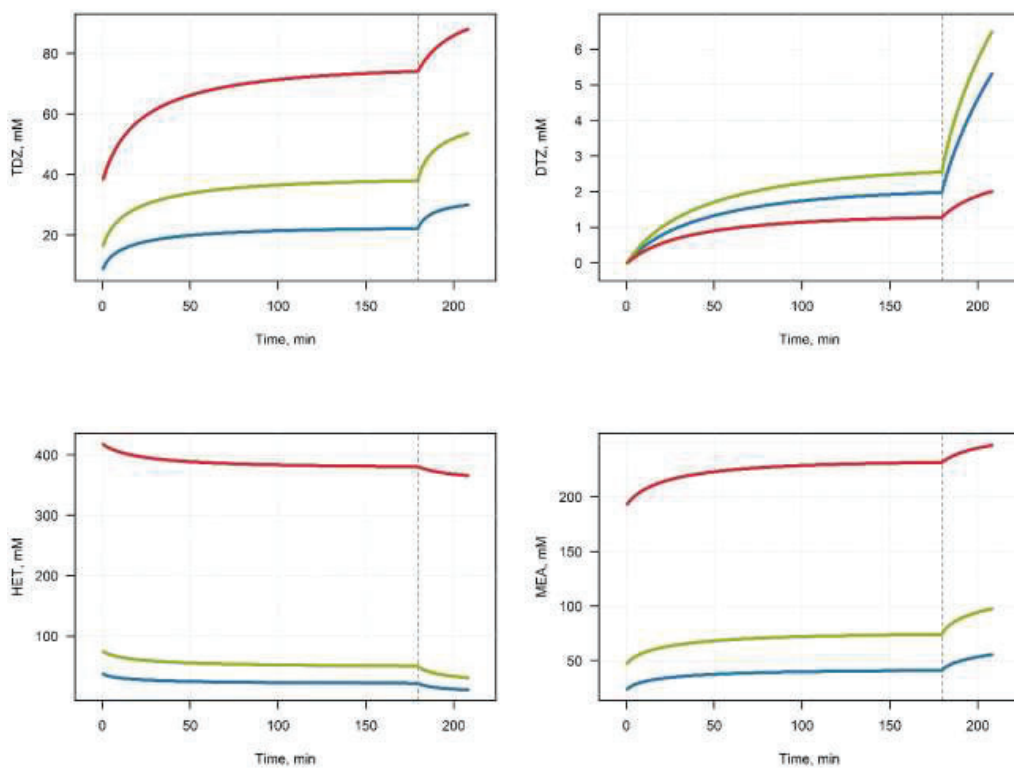


**Figure S14.** Calculated concentration of the main reaction components: HET, TDZ, DTZ, and MEA for the reactions run at 25 °C. Blue for 46 mM HET, green for 91 mM HET and red for 456 mM HET. Dashed vertical line represents the time of system reacidification (180 min).

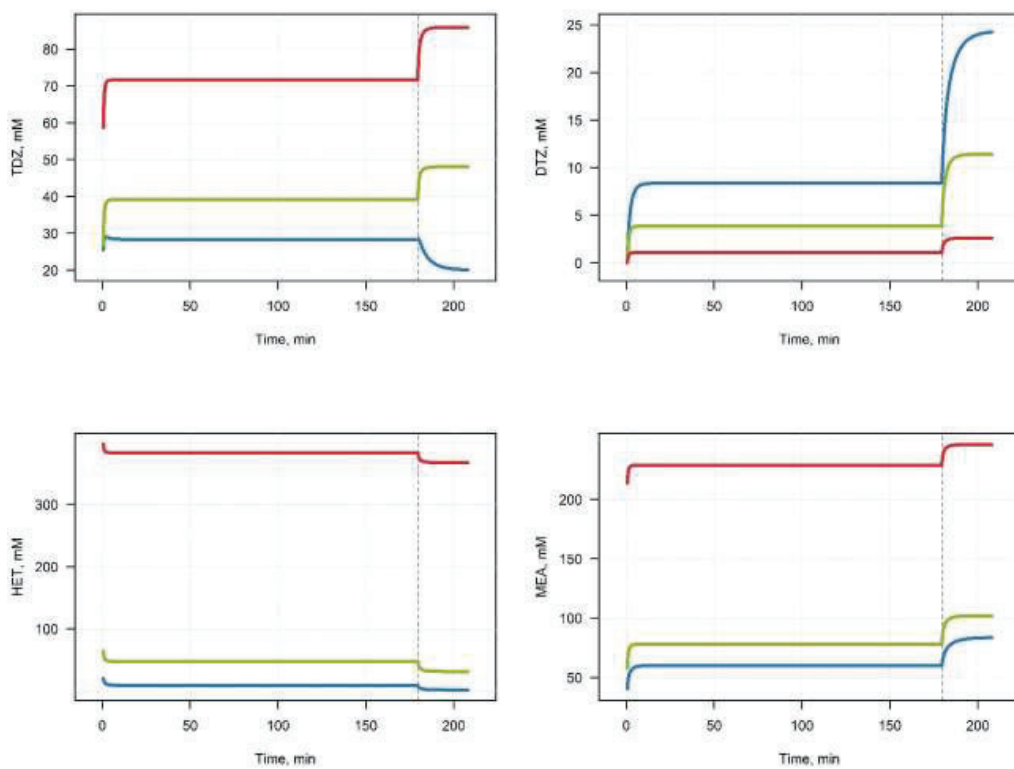


**Figure S15.** Calculated concentration of the main reaction components: HET, TDZ, DTZ, and MEA for the reactions run at 75 °C. Blue for 46 mM HET, green for 91 mM HET and red for 456 mM HET. Dashed vertical line represents the time of system reacidification (180 min).



ISSN (online): 2446-1636  
ISBN (online): 978-87-7573-653-9

**AALBORG UNIVERSITY PRESS**